A parametric investigation on the shear strength and bearing capacity of Cenozoic Berea Red Sand with geosynthetic reinforcements.

by

Ellisha Angath

19315628

UNIVERSITEIT VAN PRETORIA
UNIVERSITY OF PRETORIA
YUNIBESITHI YA PRETORIA

Department of Geology

Faculty of Natural and Agricultural Sciences

University of Pretoria

Submitted in accordance with the requirements for the degree of Master of Science September 2021

Study Supervisor: Prof J. Louis Van Rooy

The financial assistance of the University of Pretoria towards this research is hereby acknowledged. Opinions expressed and conclusions arrived at, are those of the author, and are not necessarily to be attributed to the University of Pretoria.

Declaration

This dissertation represents the original work of the author and has not otherwise been submitted to any tertiary institution in the form of a diploma or degree. The work of others has been duly acknowledged in the text, when used.

This study was undertaken in a commercial laboratory.

The dissertation was supervised by Prof J. Louis Van Rooy.

Ellisha Angath
19315628

Signature: _______________
Date (of resubmission): _____25/08/22____________

Abstract

The use of Berea Red sands can be seen extensively among civil infrastructure particularly along the eastern coast of South Africa. These cohesive soils vary in colour, composition, and strength. Despite the understanding of limited works being published on the geotechnical properties on Berea Red sands as well as the implementation of reinforcing agents to improve it, this study was undertaken to investigate the bearing capacity and shear strength of Berea Red sands with and without reinforcing agents. In addition, the concept of reinforcing materials was investigated with the probability of improving the Berea Red sands regarding the abovementioned properties, thereby displaying the novelty of this study. Deformation behaviour under an increasing compressive load of 100kPa, 200kPa and 300kPa was implemented through a suite of consolidated undrained triaxial tests. The triaxial tests provided an appropriate technique to study the effects of stress and strain correlation as well as in obtaining the parameters needed to calculate bearing capacity and shear strength. The triaxial tests compared the behaviour of Berea Red sands under reinforced and unreinforced conditions. The implementation of two different reinforcing parameters were investigated and compared with each other as well as with the original unreinforced test results. The two reinforcing agents used resembled that of a diamond mesh and a mosquito net. Different configurations and layers of reinforcement were implemented in the triaxial tests to better study its contribution and influence on the bearing capacity and shear strength of Berea Red sands. The Berea Red sand properties of bearing capacity, shear strength and strength ratio increased by the implementation of reinforcing agents as well as the increase in reinforcing layers with the 4 layer diamond mesh exhibited the best strength properties when compared to unreinforced samples and 2 layer reinforced samples, across all confining pressures (100kPa, 200kPa and 300kPa).

Contents

List of Figures

List of Tables

List of Graphs

1. Introduction

1.1. Background

With an increase in urbanisation, the growth of infrastructure and road development has increased along the eastern coastline of KwaZulu Natal. Most of these developments have been established on typically unconsolidated sediments known colloquially as “Berea Red sands” which form part of the late Cenozoic Maputaland Group. These sediments stretch along the KwaZulu Natal coastline and creep northward into Mozambique.

Berea Red sands have been classified as collapsible soils with poor geotechnical properties as well as limited foundation treatments, regarding a variety of engineering prospects (Schwartz, 1985). Due to this, specialised foundation designs and construction methods are required when constructing on these materials. When developing structures on unfavourable materials, the primary development would be the construction of traditional solutions such as piling. An alternative under consideration is the use of geosynthetics as basal reinforcement (Jones, 2014). Geosynthetics can potentially provide an alternative technique to the traditional methods which have been supported in case studies by Purchase and Van der Merwe, 2017 and Pequenino et al., 2018

Due to Berea Red sands being under constant speculation due to its behavioral change when under pressure, the study attempts to analyse the bearing capacity and shear strength properties with and without geosynthetic reinforcement of Berea Red sands, to develop a better understanding of these sediments for future civil infrastructure. Understanding subsoil behaviour upon foundation loading can help understand the failure mechanisms which are an essential component of stability analysis of earth structures (Jones, 2014).

In qualitative terms the study of bearing capacity and shear strength will contribute to further knowledge, improvement and determining techniques on stabilizing Berea Red sands as well as if it requires reinforcement.

In general, it can be noted that there is a limited supply of published works regarding the geotechnical properties of Berea Red sands as well as the implementation of reinforcing parameters such as geosynthetics on this particular material as well as in general. With that being said, vast civil infrastructure can be seen developing on and with these sediments. This fact forms additional motive in undertaking this investigation, to better understand the properties of Berea Red sands from a geotechnical perspective.

1.2. Aim of Study

The aim of this study investigates the properties of Berea Red sands, in particular the ultimate bearing capacity and shear strength properties, with and without geosynthetic reinforcements by undertaking a parametric study.

1.3. Objectives

The following are the primary objectives of the project:

The analysis of a series of consolidated undrained triaxial test specimens to correlate the stress-strain properties of Berea Red sands.

To evaluate the effect of geosynthetic reinforcement implementation in Berea Red sands.

To analyze the effect of geosynthetic reinforcement layers in Berea Red sands, based on quantity and type.

To contrast the stress-strain behaviour between the natural state and reinforced specimens.

To correlate the ultimate bearing capacity between unreinforced and reinforced specimens for continuous/strip footing foundations, square foundations, and circular foundations.

To analyze the shear strength properties of unreinforced and reinforced specimens.

1.4. Organization of Dissertation

Chapter 1- Introduction

The background to the research by introducing the key factors; namely Berea Red sands and reinforcing parameters. The aims and objectives are stated as well as the approach.

Chapter 2- Literature review

The literature review serves as a basis for the dissertation and was carried out to gain knowledge on previous studies, limited as they may be, with regard to bearing capacity and shear strength parameters on Berea Red sands and soils of similar characteristics, with and without geosynthetic reinforcement. Previous research on triaxial testing of soils with geosynthetic reinforced sands with a variety of type and configuration of reinforcement was incorporated into this review.

Chapter 3- Materials and Methodology

General background information on the geographic and geological setting of KwaZulu Natal and introduction of Berea Red Sand. The methodology followed by each triaxial test was outlined. This included the model phase, the design and preparation as well as the selection of materials. The process followed for the model construction is stated, together with any problems experienced.

Chapter 4- Results and Analysis

Data and gathered from the triaxial tests are presented and analyzed. The difference in bearing capacity between the reinforced and unreinforced scenarios were identified. The deformation behaviour between the unreinforced and reinforced scenarios is investigated as well as the number and type of reinforcement is compared. The ultimate bearing capacity of Berea Red sands are interpreted based on the impact of reinforcement.

Chapter 5- Conclusion and Recommendations

By reviewing the data provided from the consolidated undrained triaxial tests, conclusions were made to satisfy the intended scope of work.

2. Literature Review

2.1. Cenozoic-age Berea Red Sands

According to soil engineers' soils can be used in any kind of civil engineering job as construction or foundation material (Tuncer, 1976). The colloquially termed "Berea Red sands" form part of the Cenozoic-age Maputaland Group, which extends from the Mtentu River to the Mozambique border, comprising coastal aeolian sands which range in colour and age, depending upon their period of exposure (Botha, 2018). These sediments can be classified as decalcified and rubified clayey sands of the Berea Formation and are described as unconsolidated aeolian sediments which are categorized into two horizons, which formed due to the weathering of feldspar minerals to clay. The upper horizon can be identified by its slightly clayey sandy composition whereas the lower horizon is described as having a sandy clay composition due to the leaching of the clay from the upper horizon. The Berea Formation have obtained an orange to red colour as a result of the weathering of the high iron content from the parent rock to form iron hydroxide. Berea Reds are weathered products of aeolinite which are soft and porous rocks and differ in colour, clay content and weathering thickness in areas underlain by the Umkwelane Formation aeolianites (Botha, 2018). Berea Reds may be defined as sand, but it was reported to have significant amounts of clay which is a result of in situ feldspar weathering (Clayton, 1989). A varying clay content of less than 5% to more than 40% can be found in this sand (Rust et al., 2005). Berea Red sand is a highly erodible aeolian deposit with a highly variable plasticity index which range from non-plastic to a plasticity index of 12% (November, 2014). There is an abundant exposure of Berea Red sand distributed along the East coast of South Africa from the KwaZulu Natal coastline up to Mozambique (Bergh et al., 2008). The Berea Formation also occurs sporadically onto the Transkei coast till the north of East London (Clayton, 1989).

2.1.1. Collapse phenomenon

Berea Red sands have been associated with failures of buildings, roads and slope instability problems (Okonta & Govender, 2011). These problems arise due to the physical and engineering properties of the sand varying significantly both vertically and laterally in relation to clay content and moisture content (Clayton, 1989). Berea Reds are interesting soils from a geotechnical point of view, ever since they were recognised as collapsible soils in the insitu undisturbed state (Schwartz, 1981).

The term collapse potential was first recognised by Jennings and Knight, 1975. Collapsible soils refer to soils that can withstand considerable amounts of stress in its dry state but undergoes a large and sudden reduction in volume if it experiences an increase in moisture content with no additional increase in stress (Clayton, 1989). Due to the exposure of partial saturation, capillary forces bring about a change in the soils compression characteristics which results in the collapse phenomenon (Schwartz, 1985). During this change in physical behaviour the soil absorbs the water and progressively loses strength thereby decreasing the bearing capacity.

Collapsible soils are termed to be geologically young and are formed by alluvial, colluvial or aeolian deposition. These soils are often described as open textured silty sandy soil that have a high void ratio and are extremely leached as a result of chemical weathering (Clayton, 1989). According to recent studies, the geological origin of the material does play a vital role in determining a collapse mechanism in that particular material. The collapse phenomenon has been identified in many different transported soils as well as soils such as granitic soils associated to the Basement Complex of South Africa and have thence lost the assumption of being restricted to loose aeolian deposits as previously stated (Brink and Van Rooy, 2015). Collapsible soils can be subdivided into two broad groups namely wet collapsible soils and dry collapsible soils (Fredlund and Gan, 1995). Soil that is partially saturated often have a high bearing capacity due to it being dense and will subsequently suffer low amounts of compression when under a normal foundation load, however when wetted under a load many soils undergo a sudden increase in settlement known as the collapse settlement (Brink and Van Rooy, 2015).

Schwartz, 1985, states the degree of saturation is an important aspect in the collapse phenomenon and should be the determining factor for collapse estimates (Rust et al., 2005). Collapsible soils can be subdivided into two groups; namely dry collapsible soils and wet collapsible soils (Fredlund and Gan, 1995).

The relationship between collapse potential index and dry density for both Aeolian and sands of mixed origin were proposed by Brink, 1985, by the following equations:

Aeolian sands:

$$CP = \frac{1672-\gamma_d}{22} \quad \text{Eq. 1}$$

With a coefficient of correlation= 0.73

Mixed origin:

$$CP = \frac{1590-\gamma_d}{18.9} \quad \text{Eq. 2}$$

With a coefficient of correlation= 0.77

These equations indicate that dry densities greater than 1672 kg/m^3 and 1590 kg/m^3 are usually not regarded as collapsible soils for Aeolian sands and sands of mixed origin respectively (Brink, 2011).

In order for collapse to occur, there are specific conditions that need to be met according to Schwartz, 1985. These are 1. Soils need a collapsible fabric, 2. The soil should be partially saturated, 3. An increase in moisture content must be present and can be the main reason for collapse, 4. An applied pressure should be greater than the overburden pressure prior to collapse (Brink and Van Rooy, 2015). According to Klukanova and Frankovska, 1995, once these factors have been attained the process of collapse can be divided into three separate phase which can occur simultaneously:

Phase 1: due to an increase in moisture and applied stress this phase represents the first stage of destruction of the original microstructure.

Phase 2: continued disintegration of the microstructure as well as a decrease in carbonate. Fabric elements compress and the entire soil volume decreases.

Phase 3: after collapse a new microstructure is formed. Clay particles are aggregated, and clay coatings are removed or destroyed.

Berea Reds have experienced collapse particularly when the content of clay is low, however at depths lower than 5 m this phenomenon is rarely seen (Rust et al., 2005). With regard to road construction, Berea Reds are considered unsuitable natural subgrade material due to them being collapsible soils.

2.1.2. Stabilisation of Berea Red sands

It is vital to investigate any natural material needed for construction to determine its quality and properties to accomplish a successful development. Berea Red sands are seldomly used as base and sub-base material even on lightly trafficked roads (Bergh et al., 2008). This is due to the speculative views on the variability of the material and it being supposedly substandard. According to recent studies Berea Red sands do show certain limitations such as the grading modulus however it is the lack of knowledge on this material which is the prime shortcoming.

A variety of stabilisation techniques to modify Berea Red sands and improve the grading modulus have been evident in past research, by the addition of lime; crushed aggregates and grade emulsion and cement. An improvement of CBR was noticed in Berea Reds which were stabilised by lime and have been used as both base and subbase layers on low trafficked roads

(Bergh et al., 2008). On another account specific for low traffic volume roads, foamed bitumen mixed with Berea Red sand and cement show excellent performance as base material (Paige Green and Garryts, 1998).

The addition of <9.5 mm crushed stone aggregate was tested only to establish a trend using uniform material and by that determine its effect on the grading modulus. By adding 25% of <9.5 mm aggregate shows a significant increase of 60% in CBR value. The addition of emulsion to Berea Red sand helps increase the compactive densities which result in higher CBR strengths. Coarse crushed stone aggregate was also added prior to emulsion and show positive results with increased CBR values (Bergh et al., 2008).

Geotextiles have been studied on Berea Reds to investigate its filtration properties and behaviour. The outcome of the study showed to have a failure rate of 58.33% due to the geotextiles clogging and blocking filtration of water (November, 2014). These mostly occurred on non-plastic Berea Red sands. This study had encountered challenges however it has highlighted potential risks and given rise to the importance of the permeability factor with reference to filtration. The use of geogrid reinforcements was used over soft thin shallow clay layers along the eastern coast of South Africa as a means of basal reinforcement of warehouse floors (Jones et al., 2016). These deposits were estuarine and not aeolian like that of Berea Reds, however the concept of geosynthetic reinforcements allowing large surcharge loads to be applied on clayey sands shows most beneficial.

As a result, Berea Reds can be used as subbase or base construction material given that they are modified or stabilised by an outside source either a chemical or physical source. Chemical stabilisation of Berea Reds has seen good outcomes and have even lasted up to 30 years (Bergh et al., 2008). Physical stabilisation of Berea Reds may be accomplished by the use of geosynthetics overlying the sands.

With the increase in population, the demand for development and urbanisation has risen particularly in KwaZulu Natal. With this in mind, road building materials such as natural gravels are becoming more difficult to find and costly to transport to construction sites. In addition, the usage of crushed aggregate adds onto the cost of road construction in particular. By sourcing out other aggregates for subbase and base construction the economy is affected, whereas by using material locally available and in plentiful amounts, such as Berea Reds, would be a more viable option. Berea Reds have not been vastly used for subbase and base construction due to it usually having a grading modulus of less than one however it is classified as A-2-4 (0) to A-6 according to AASHTO classification (Bergh et al., 2008).

The Mt Edgecombe Interchange project was based on the improvement of an existing diamond shaped interchange between the M41 Motorway and the N2 Freeway in uMhlanga Durban. The improvements would lead into a free flow, four level interchange (Purchase and Van der Merwe, 2017). At the project site Berea Red sands are medium dense clayey fine sands which vary in thickness due to the undulating surface topography and bedrock profile. The project included six new and four upgraded bridge structures. Carefully considered foundation design and geotechnical risks were taken into consideration as well as strict settlement criteria to consider the exceptionally high vertical and horizontal loads and movements from load launchings, bridge piers up to 26m high and lengths of up to 65m for this project. Both bearing capacity and circular slip failure checks indicated that additional ground improvement was needed below the foundation of MSE Wall 6 and 7. These improvements consisted of Replacement Stone Columns installation with Dynamic Compaction with a G6 raft and high strength bi-directional geotextile for areas of MSEW 6 exceeding 7m in height. In areas where the heights range between 4m and 7m, only a G6 raft was used, and no foundation improvement was specified for wall heights below 4m.

2.2. Bearing Capacity

Bearing capacity of foundations are important when it comes to analyzing the settlement of soils as an increase in load on the foundation will be accompanied by an increase in settlement as well as when determining the footing designs of structures and assessing the economical dimensions of foundations. The ultimate bearing capacity, q_u, is the load per unit area at which movement of the foundation occurs because of a sudden failure of the foundation with the failure surface of the soil extending to the surface of the ground (Das, 2011).
Beyond this point, an increase in load will result in foundation settlement of vast proportions with this being referred to as the local shear failure in soil.

The principal modes of failure can be described as, general shear failure; local shear failure and punching failure. The general shear failure is most commonly seen in dense sands and reacts due to a sudden failure in the soil and results in bulging of the ground surface next to the foundation (Figure 1.a). The local shear failure is commonly seen in sand or clays with medium compaction and reacts due to a vast amount of settlement due to loading and results in a small amount of bulging adjacent to the foundation (Figure 1.b). The punching failure (Figure 1.c) is commonly seen in soft clay or fairly loose sand and is initiated due to extensive settlement and results in a wedge-shaped soil zone beneath the foundation in the elastic equilibrium (Sachan, 2015).

Depending on the type of soil the load is carried out on, such as sand or clayey soil (Figure 1.b) or fairly loose soil (Figure 1.c), the bearing capacity will react accordingly.

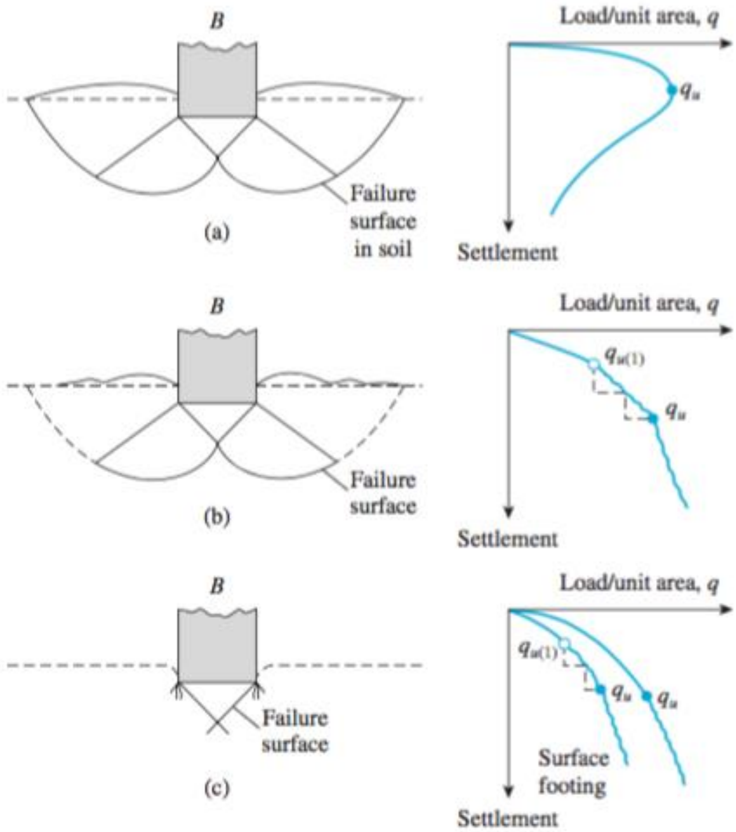

Figure 1: Nature of the bearing capacity failure in soils- a.) general shear failure, b.) local shear failure, c.) punching shear failure (Vesic, 1973 from Das, 2011).

In the case where the failure surface in soil does not extend to the ground surface, such as in fairly loose soils, is referred to as the punching shear failure (Figure 2).

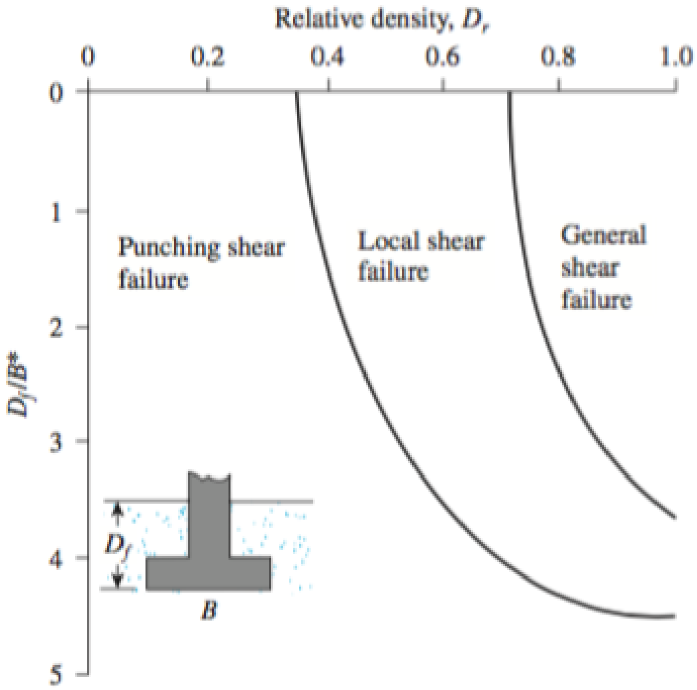

Figure 2: Modes of foundation failure in sand (After Vesic, 1973 from Das, 2011).

2.2.1. Terzaghi's theory

Ultimate bearing capacity according to Terzaghi, 1943, is considered shallow if the depth, D_f, is less than or equal to its width, however later analysis have suggested that depths equal to three to four times their width is also considered shallow (Das, 2011). With regard to continuous/strip footing foundations, Terzaghi states the failure surface in soils at ultimate load may be similar to that in Figure 3. A surcharge $q = \gamma D_f$, where γ is the unit weight of the soil, is assumed to replace the effect of the soil above the bottom of the foundation. It should be noted that the failure zone beneath the foundation can be separated into three sections, namely the triangular zone ACD; the radial shear zone ADF and CDE and two triangular Rankine passive zones AHF and CEG, as shown in Figure 3 (Das, 2011). Due to an equivalent surcharge, q, replacing the soil above the bottom of the foundation, the shear resistance of the soil was neglected, along the failure surfaces GI and HJ.

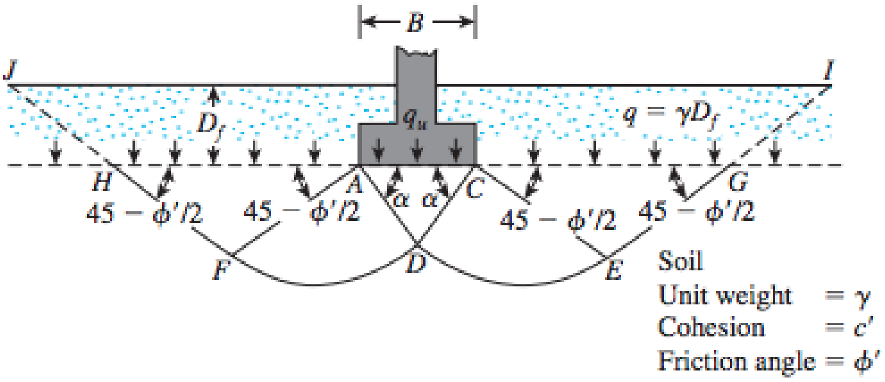

Figure 3: Bearing capacity failure in soil for continuous/strip foundations (Das, 2011)

Terzaghi showed the ultimate bearing capacity for continuous/ strip foundations as:

$$q_u = c'N_c + qN_q + \frac{1}{2}\gamma BN_\gamma \qquad \text{Eq. 3}$$

Where,

c'= soil cohesion

γ = unit weight of soil

$q = \gamma D_f$

N_c, N_q and N_γ = non-dimensional bearing capacity factors which are functions only of the soil friction angle, ϕ' and can be defined by:

$$N_c = \cot\phi' \left[\frac{e^{2(\frac{3\pi}{4}-\frac{\phi}{2})\tan\phi\prime}}{2Cos^2(\frac{\pi}{4}+(\frac{\phi'}{2})} - 1\right]$$

$$N_c = \cot\phi' \ (N_q - 1) \qquad \text{Eq. 4}$$

$$N_q = \frac{e^{2(\frac{3\pi}{4}-\frac{\phi}{2})\tan\phi\prime}}{2Cos^2(45+(\frac{\phi'}{2})} \qquad \text{Eq. 5}$$

and,

$N_\gamma = \frac{1}{2}\left(\frac{K_{p\gamma}}{Cos^2\phi'} - 1\right)\tan\phi'$ Eq. 6

Where $K_{p\gamma}$ = passive pressure coefficient

The bearing capacity factors can be defined by the above equations in Table 1 below.

Table 1: Terzaghi's bearing capacity factors (Kumbhojkar, 1993, from Das, 2011)

ϕ'	N_c	N_q	N_γ^{a}	ϕ'	N_c	N_q	N_γ^{a}
0	5.70	1.00	0.00	26	27.09	14.21	9.84
1	6.00	1.10	0.01	27	29.24	15.90	11.60
2	6.30	1.22	0.04	28	31.61	17.81	13.70
3	6.62	1.35	0.06	29	34.24	19.98	16.18
4	6.97	1.49	0.10	30	37.16	22.46	19.13
5	7.34	1.64	0.14	31	40.41	25.28	22.65
6	7.73	1.81	0.20	32	44.04	28.52	26.87
7	8.15	2.00	0.27	33	48.09	32.23	31.94
8	8.60	2.21	0.35	34	52.64	36.50	38.04
9	9.09	2.44	0.44	35	57.75	41.44	45.41
10	9.61	2.69	0.56	36	63.53	47.16	54.36
11	10.16	2.98	0.69	37	70.01	53.80	65.27
12	10.76	3.29	0.85	38	77.50	61.55	78.61
13	11.41	3.63	1.04	39	85.97	70.61	95.03
14	12.11	4.02	1.26	40	95.66	81.27	115.31
15	12.86	4.45	1.52	41	106.81	93.85	140.51
16	13.68	4.92	1.82	42	119.67	108.75	171.99
17	14.60	5.45	2.18	43	134.58	126.50	211.56
18	15.12	6.04	2.59	44	151.95	147.74	261.60
19	16.56	6.70	3.07	45	172.28	173.28	325.34
20	17.69	7.44	3.64	46	196.22	204.19	407.11
21	18.92	8.26	4.31	47	224.55	241.80	512.84
22	20.27	9.19	5.09	48	258.28	287.85	650.67
23	21.75	10.23	6.00	49	298.71	344.63	831.99
24	23.36	11.40	7.08	50	347.50	415.14	1072.80
25	25.13	12.72	8.34				

The Equation 3 can be modified when estimating the ultimate bearing capacity for square foundations:

$q_u = 1.3c'N_c + qN_q + 0.4\gamma BN_\gamma$ Eq. 7

And circular foundations:

$q_u = 1.3c'N_c + qN_q + 0.3\gamma BN_\gamma$ Eq. 8

2.2.2. Factor of safety

The factor of safety (FS) to the gross ultimate bearing capacity allows the calculation of the gross allowable load-bearing capacity for shallow foundations by the following equation:

$$q_{all} = \frac{q_u}{FS} \qquad \text{Eq. 9}$$

An alternative to Equation 9 is,

$$Net\ stress\ increase\ on\ soil = \frac{net\ ultimate\ bearing\ capacity}{FS} \qquad \text{Eq. 10}$$

Where the net ultimate bearing capacity is defined as the ultimate pressure per unit area of the foundation which is supported by the soil over and above the pressure as a result of the surrounding soil at the level of foundation (Das, 2011).

2.3. Modulus of Elasticity and Poisson's Ratio

The modulus of elasticity, E, and Poisson's ratio, ν, of soils are needed when calculating the stress distribution in soil and can be determined from a triaxial test by reading the results of the plot σ_1'- σ_3' versus axial strain where σ_3 is kept constant (Figure 4) (Das, 2008). The modulus of elasticity varies with confining pressure, such as the greater the confining pressure the greater the E value (Molla, 2017).
The modulus of elasticity can be defined as,

$$E' = \frac{\Delta\sigma}{\Delta\varepsilon} \qquad \text{Eq. 11}$$

Where $\Delta\sigma$ is the change in stress and $\Delta\varepsilon$ is the change in strain. Both these parameters can be obtained from the triaxial test results. The initial tangent modulus can be estimated as,

$$E_i = Kp_a\left(\frac{\sigma'_3}{p_a}\right)^n \qquad \text{Eq. 12}$$

Where,
p_a= atmospheric pressure
K= modulus number

n= exponent determining the rate of variation of E_i and σ'_3

The values of *K* and *n* for different soils mainly falls within the range of 300-2000 and 0.3-0.6 respectively.

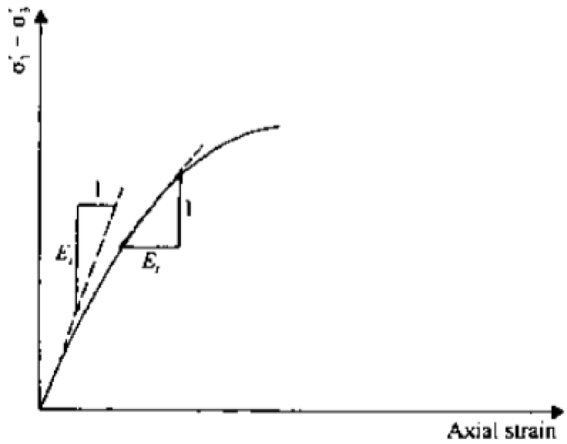

Figure 4: Triaxial test result showing the definition of E_i and E_t (Das, 2008).

Poisson's ratio can be determined by using the formula,

$$\nu = \frac{\Delta\epsilon_a - \Delta\epsilon_v}{2\Delta\epsilon_a} \qquad \text{Eq. 13}$$

Where,

$\Delta\epsilon_a$ = increase in axial strain

$\Delta\epsilon_v$ = volumetric strain

$\Delta\epsilon_r$ = lateral strain

2.4. <u>Shear Strength</u>

Shear strength of soils are important when determining the bearing capacity of piles and shallow foundations as well as many other foundation problems (Das, 2011). It is defined by Mohr's theory that both the normal and shear stresses together produce failure along a plane in a material.

The shear strength of a soil can be classified according to the effective stress in the Equation 14, also known as the Mohr-Coulomb failure criterion (Das, 2011).

$$S = c' + \sigma' \tan\phi' \qquad \text{Eq. 14}$$

Where,

c' = cohesion

σ' = effective normal stress

ϕ = angle of internal friction

The cohesion and angle of internal friction can be determined by either triaxial or direct shear tests.

The shear strength envelope equation put together by Fredlund, 1979, is,

$$\sigma' = c' + (\sigma - u_a)\tan\phi' + (u_a - u_w)\tan\phi^b \qquad \text{Eq. 15}$$

Where, ϕ' and ϕ^b are the angle of friction for changes in $(\sigma-u_a)$ and $(\sigma-u_w)$ respectively (Okonta, 2005). The outcome of using this formula has revealed some restrictions due to incorporating the two stress variables. In terms of describing the volume change behaviour of soils that are unsaturated, most ideas and suggestions have not been entirely successful (Maswoswe, 1982, from Okonta, 2005).

Both Bishop, 1959 and Fredlund, 1979, express the component of shear strength with regard to suction as $\chi\ (u_a-u_w)$ and $(u_a-u_w)\tan\phi^b$ respectively. It can be seen that both these concepts are based on different factors such that the effective stress concept of Bishop's equation is based on the degree of saturation, which is expressed as χ, whereas Fredlund's approach is based on a direct relationship between suction and shear strength (Okonta, 2005).

Shear strength publication on Berea Red sands is largely limited despite the extensive development on these sediments. The two previous works related to triaxial testing on Berea Red sand were written by Clayton, 1989 and Boniface and Olivier, 1979; who performed consolidated undrained triaxial tests as well as many insitu and disturbed tests during the construction of the Glenwood tunnel. Boniface and Olivier, 1979, obtained a Young' modulus of between 10-52MPa from the triaxial tests, which correlated Clayton's, 1989, values from ITS tests on natural Berea Red sand. Clayton, 1989 indicated the coefficient of compressibility as well as shear strength of these sediments are sensitive to changes in moisture content. By investigating the effect of saturation periods on lime stabilized Berea Red sand, the shear strength was investigated on only 2% lime stabilized Berea Red sand as well as on natural Berea Red sand with a 100% mod AASHTO density (Clayton, 1989). The experiments evaluated the effects of the lower compacted density by performing three sets of tests at 95% mod AASHTO density by taking into account the shear strength parameters.

The results indicated that high shear strength levels were maintained due to the dilatancy of the specimens, which increased the confining stress due to pore pressure reduction, which in turn only resulted in a low reduction of peak failure deviator stress. Clayton, 1989, indicated the need of pore water pressure results in order to calculate the undrained shear strength of the soil under investigation. The lack of published properties regarding Berea Red sands is evident despite the substantial development on these sediments.

2.5. Soil Reinforcements

Soil reinforcement is solely concerned with increasing the strength properties of soils by incorporating a resisting element comprising of different materials and forms which are dependent upon the intended use. The use of reinforcements also increases the strength of adjacent structures and can either be permanent or temporary. Based on the concept produced by Vidal, 1969, namely Vidal’s concept, the interaction between soil and horizontal reinforcement is generated primarily by friction due to gravity (Patil et al., 2016). Due to the relative displacement between the soil and reinforcement, a frictional force is induced at the soil-reinforcement interface (Jones, 2014). Thereby causing the potential tensile strain of the reinforced soil to be restrained which results in the reduction of the soils vertical deformation. Soil reinforcement is carried out by the anisotropic reduction of normal strain rate. The reinforcement of soil is essential in areas where erosion is high as well as on soft soil due to it being susceptible to environmental factors and not being able to support structures independently. An increase in the compressive strength of the soil can be improved by lateral confinement which in turn improves the bearing capacity of the reinforced soil (Jones, 2014). A large variety of reinforcements can be used on insitu soils or fill material based on the type of civil engineering infrastructure they will support, such as foundations, retaining walls, railways and road embankments.

2.5.1. Geosynthetics

Geosynthetic reinforcements are a modern approach to helping construction and infrastructure design and engineering. They are able to provide maximum reproducibility of the soil and also thicken the soil volume for increased strength. Geosynthetics are widely used for strengthening insitu soil as well as mechanical improvement of pavement layers (Zannoni, 2013). These products are engineered to be highly durable, resistant and adaptable.

ASTM defined geosynthetics as ‘planar products’ that have been manufactured from polymeric materials and used on or with soils and rocks in civil engineering applications or projects. The name ‘geosynthetic’ is able to define itself, by the prefix ‘geo’ indicating the use of geotechnical materials such as soil; sand and rock and the suffix ‘synthetic’ stating that geosynthetics are made from synthetic material (Ghafoori and Sharbaf, 2016). These products are made from a variety of polymers such as, polypropylene; polyester; polyvinyl chloride and polyethylene. There are some cases when natural materials such as coconut husk and jute fibers were used to make geosynthetics.

The reinforcement function provides increased tensile strength to the geotechnical material used. Geosynthetics have transformed many aspects of civil engineering practices in less than 30 years and in some cases have completely replaced traditional construction materials (Holtz, 2001). There are many factors contributing to this decision, such as environmental impacts and socio-economic impacts. Geosynthetics have been used in many different applications in both civil and underground engineering where in most cases geosynthetics replace mineral based materials such as gravel, lime and concrete in applications like foundation stabilization; slope retention and filter layer construction (Stucki et al., 2011). Geosynthetic reinforcements can be used in cases where the geotechnical material is not able to withstand the pressures exerted on by structures and highways and are able to form a stability barrier for subgrade material. These revolutionizing reinforcement agents are extensively used to strengthen residual soils and enhance pavement layers by improving the subgrade bearing capacity (Zannoni, 2013). The use of geosynthetics as reinforcement material can improve design technique, performance, and safety factor. Geosynthetics have become the key component in designing better roads and providing up to date maintenance on highways and infrastructure. They have also contributed to projects by being able to reduce layer thickness in pavement design and promote the use of lower quality materials as subbase construction fill thereby resulting in cost effective projects (Christopher, 2014).

With regards to soil reinforcement Holtz, 2001, describes three primary applications which are namely:

1. Reinforcing embankment bases on very soft foundations
2. Increasing slope stability and steepness
3. Reducing earth pressures behind retaining walls

Geosynthetics are also able to provide reinforcement and stabilization in roadways; railways; natural slope reinforcement and stabilization of large areas such as warehouse development and harbor ports. Jones et al, 2016 discusses the horizontal deformation and non-uniform settlement of a warehouse floor that could be caused by an increased load pressure on the floor which results in the increase of the undrained strength of the clay, which ultimately fails by being squeezed out at the sides. To avoid this effect, the use of reinforcements in the sand layer is able to control horizontal deformation and strengthen the sand to enhance the rigidity of the floor. The outcome of this investigation allowed for larger surcharge loads to be applied on a specific amount of settlement as well as the reinforcing effect on the geogrid having complete mobilization at 5% vertical compression of the clay layer.

Latha and Murthy, 2006, investigate the effect of quantity and type of geosynthetic reinforcement as well as tensile strength of the materials on the mechanical behaviour of geosynthetic reinforced sand. The three different types of geosynthetics used were woven geotextile; geogrid and polyester film, typically used as overhead projection transparency film. The frictional efficiency for the geosynthetic material varied from 0.45 to 0.78 thereby indicating that the soils used has good frictional interaction with the geosynthetic materials. The results conclude reinforced sand exhibit improved stress-strain behaviour with regard to an increase in peak deviatoric stress and failure strain irrespective of the type of geosynthetic reinforcing material used. It should be noted the increase in shear strength of the sand due to reinforcement cannot be directly related to the tensile strength of the reinforcing material. The stiffness of the reinforced specimens are observed to be less in comparison to the stiffness of the unreinforced specimens at all strains. The increase in cohesive strength is directly proportional to the number of reinforcing layers with little or no effect to the internal friction.

2.6. Triaxial Modelling

Triaxial tests typically involves confining a cylindrical soil or rock sample into a pressurised cell which stimulates a stress condition. This test is then sheared to failure to determine the shear strength conditions of the sample. Therefore, the principal idea of a triaxial test is to determine the stress-strain and shear characteristics of the soil under a predetermined stress state. The triaxial compression test is a versatile soil test which is generally used in geotechnical engineering, in which triaxial compression is applied where $\sigma_1 > \sigma_2 = \sigma_3$ with the σ_1 (axial principal stress) acting vertically (Clayton, 1989). The behaviour of a soil's stress-strain is not linear and may depict different forms such as elastic to an elastic-plastic state which can be compared to the behaviour of rubber or mild steel (Clayton, 1989).

Normally reinforced soil structures are constructed on good quality granular fill material; however, this is not always the case due to availability being uncertain. Soils can be used as backfill materials sometimes without compromising the stability and serviceability (Carlos et al., 2016). To determine the analysis of reinforced soils with geosynthetics, triaxial tests have been used on several accounts on both granular and fine soils (Nair and Latha, 2014, and Noorzad and Mirmoradi, 2010).

Triaxial tests are carried out based on the type of engineering application needed. There are three different types of triaxial tests which can be conducted under laboratory conditions, namely unconsolidated undrained (UU); consolidated drained (CD) and consolidated undrained (CU).

The unconsolidated undrained test loads soil samples whilst the total stresses are controlled, therefore allowing for the undrained shear strength, C_u, to be determined and can analyse short term soil stability. This is also the quickest and simplest of the three tests and is normally performed on cohesive soil samples.

The consolidated drained (CD) test provides strength parameters which are determined by effective stress control, such as the cohesion intercept and effective friction angle, and is associated with long term loading response. This test, unlike the unconsolidated undrained test, takes a significant amount of time to complete when investigating cohesive soils due to the shear rate being slow in order to account for pore water pressure changes.

Consolidated undrained test can determine strength parameters from effective stress such as cohesion and effective friction angle. This can be obtained by allowing a faster rate of shearing compared with that of the consolidated drained test. A faster rate of shearing is achieved by recording the excess pore pressure changes within the sample whilst shearing occurs.

The triaxial test apparatus is a complex piece of machinery which consists of a triaxial cell (Figure 5). The sample being tested is encased inside a rubber membrane and then surrounded by water which equates to the cell pressure. This pressure is then used to apply a stress to the sample (σ_3). The sample is axially loaded whilst shearing and the load cell measuring the force applied onto it. The deformation of the cell is measured by the displacement transducer with pore pressure being measured by LVTDs. The volume of the sample can be measured by an automatic pressure controller or by the back-pressure line.

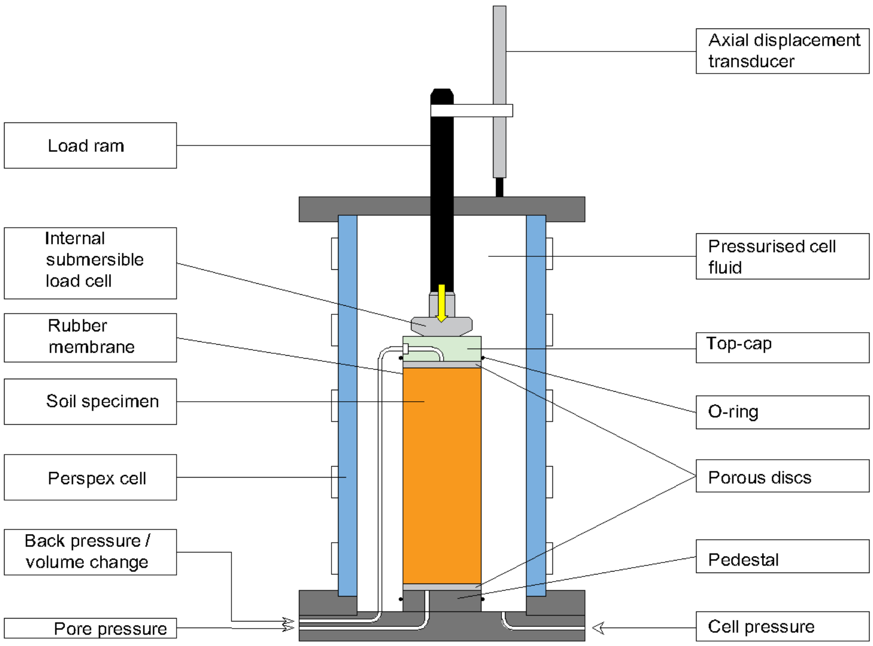

Figure 5: Schematic diagram showing a triaxial cell.

The typical triaxial system used in this investigation is the hydraulic pressure controller which consists of the following components:
Load cell- this measuring device provides the loads required to shear the triaxial sample under investigation.

Triaxial cell- this cell contains the triaxial sample and is pressurized throughout the experiment. These cells come in different sizes and pressure rates. The main features of the cell are the cell top plate of corrosion resistant material which is fitted with an air bleed plug; the loading piston for applying axial compressive forces onto the sample; the cylindrical cell body which is removed for inserting the sample and shall be sealed at the top and base plate; and the cell base f corrosion resistant rigid material which incorporates connection ports.

Load frame- the load frame has a built-in data logger to log transducer data during the test. The load frame is primarily used to apply deformation to the triaxial sample and can be controlled to high levels of accuracy.

Distribution panel- this device is used to connect the dual pressure controller to the triaxial cell. The panel allows for easy movement of water to allocated locations without the disconnection of lines.

Displacement transducer- is used to measure the deformation applied on to the triaxial sample whilst shearing.

Pore pressure transducer- this device is attached to the base of the triaxial cell and measures the pressure inside the triaxial sample for both consolidated undrained and consolidated drained triaxial tests.

Automatic pressure/ volume controller- the pressure controller is able to measure the change in volume whilst the test is ongoing. This device is used to generate pressure for the triaxial test by using stepper motors to pressurize each cylinder of water to create cell pressure as well as back pressure.

The pressure systems for the triaxial test shall be two independent systems, for applying and maintaining the allocated pressure in the cell as well as in the sample drainage line, a calibrated pressure gauge of test grade for independent measurements of the cell pressure and back pressure, a calibrated pore water pressure measuring device containing an electric pressure transducer measuring to 1kPa and a calibrated volume change indicator which is connected to the back pressure line.

A triaxial test creates a series of applied stresses onto the sample of soil or rock (Figure 6). The confining stress, σ_c, is equal to the minor principal stress σ_3 or the radial stress σ_r. The confining stress is applied by pressurising the cell fluid surrounding the sample. The deviator stress, q, acts in addition to the confining stress in the axial direction. The deviator stress is created by applying an axial strain ε_a to the soil. Both the deviator stress and the confining stress combined equal to the axial stress σ_a, or the major principal stress σ_1. When $\sigma_1 = \sigma_3$ the stress state is said to be isotropic, and when $\sigma_1 \neq \sigma_3$ it is anisotropic.

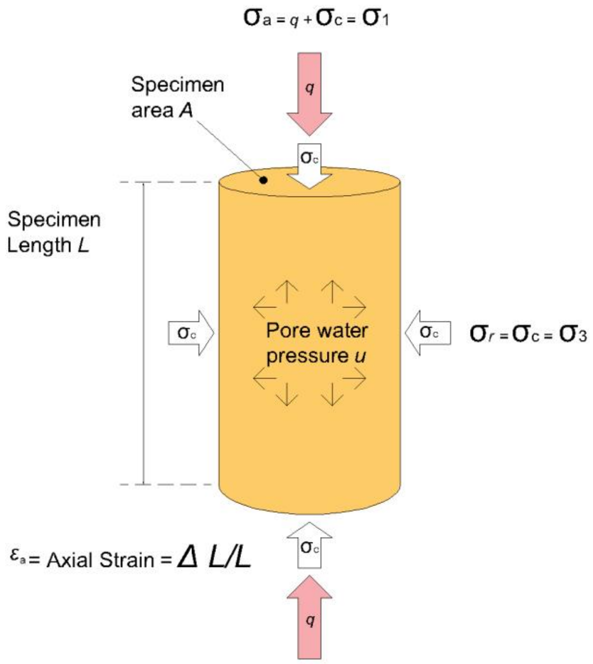

Figure 6: Schematic drawing showing stress states during triaxial compression

2.6.1. Triaxial testing advancements

Over the past two decades there have been vast improvements made on both measurement instrumentation and measurement techniques of triaxial testing. These advancements enable a better conceptual understanding of soil behaviour (Heymann, 2000). Triaxial tests are widely used to investigate soil strength behaviour with the relative techniques being drained and undrained. Instrumentation improvements have been a priority in advancing triaxial tests to measure soil response during testing. The instrumentation improvements have led to a various new measurement technique such as the measurement of soil stiffness, which has shown to be most noted (Heymann, 2000). Being said in theory, triaxial tests are relatively simple to undertake and can be a single element test in which both stress and strain occur throughout the sample. Control over different variables need to be noted for triaxial tests such as the drainage condition, the cell pressure and the axial load applied to the sample (Heymann, 2000). However, during complex triaxial tests measurements of pore fluid pressure, radial strain, axial strain, body wave velocities and volume change are considered.

The measurement of pore fluid pressure is essential for effective stress testing in which many factors need to be addressed such as pressure gradient, the state of pore fluid pressure either being positive or negative as well as the degree of moisture in pore spaces. During saturated triaxial tests it is vital for the entire sample to be saturated as well as the backpress system to ensure no error occurs when measuring pore pressure. The pore fluid pressure under such conditions could be measured at the back pedestal however uniform pore pressure are not likely to occur due to end constraints (Bishop et al., 1960, from Heymann, 2000). When undertaking the measurement of pore fluid pressure, no air should enter the sample and the water should be de-aired. A self-contained water pressure source was developed based on the screw pump mechanism. This mechanism enables pressure to be applied directly onto the water by a piston where the pressure is controlled by a micro-processor feedback system (Heymann, 2000). This system is able to apply high pressures up to 5000 kPa.

Axial force is measured to determine the total vertical stress of the sample. Initially the measurement was executed externally however this brought about inaccuracies for the ram friction. Internal load cells were introduced and directly measure the applied load on the sample. These improvements are insensitive to changes in cell pressure and are evidently more accurate in measuring load than external transducers.

The axial strain or deformation measurements were measured externally just as axial force. This was performed by measuring the relative movement between the loading ram and a remote area of the triaxial cell (Heymann, 2000). Many inaccuracies followed such as seating errors due to gaps between components, non-uniform sample strains and errors from the apparatus; loading ram and load cell. These errors may be rectified by using a new method of measuring strain directly on the sample, namely local strain measurement.

2.6.2. Triaxial sample setup

The preparation of soils for a triaxial test depends on the experiment being performed in the dry state or saturated state to measure the pore pressure response and volume change. In this study both experiments will take place. For dry test conditions the sample need to be placed into the triaxial cell by a funnel and then tamped. The consolidated undrained triaxial tests followed the ASTM D4767-11 triaxial testing standards, which was able to provide useful data in determining the strength of the samples as well as the deformation. Specific testing standards regarding the inclusion of geosynthetics was not found.

Completely saturation of the soil sample from an initial dry state is very complicated. Conventional methods include using a soluble gas to displace the air prior to passing water through the sample however effective stress can be difficult to control when undertaking this approach (Harikumar et al., 2014). Another approach is filling the membrane with de-aired water and depositing the soil sample via a funnel into the rubber membrane and sealing it tightly. In this case the soil sample can result in segregation of particles. All conventional methods of preparing saturated samples for a triaxial test involve tamping, air pulviation and water pulviation (Harikumar et al., 2014).

The degree of saturation is defined by:

$$S = \frac{V_w}{V_v} \quad \text{Eq. 16}$$

Where *S*= 0 for dry soil mass and *S*= 1 for fully saturated soil sample.

The water content that is required for complete saturation of a given mass of dry soil/sand with a certain void ratio and specific gravity can be calculated as (Harikumar et al., 2014):

$$w = \frac{eS}{G} \quad \text{Eq. 17}$$

Where *w* is the water content; *e* is the void ratio, *S* the degree of saturation and *G* the specific gravity. Therefore, the theoretical weight of the saturated sample is:

$$w_1 = \left(1 + \frac{w}{100}\right) \quad \text{Eq. 18}$$

Where w_1 is the dry weight of the sample.

Generally, triaxial tests are conducted on undisturbed samples however remolded samples can be tested under relevant standards.

The sample preparation has a ratio of 2:1 regarding height and diameter, respectively. The samples need to be level and flat at both sides and can be obtained by trimming the ends of the samples. Measurements of the samples bulk density need to be obtained to calculate the volume and area of the sample. If it important to ensure that the measurements of the sample are accurate so the stress and strain being applied to the sample can be calculated accordingly. When setting up a triaxial test sample it is important to undertake certain checks such as to ensure the membrane does not have any holes; the porous discs are clean, and no loose materials are present due to these causing leaks in the sample.

When preparing the triaxial sample it is important to minimize disturbance of the sample due to it affecting the final results.

This study will be conducting a compacted sample investigation. The sample can be compacted in one of two ways, by compacting the soil into a mould at a specific moisture content by applying a specific compactive effort or by compacting the soil into a mould at a specific moisture content to achieve a particular dry density.

When preparing and mounting the triaxial test sample the following steps should be followed:

Assemble a spilt mould on to the triaxial cell base with a latex rubber membrane fitted within and around the base pedestal

Place the soil in the split mould in layers and compact or tamp each layer with a tamping rod

Use a controlled effort to achieve the specific sample density

Do not disturb or puncture the membrane

Remove the split mould carefully when assembling the triaxial cell.

Place the soaked rubber membrane around the sample, using a membrane stretcher.

Seal the membrane to the base pedestal using two rubber O rings.

Remove all air pockets from the membrane and sample.

No addition of water should be added to the membrane or sample.

Place the two O rings around the drainage lead which is connected to the top loading caps.

Ensure the back-pressure valve is open to moisten the top cap.

Fit the cap on to the porous disc without entrapping any air.

Using the spilt ring stretcher, seal the membrane on to the top cap with the O rings.

Ensure that the drainage line from the top cap will not interfere with the fit of the cell body.

Ensure the sample has a vertical axis alignment.

Install the cell body using the loading piston without touching the top cap.

Ensure alignment of the sample by sliding the piston slowly until it makes contact with the bearing surface on the top cap. Once contact is made retract the piston.

Fill the triaxial cell with de aerated water quickly without creating turbulence.

Close the bleed plug only once the sample is ready to be pressurized.

Apply the first cell pressure as soon as possible, as required by the saturation process.

The triaxial tests being investigated in this study are effective stress triaxial since the tests conducted are consolidated undrained and consolidated drained. These tests require the sample to be saturated for testing thereby providing pore pressure measurements by removal of air from the voids within the sample. This can be achieved by increasing the pore pressure in the sample which can be increased by either increasing the cell pressure only or by applying water pressure to the sample and simultaneously increasing the cell pressure which produces a positive effective stress.

When saturating a sample, it is vital to consider the applied effective stress, which should not over consolidate the sample, and the effective stress, which should not fall below the requirements needed to prevent swelling of the soils.

The basic requirements when saturating a sample for a triaxial test is stated as follows:

The water should always be de aerated when applied to the sample.

The cell pressure magnitude should not exceed 50kPa or the effective stress which is used for the consolidation of the sample.

The cell pressure and back pressure difference should not be more than 20kPa or the desired effective stress pressure nor shall it be less than 5kPa.

When saturating a sample under constant moisture conditions, such as the case in this investigation, the following guidelines should be adhered to:

Water should not enter or leave the sample whilst this experiment is ongoing.

Saturation is achieved by increasing the cell pressure only by a nominal level of 50kPa or 100kPa.

Allow the pore pressure to reach equilibrium.

Apply equal increments of cell pressure and record the pore pressure values accordingly.

Calculate the *B* value by $B = \frac{\delta u}{50}$ where δu is the pore pressure in kPa.

The sample is considered saturated when the pore pressure remains stable after 12 hours or overnight as well as the *B* value is equal to or greater than 0.95.

Once the above is achieved the sample is ready for consolidation to the allocated effective stress.

Once the saturation process is complete the consolidation stage follows immediately. The main objective of the consolidation stage is to bring the sample to the state of effective stress required for undertaking the compression test. A suitable strain rate which is to be applied during compression, is obtained from the consolidation stage. The effective stress in the sample should be increased to the appointed value by increasing the cell pressure and dissipating the pore pressure to an appropriate back pressure. In the final saturation stage, the back pressure should not be lower than the level of pore pressure or 300kPa.

The following steps should be followed when carrying out a consolidation procedure:

A record of the final pore pressure and volume change indicator readings should be taken prior to commencing the consolidation process.

The back-pressure valve should remain closed during this stage.

Increase the cell pressure line to give a difference equal to the required effective consolidation pressure (σ_3') such that: $\sigma_3' = \sigma_3 - U_b$

Once a steady pore pressure (U_i) value is obtained, record this value.

Record the change in the volume at the volume-change indicator.

At zero time commence the consolidation stage by opening the back valve/s.

Record the volume-change indicator values at incremental intervals.

2.6.3. Triaxial testing of reinforced soils

Many studies and investigations have been undertaken with the aid of triaxial tests in determining the shear strength and stress-strain behaviour of sediment along with analysing the effects of geosynthetic reinforcement. These experiments investigated the effect of reinforcing parameters on a variety of soils by using triaxial equipment.

Latha and Murthy, 2006, was one of the first papers encountered to investigate the mechanical behaviour of geosynthetic reinforced soil, using three different types of reinforcement, namely geogrid, geotextile and polyester film. This investigation also used different horizontal layer arrangements of two, three, four and eight to study the effect of reinforcement quantity and tensile strength of the geosynthetic reinforcement used. A total of 36 undrained triaxial tests were conducted to understand the mechanical properties of reinforced sand with different types of geosynthetic reinforcement in different layered configurations. Three different confining pressures of 100kPa, 150kPa and 200kPa were used with the shear strength of the natural sand samples being 70% relative density. The outcome of these tests indicates a gradual increase in cohesive strength with an increase in the number of layering of reinforcement, regardless of the type, with little to no effect on the internal friction angle. It was noted that the improvement of strength in the sands depend upon the properties of the reinforcements used for the same quantity of reinforcement of any type, with polyester film providing the most strength improvement in the sand with geotextile and geogrid following respectively, at all confining pressures and for all the layer configurations. This indicates the use of geosynthetic reinforcement improves the stress-strain response in triaxial tests, in comparison to unreinforced test results for all confining pressures and layer arrangements. Geogrid was found to be inferior due to the inferior load-elongation properties, in all layer configurations whereas polyester film proved highly efficient with regards to strengthening the sand however tensile strength was lower that of geotextile. This was due to indentations on the surface of the film made by sand particles.

The shear strength of a sandy soil was interpreted by incorporating geotextile reinforcement by Denine et al., 2016. A series of undrained triaxial tests were performed on sandy soils with and without geotextile reinforcement to study the confining stress effect on the mechanical behaviour of the reinforced soil. The triaxial tests used different number of reinforcement as well as different arrangements of layers at different heights such as one or two layers. The confining pressures were also consolidated to three levels, as Latha and Murthy (2006), at 50kPa, 100kPa and 150kPa and a relative density of 30%. The sand used in the experiments were poorly graded Chlef sand of alluvial nature with a specific density of 2.70g/cm^3 and a 5.5% silt plasticity index. The geotextile showed a maximum tensile strength between 12 to 14kN/m. The results showed a significant increase in deviator stress for reinforced tests, particularly under low confining pressures in comparison to unreinforced test results. However, the effectiveness of the reinforcement decreased with increasing confining pressures in tests with the same reinforcement arrangement, such as in two-layer configuration at 50kPa the deviator stress increases by 97% whereas at 100kPa it increases by 82%. Regarding the strength properties, the incorporation of geotextiles reduces the contractive behaviour of samples at low stress. The higher the confining pressure the more enlarged the contractancy of the reinforced sand, in particular two-layer arrangements. The cohesion results tend to show correlative tendencies with an increase in the number of geotextile layers, which was also found in Latha and Murthy, 2006. The angle of friction, on the other hand, tends to decrease with an increase in the number of geotextile layers. Both the cohesion and the friction angle trends can be based on the interlocking of soils particles due to the reinforcement. This reduces the number of contact points between the layers of soil particles. It was noticed in reinforced specimens, an increase in the confinement of the specimen which led to an increase

in deformation of the specimens, with reinforced specimens displaying a bulging deformation up the layers of geotextile reinforcement without shear band rupture. That being found, this study concludes that the presence of geotextile reinforcement does improve the behaviour of the sand by increasing the shear resistance with an increase in the layers of reinforcement.
Goodarzi and Shahnazari, 2019, studied the effects of geotextile reinforced carbonate sand by performing a series of drained compressional triaxial tests with a range of geotextile arrangements, layers, and types as well as unreinforced. The study emphasised on the effect of geotextile layers and arrangement being important due to the overall costs of projects being affected by the increase in vertical distancing of reinforcing agents. Two particle size distributions and three types of geotextiles were used in this study. Four different arrangements of geotextiles were observed in this study with one, two and four layers of reinforcement. Two tests, using two reinforcing layers differed in arrangement by one maintaining equal distance in layers whereas the other distributed the layers to either side of the triaxial cell. The outcome of this resulted in the strength parameters being stronger in the equally distanced layers due to the maximum radial strain being distributed to the middle of the specimen in triaxial tests. Thereby indicating the importance of arrangement as well as layers of reinforcement. The overall results of the tests states that geotextile reinforcement reduces the post peak strength loss of carbonate sediments as well as increases the peak strength and axial strain at failure. It was also deduced that the increase in geotextile layers, increased the strength parameters of the specimens. Both reinforced and unreinforced carbonate specimens displayed a more contractive behaviour and dilated at higher axial strains than siliceous specimens. Visible deformation of specimens could be seen by bulging between adjacent layers which implies the lateral expansion limitations of the specimens. It was observed that the strength ratio displays a correlative relationship with the relative density of reinforced specimens, if the geotextile does not break, as observed in type 3 geotextile where the strength ratio increased by increasing the relative density from 70% to 94% (Goodarzi and Shahnarzi, 2019).

Geogrids is observed to positively contribute to geotechnical construction, when taking the shear strength into consideration, as stated in Skuodis et al., 2020. This study investigated the shear strength of geogrid reinforced sand using triaxial tests. The sand used for these tests were Klaipeda sand of Baltic Sea origin and did not contain clay or silt. A variety of geogrids were used that were commonly found within the area of the investigation, namely Lithuania. The outcome of these tests indicates a high max stress deviator for geogrid reinforced samples due to the failure planes starting from the top of the sample and extended to the middle, where the geogrid was placed. The confining pressures of the samples played a key role in deducing the outcome of utilising geogrid reinforcement such as 100kPa and 200kPa indicate a higher resistance and residual strength when compared to unreinforced samples. However, when undergoing tests at a cell pressure of 300kPa, a similar resistance with unreinforced samples was observed, due to high cell pressures having an influence on stress distribution in samples. Therefore, it was noticed that an increase in confining pressure, reduces the effect of the geogrid reinforcement in the sample thereby displaying low productivity at high confining pressure. Nevertheless, these test samples provided an insight into the shear strength properties of reinforced sand samples which show a positive response when compared to unreinforced samples. The shearing strength increment increased from 1.09 to 1.43 for reinforced samples. Both the angle or internal friction and cohesion varies, depending upon the type of geogrid reinforcement used.

3. Materials and Methodology

3.1. Physiography

The province of KwaZulu Natal is bound by the warm Indian Ocean in the east and land bound by Mpumalanga, Mozambique and Swaziland in the north , the Eastern Cape in the south and Free State and Lesotho in the west with an approximate areal extent of 93000km^2. The main urban city centres include Durban, Richards Bay or Empangeni and Pietermaritzburg with other important urbanized areas being Vryheid, Newcastle, Ladysmith, Dundee, and Ulundi. A high portion of the population of KwaZulu Natal is concentrated in the main city centres like Durban however a significant amount of the populace resides in non-urban settings thus resulting in many poorly developed rural communities across the province. On the other hand, KwaZulu Natal has well developed road networks made up of the N3 and N2 national highways and boasts modern designed high-rise infrastructure. KwaZulu Natal thrives on the agricultural produce, forestry, tourism, and mining such as coal.

KwaZulu Natal exposes the breath-taking Drakensberg Mountains, Lebombo Mountains and Biggarsberg and Balelesberg. KwaZulu Natal can be broadly divided into three geographical regions namely, rolling hills in the central regions, lowland plains along the Indian Ocean and mountainous areas to the west and north (Kruger, 1983 in Singh, 2009). The major rivers in the province include the Tugela, Mfolozi, Mkomaas and Msunduzi which help drain and irrigate the land and the people.

3.2. Climate

The province of KwaZulu Natal experiences all four seasons in a year. During the summer, a subsidence inversion occurs and rises above the escarpment producing an influx of humid air by south easterly winds from the Indian Ocean. KwaZulu Natal often experiences rainfall which occurs due to convective thunderstorms or is orographically induced along the escarpments (Singh, 2009). During these months of rain many floods' events occurs which are caused by cut off low pressure systems. In September 1987, a disastrous flooding event occurred in the province, due to a cut off low which formed in the upper air with strong surface high pressure system (Tennant and Heerden, 1994) (Figure 7). The city of Durban experiences an annual rainfall of 866mm and a maximum annual temperature of 24.1^{o}C and a minimum temperature of 5.5^{o}C for the year 2018 (Table 2.a and b).

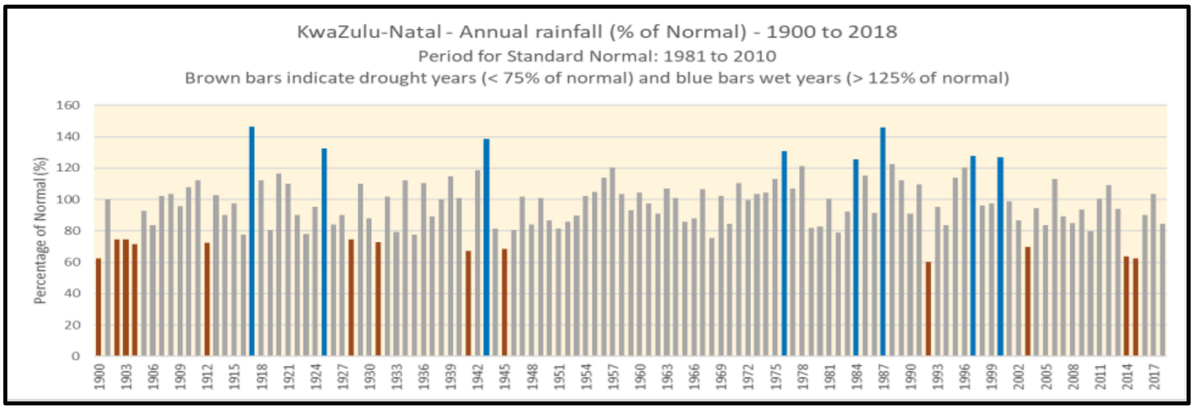

Figure 7: Graph showing the annual rainfall from 1900-2018 for KwaZulu Natal. (South African Weather, 2018).

Table 2.a: Table showing the annual climate summary for 2018 for temperature (SAWS, 2018).

Annual Climate Summary 2018									
Minimum Temperature (°C) overview for some long-term climate stations for 2018									
Station:	Avg (2018)	Normal (1981-2010)	Rank Highest (Since 1981)	Highest Annual Avg (Since 1981)	Lowest Annual Avg (since 1981)	Highest Daily (2018)	Highest Daily (Since 1981)	Lowest Daily (2018)	Lowest Daily (Since 1981)
Ladysmith	9.4	10.7	37	13.6 (1988)	8.6 (2017)	21.9	23.8 (1990-11-14)	-4.2	-5.8
Durban	17.3	16.5	7	17.5 (1985)	16.1 (2013)	24.1	26.1 (1983-01-11)	5.5	2.6

Table 2.b: Table showing the annual climate summary for 2018 for rainfall (SAWS, 2018).

Annual Climate Summary 2018								
Rainfall (mm) overview for some long-term climate stations for 2018								
Station:	Total (2018)	Normal (1981-2010)	Highest Annual Total (Since 1981)	Lowest Annual Total (Since 1981)	Highest Daily Total (1981)	Highest Daily Total (Since 1981)	No. of days with rain >=1mm (2018)	Avg No. of days per year with rain >=1mm
Ladysmith	597	749	1111	300	44	141	70	68
Durban	866	1021	1422	471	52	265	79	87

In April and November 2019 heavy rainfall occurred and caused large scale damage consisting of a collapsed reservoir and flooding (Figure 8.a and b). These rainfalls are also associated with slope failure.

The KwaZulu Natal province is situated between the high escarpment of the Drakensberg in the west and the warm Indian Ocean in the east thus resulting in localised climatic variations. The inland regions of the province experience colder weather than the coastal areas, which are subtropical in climate and experience hot, humid during the summer and in general whereas during winter the weather is generally mild. In the north coast or Zululand region, the climate is the warmest and most humid. The inland areas such as the Midlands and Pietermaritzburg experience cooler climates, especially in winter. Regions such as the Drakensberg and Ladysmith experience very dry cold to very cold climate in winter and at times receiving frost and snow at high elevations.

The general airflow over the area is controlled by the South Indian anticyclone which strongly influences the weather patterns of the province. During the winter months also known by the locals as the dry season, a subsidence of air occurs which bring about atmospheric stability.

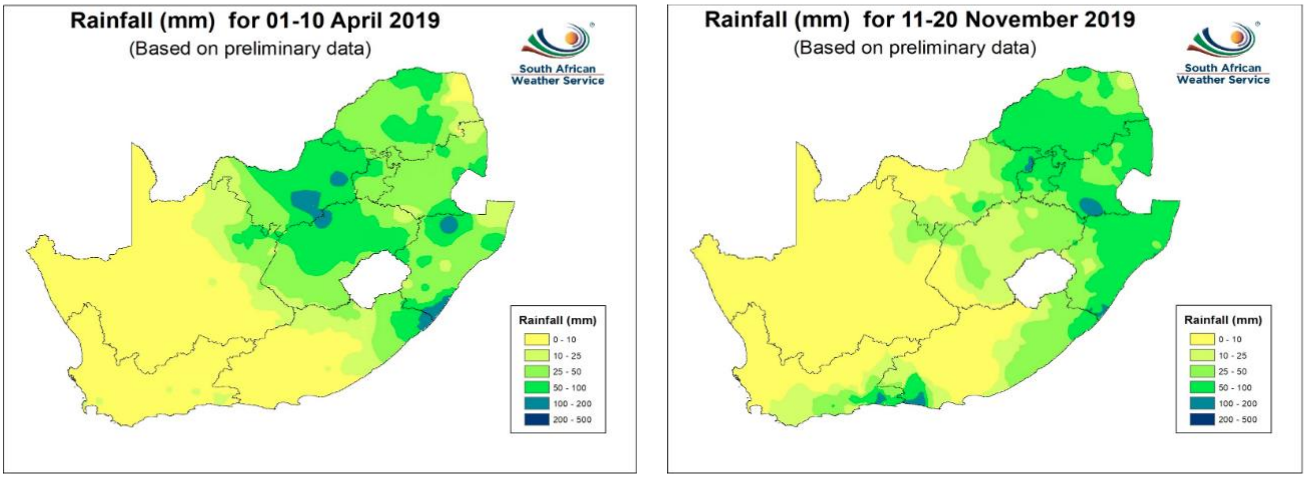

Figure 8.a: Map of South Africa showing rainfall in April 2019, 12.b: Map of South Africa showing rainfall in November 2019.

3.3. <u>Regional Geology</u>

The geological evolution of KwaZulu Natal extends approximately 3500 million years ago (Figure 9). The foundation of KwaZulu Natal can be subdivided into two distinct geological units, namely the Kaapvaal Craton (~3000 Ma) and the Natal Metamorphic Province. The Kaapvaal Craton is among the very few remaining pristine crusts on the Earth and predominantly comprises granitoids with subordinate gneisses. The Natal Metamorphic Province (NMP) was formed ~1000 million years ago through the subduction and collision along the southern margin of the Kaapvaal Craton.

The Karoo Supergroup extends over most of southern Gondwana and holds ~120Ma of geological history. This supergroup preserves a large variety of depositional paleoenvironments from glacial to deep marine, aeolian to fluvial.

The Gondwana breakup begun with outpourings of lava ~180Ma which formed the Drakensberg and Lebombo Groups. A second phase of volcanic eruption occurred spewing rhyolites and volcanic ash. Due to uplifting and faulting after the volcanism period, the separation of Africa and Antarctica commenced. Sea levels began to drop from high levels in the Cretaceous during the Cenozoic. This promoted the formation of large dune complexes situated parallel across the coastline. These sediments now make up the Berea and Bluff Ridges. The weathering of old dunes formed a dark red coloured sand which is known as Berea Red Sand. Berea Formation is found along most of the eastern coastline of KwaZulu Natal spanning as far up to Mozambique. Berea Red sand can be located along the coastline as well as inland (Clayton, 1989). The age of this formation can be placed as increasing away from the coast and can be dependent on the colouring and pedogenesis. Berea Red sand is dispersed as a narrow belt but can be sporadically encountered along the Transkei coast and East London (Clayton, 1989). The Berea Dune consists of fine-grained sand due to being blown inland from the shoreline, was formed over thousands of years, and resulted in the Berea Ridge.

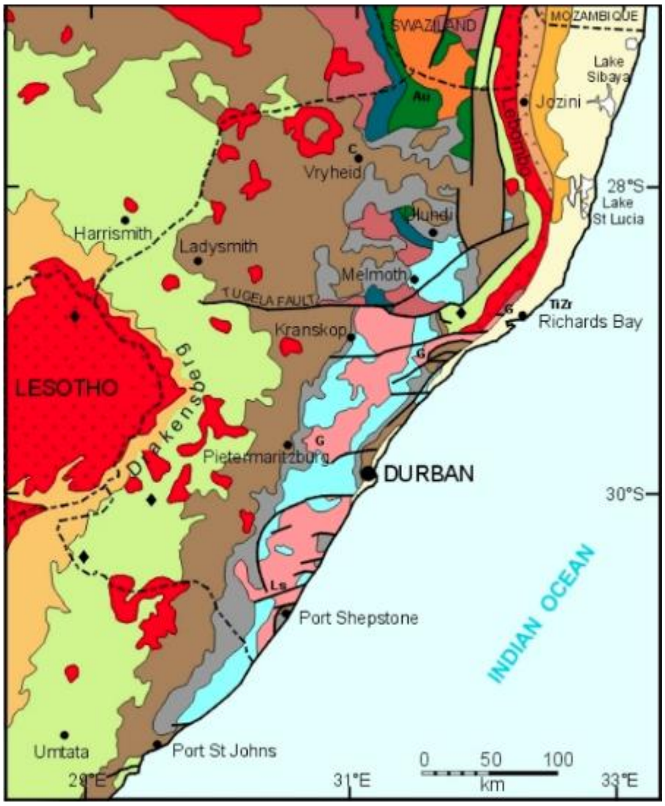

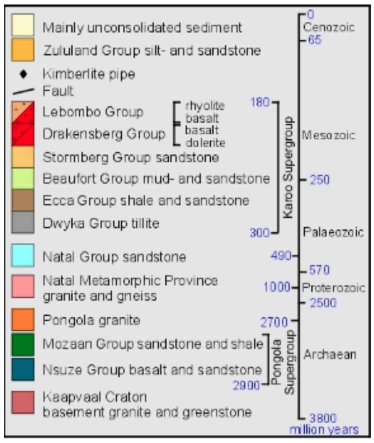

Figure 9: Geological Map and key of KwaZulu Natal.

(Geological Survey, 1984)

3.4. Soil Materials

Berea Red sand utilized in this study was obtained from the eastern coastline of KwaZulu Natal, in the newly developed area of Sibaya within the Sibaya Signature estate construction site, located on the outskirts of the coastal town of Umhlanga, north of Durban (Figure 10). It should be noted that the sand sampled was not cemented. According to the geological map of South Africa, the insitu and foundation material of the site is consolidated Berea Red sand, situated among quaternary age. Berea Red sand which is the basis of this study is derived from aeolian deposition of coastal sediment and spans to Cenozoic in age. These sediments form part of the Phanerozoic cover succession of the eastern portion of South Africa.

Figure 10: The sample area (red triangle) on the outskirts of Umhlanga, KwaZulu Natal (Google image)

The site houses new upscale modern developments used for residential purposes, which indicate the compressibility of the soil (Figure 11).

Figure 11: Local site undergoing residential construction.

Sampling was carried out on a platform using a shovel and spade, within the estate which is currently undergoing development for a residential building (Figure 12). A profile of the Berea Red sand sampled displays very slight variations among horizons, mainly in colour.(Figure 13). Two distinct horizons were profiled with the descriptions reading from 0-1.2m as medium dense, dark brown to orangey red slightly silty SAND, 1.2-3m as medium dense, dark orange red slightly clayey silty SAND. Berea Red sand was sampled from the second horizon (1.2-3m) for this study.

Figure 12: Site location platform, Sibaya, KwaZulu Natal.

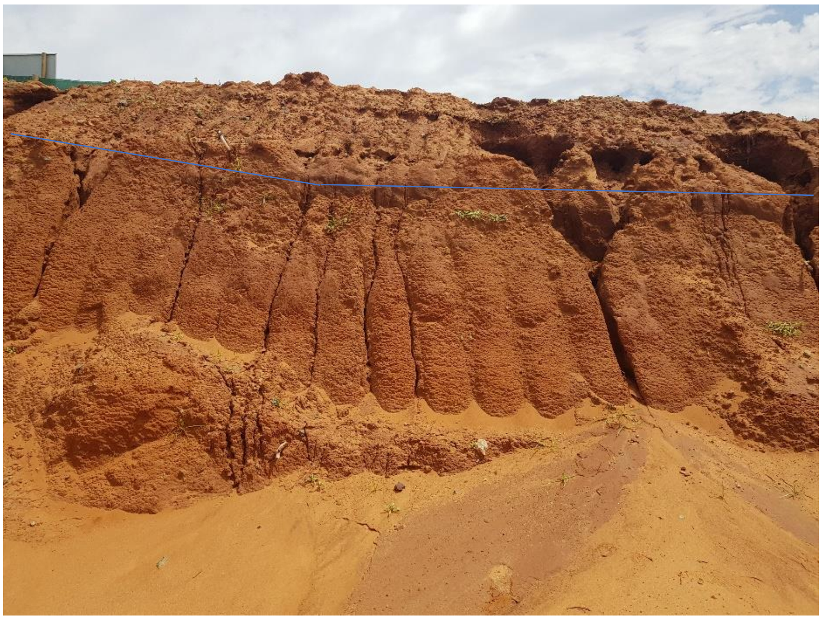

Figure 13: Berea Red soil profile depicting two horizons.

The Berea Red sand was subjected to laboratory investigation having undergone Atterberg Limits, Mod AASHTO tests and California Bearing Ratio (CBR) tests, tabulated in Table 3 below. The Berea Red sand used for this study is categorised as a fine sand and with a low clay content of 6.4%, indicative of a low potential expansiveness index shown in Graph 1 below. The cohesion results from the triaxial test for unreinforced Berea Red sand was 15kPa, considering the low clay content in the sand. The AASHTO soil classification was defined as A-3 (0) with a grading modulus of 0.94. The Berea Red sand sampled resulted in a unified classification of SP-SM which validates the high sand content. A comparative analysis between the sampled index test results and published Berea Red sand index values from Clayton, 1989, show a similar reading regarding the liquid limit which is 19.6 and 20 respectively (Table 4). Published results between Clayton, 1989, and Okonto and Manciya, 2006, show similarities between the plasticity index and the same results for linear shrinkage at 2%. Tests such as cone penetration and bulk density tests on the site materials were not obtained due to budgetary constraints. These test results were requested from the developers but were not provided.

Graph 1: Showing the grading curve of the Berea Red sand sample

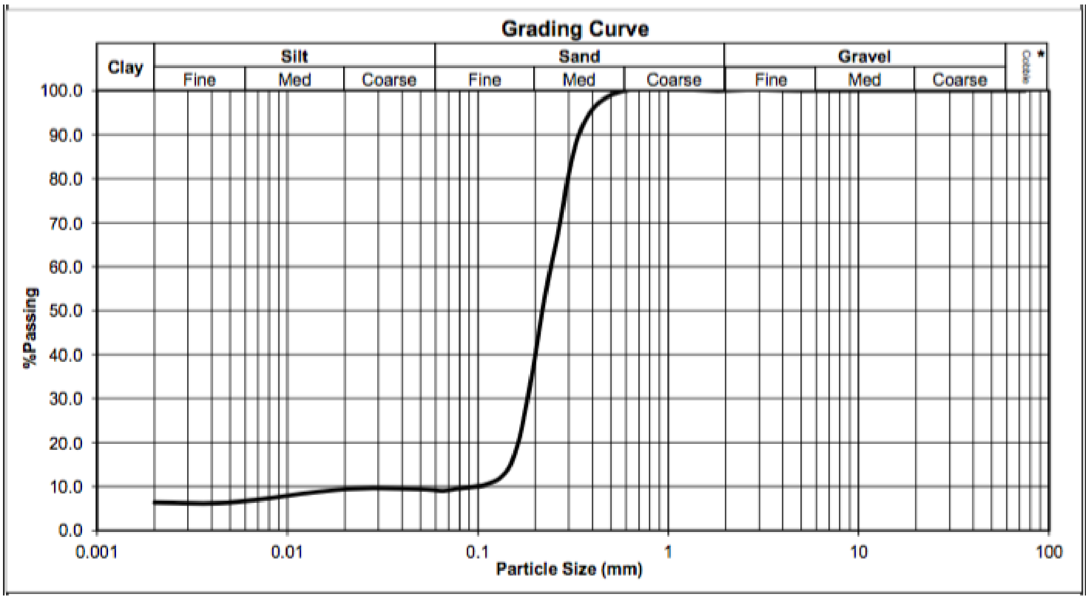

Table 3: Laboratory results of Berea Red Sand samples

CBR	100%	11
	98%	7.7
	95%	4.4
	93% (Inferred)	4
	90%	3.7
	CBR Swell	0.00
Grading Modulus	TRH 14 (1985)	G10
Mod AASHTO Density	Density Kg/m^3	1739
	OMC	11.7
Atterberg Limits	Liquid Limit	19.6
Classification	Potential Expansiveness	Low
	Group Index	0
	AASHTO Soil Classification	A-3
	Unified Classification	SP-SM

Table 4: Index properties of the site samples vs published index values of Berea Red sands

	Site Index Values	Clayton (1898) Index Values	Okonto & Manciya (2006) Index Values
LL	19.6	20	-
PI	0	7	6-8
LS	0	2	2

Laboratory analysis observed only 6.4% clay within the Berea Red sand samples and a Mod AASHTO density of 1739kg/m^3. According to Clayton, 1989, Berea Red sands can be distinguished based upon clay content, either being less than 5% or more than 30%. Berea Red sands with a clay content less than 5% were classified to obtain in situ bulk density between 1600-1750kg/m^3 whereas Berea Red sands with a clay content more than 30% were classified to have a range of 1550-1700kg/m^3. Based on Clayton's, 1989, analysis and due to the Berea Red sand samples investigated for this study being 6.4% clay, a dry density of 1652kg/m^3 was used for all the triaxial tests.

3.5. <u>Geosynthetic Material</u>

For the purpose of this dissertation, a parametric study was undertaken with two reinforcing materials, posing as geogrids, namely diamond mesh and mosquito net. Two different materials were used to correlate the results accordingly. The material had undergone laboratory analysis which resulted in the following:

Table 5: Properties of Diamond and Mosquito mesh reinforcements

Specimen	Peak Load (kN)	Strain at Peak	Peak (kN/m)	Width (mm)
Diamond Mesh	0.240	116.010	1.199	200
Mosquito Mesh	0.136	34.756	0.678	200

Graph 2: Showing the load versus extension on the Diamond Mesh reinforcement.

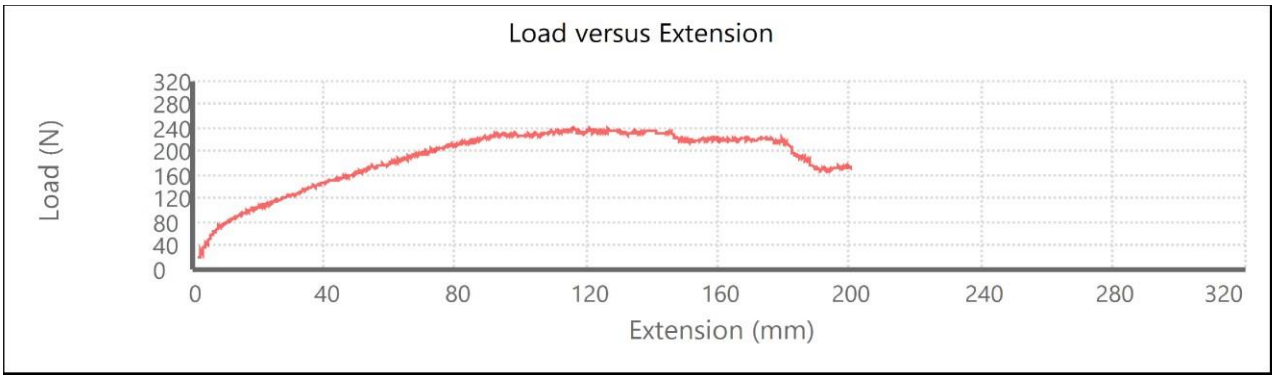

Graph 3: Showing the load versus extension on the Mosquito Net reinforcement.

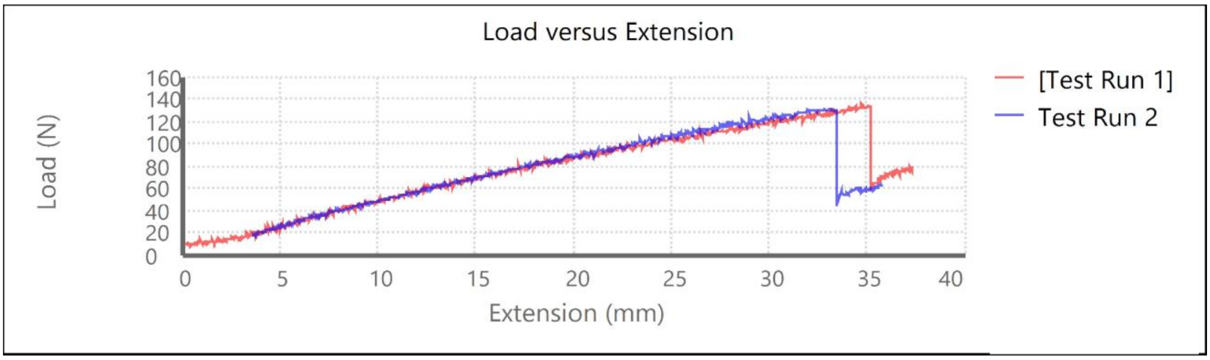

For the purpose of this research, two different reinforcing specimens were tested namely, diamond mesh (Figure 14) and mosquito net (Figure 15) of plastic and fabric origin respectively. The reason for choosing two different geosynthetic material was to assess the strength parameter based on the different material makeup of the products, being of a plastic and fabric nature. The plastic-based material or diamond mesh is more rigid than the fabric based or mosquito net geosynthetic thereby indicating a difference in strength parameter. Tensile strength testing was performed on the reinforcements and are tabulated in Table 5 above. These products were chosen based on their different strength or stability parameters to provide a comparative analysis, which is based on the number of reinforcing layers as well. The strength parameters of the reinforcements are taken into consideration due to the study being focused on the bearing capacity of Berea Red sands with and without the influence of reinforcing parameters.

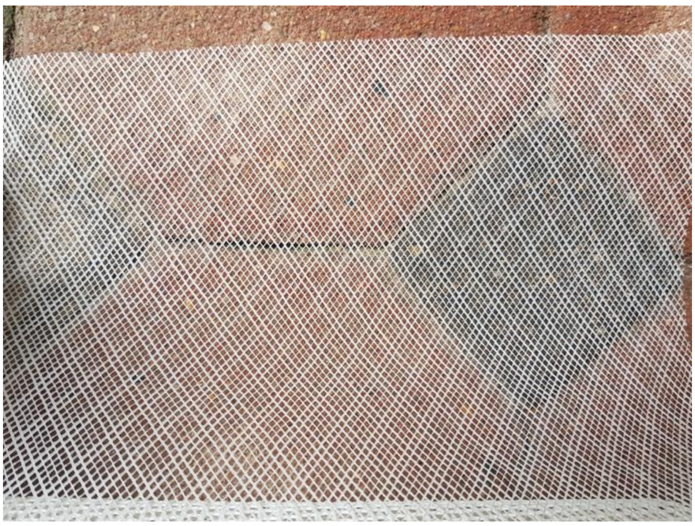

Figure 14: Image showing the Diamond Mesh (plastic) reinforcement

Figure 15: Image showing the Mosquito Net (fabric) reinforcement

3.6. Methodology

The objective of this experiment is to study the bearing capacity of soft cohesive Berea Red sands with and without reinforcement by obtaining the effective stress cohesion intercept (c’) and the effective stress friction angle (ϕ’). To study this behaviour, triaxial strength tests were conducted. Five consolidated undrained triaxial tests were performed, with two variable parameters namely the type of reinforcement and the number of layers of reinforcement.

The preparation of the soil samples is of high importance for laboratory research. The soil was prepared using the tamping method whereby the soil is placed into the rubber membrane and tamped in five equal layers. During each triaxial test the Berea Red sand was remolded and compacted to obtain a density of 1652kg/m^3. In order to fabricate reinforced sample, many layers were needed. The samples were isotropically consolidated to obtain the value of effective confining stress prior to loading. The effective pressures used were 100kPa, 200kPa and 300kPa with a rate of shear no quicker than 1% strain per hour.

This experiment consisted of five different consolidated undrained triaxial tests in order to verify and compare results. The consolidated undrained tests were conducted with and without geosynthetic reinforcements and with a variable number of layers when reinforced such as 2 and 4 layers in order to study the confining stress on the mechanical behaviour of the reinforced Berea Red sand (Figure 16). This was decided based on having a comparative data analysis of the variable tests conducted.

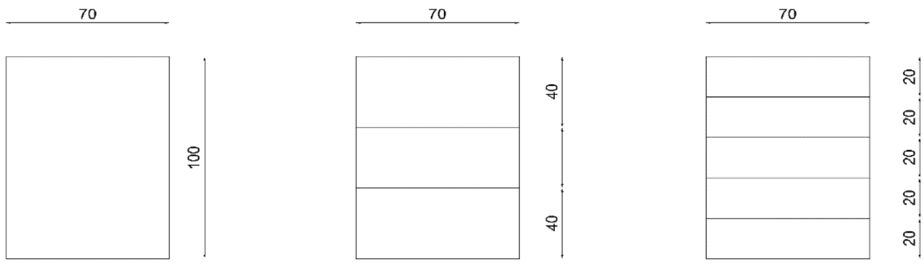

Figure 16: Schematic drawing showing the different heights and arrangements of reinforcement.

3.1.6. Test 1: Unreinforced

This experiment was performed to interpret the effect of the axle load pressure over time on Berea Red sand without reinforcement. The Berea Red sand was remolded and modelled into the triaxial cell by the tamping method and consisted of 5 relatively equal compacted layers of a thickness of 20mm as the height of the specimen is 100mm (Figure 16). This played a vital part in obtaining the desired density of the sand. The effective pressure used on this experiment was 100kPa, 200kPa and 300kPa respectively with the rate of shear not being greater than 1% per hour. The dry density was kept constant at 1652kg/m^3. The unreinforced sample provided a base comparison on the effect of reinforcing material on the behaviour of Berea Red sand.

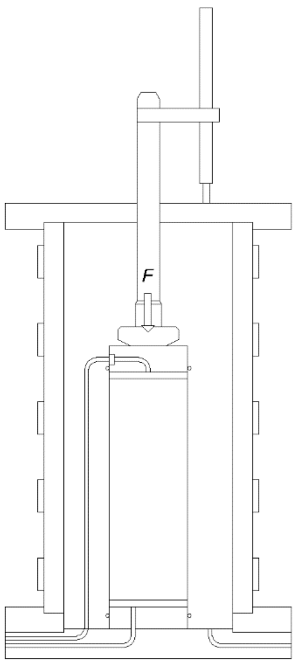

Figure 17: Schematic drawing showing unreinforced triaxial test sample.

Figure 18: Test set up of the unreinforced sample.

3.6.2. Test 2: 2-layer Diamond mesh reinforcement

This experiment was performed to study the bearing capacity and shearing behaviour of Berea Red sand with two layers of geosynthetic reinforcement. Two layers of the same geosynthetic namely diamond mesh, was used placed approximately 40mm from the top of the specimen and 40mm from the bottom of the specimen (Figure 19). The specimen was constructed in the same procedure as Test 1. The Berea Red sand was remolded and compacted into layers with the geosynthetics being placed after the second and third layers were tamped. The effective pressure used on this experiment was 100kPa, 200kPa and 300kPa respectively with the rate of shear not being greater than 1% per hour.

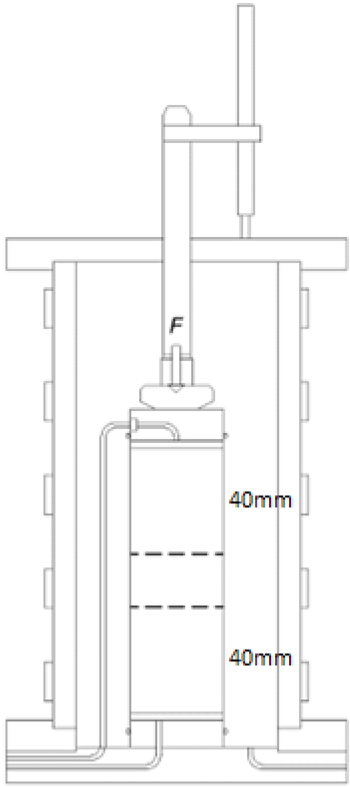

Figure 19: Schematic drawing showing 2-layer reinforced triaxial test.

3.6.3. Test 3: 4-layer Diamond mesh reinforcement

This experiment was performed to obtain a comparative study of the use of reinforcement material based on the number of layers used as well as the positioning of the layers of reinforcement. This experiment provided a basis for investigating the bearing strength of Berea Red sand. The specimen was constructed the same way as Test 1 and 2. The Berea Red sand was remolded and compacted into layers with the reinforcements placed after each sand layer was tamped therefore comprising of four layers, 20mm apart (Figure 20 to 22). It was thought that the addition of reinforcement would increase the bearing strength of the sand material and provide an increase in shear strength. The effective pressure used on this experiment was 100kPa, 200kPa and 300kPa respectively with the rate of shear not being greater than 1% per hour.

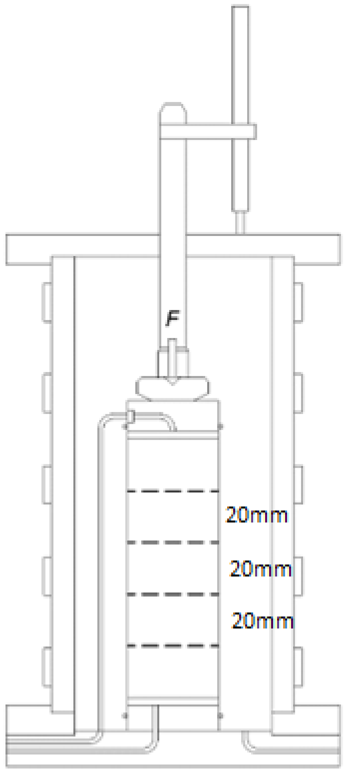

Figure 20: Schematic drawing showing a 4-layer reinforced triaxial test.

Figure 21: Triaxial test set up showing the Diamond mesh geosynthetic reinforcement.

Figure 22: The 4-layer Diamond mesh reinforced triaxial test set up.

Tests 4 and 5 are a duplication of Test 2 and 3 respectively, however with the reinforcing agent being the Mosquito net.

4. Analysis and Discussion of Results

A series of five consolidated undrained triaxial tests were conducted to investigate and evaluate the effects of the placement and quantity of reinforcing parameters on the bearing capacity within Berea Red sands. Additionally, it provides a baseline series of tests to which future tests incorporating geosynthetic reinforcement could be compared to and contrasted with.

The triaxial tests conducted used a model of inter layered geosynthetic reinforcements designed to exhibit the bearing strength and shear strength properties of the Berea Red sands.

4.1. Test 1: Unreinforced

The first triaxial test was conducted with no reinforcing agents, as seen in Figure 17 above. The axial strain results were observed to decrease with an increase in normal stress over the duration of the test with the axial strain being 11.4%, 10.2% and 7.9% over a normal stress of 100kPa, 200kPa and 300kPa respectively thereby indicating an indirectly proportional relationship and effectively displaying that strain reduces with an increase in load. The shear strength parameter namely, angle of internal friction and cohesion were found to be 29° and 15kPa, respectively. The results are indicative of the expectant behaviour of sands when under a load.

Graphs 4 and 5 show the results of consolidated undrained tests of loose Berea Red sand samples under confining pressures of 100kPa, 200kPa and 300kPa displaying deviatoric stress and pore water pressure curves, respectively. From the graphs, the unreinforced samples subjected to low confining pressure levels (100kPa) displays behaviour of limited liquefaction, whereby a limited strain is showed to soften at the start of the test. The deviator stress is observed to be rapid at the start of the test until the axial strain reached more than 10%, by which is became low. It was observed however, increasing the confining pressure increases the deviator stress of the unreinforced Berea Red sand sample which shows a steady increase trend to a relatively constant level after 6% axial strain. Graph 5 shows pore water pressure is found to develop consistently thereby indicating a contracting behaviour in the soil. It is noted the peak pore pressure is more prominent for the 300kPa confining pressure, with a progressively increasing trend to a relatively constant level as compared to samples consolidated to low effective stresses (100kPa and 200kPa), which continue to increase.

Graph 4: Test 1- Unreinforced triaxial test showing deviator stress versus axial strain

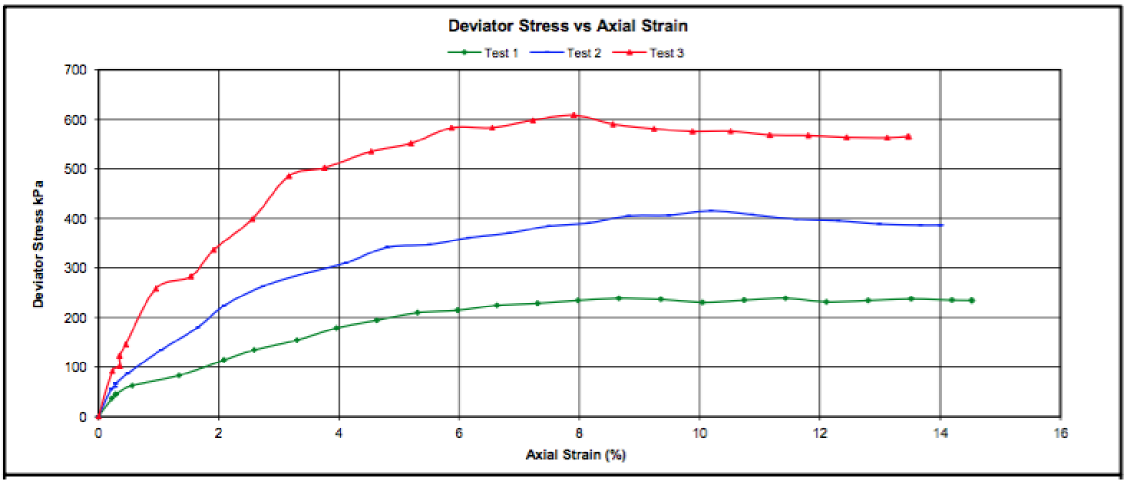

Graph 5: Test 1- Unreinforced triaxial test showing porewater pressure versus axial strain

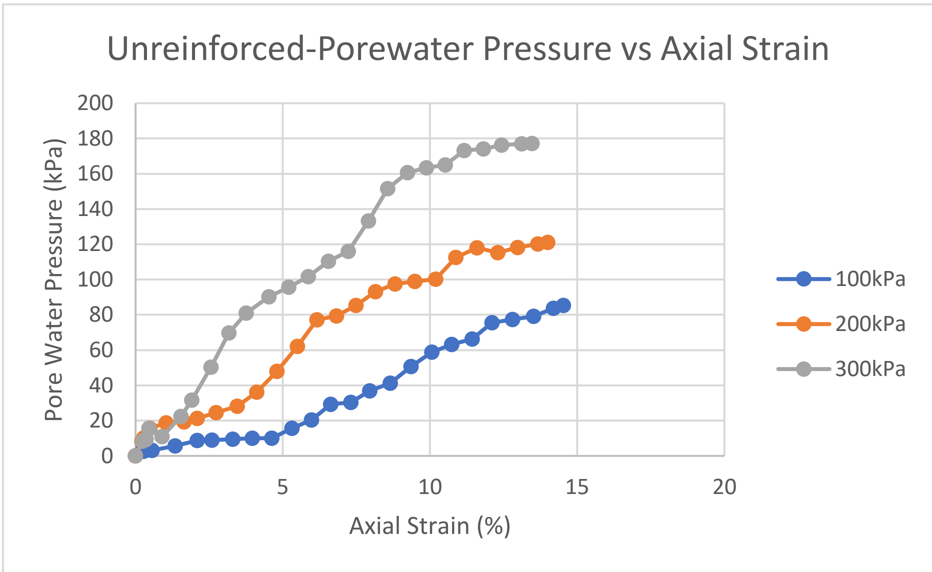

4.2. Test 2: 2- Layer Reinforced Diamond Mesh

The second triaxial test was conducted using a material ‘diamond mesh’ reinforcement, arranged in two layers, as seen in Figure 19 above. The axial strain results show an irrational trend of 11.4%, 7.5% and 13.5% at a normal stress of 100kPa, 200kPa and 300kPa, respectively. The shear strength parameters namely, angle of internal friction and cohesion were found to be 34° and 13kPa, respectively.

From the above results a 34% decrease in strain from 100kPa to 200kPa indicates that deformation has occurred as well as prevents the soil from consolidating normally whereas the sudden and significant increase in strain from 200kPa to 300kPa possibly indicates a failure of the reinforcement thereby resulting in a larger increase in deformation. It was observed however, increasing the confining pressure increases the deviator stress of the unreinforced Berea Red sand sample.

Graph 6: Test 2- 2 Layer diamond mesh reinforced triaxial test showing deviator stress versus axial strain

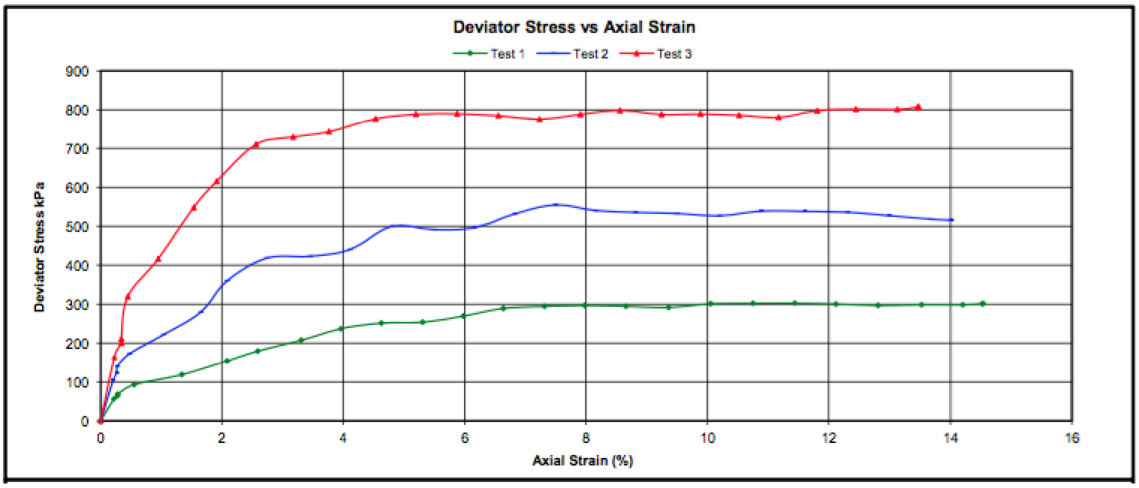

4.3. Test 3: 4- Layer Reinforced Diamond Mesh

The third triaxial test was conducted using a material ‘diamond mesh’ reinforcement, arranged in four layers, as seen in Figure 20 above. The axial strain results show an irrational trend of 10.1%, 8.8% and 12.4% at a normal stress of 100kPa, 200kPa and 300kPa respectively, which mimics the trend of the Test 2. The shear strength parameters namely, angle of internal friction and cohesion were found to be 35° and 11kPa, respectively. From the results above a 13% decrease in strain from 100 kPa to 200kPa indicates that deformation has occurred as well as prevents the soil from consolidating normally whereas the sudden and significant increase in strain from 200kPa to 300kPa possibly indicates a failure of the reinforcement thereby resulting in a larger increase in deformation as suggested for Test 2. The response of Berea Red sand shows a positive correlation between the confining pressure and deviator stress.

Graph 7: Test 3- 4 Layer diamond mesh reinforced triaxial test showing deviator stress versus axial strain

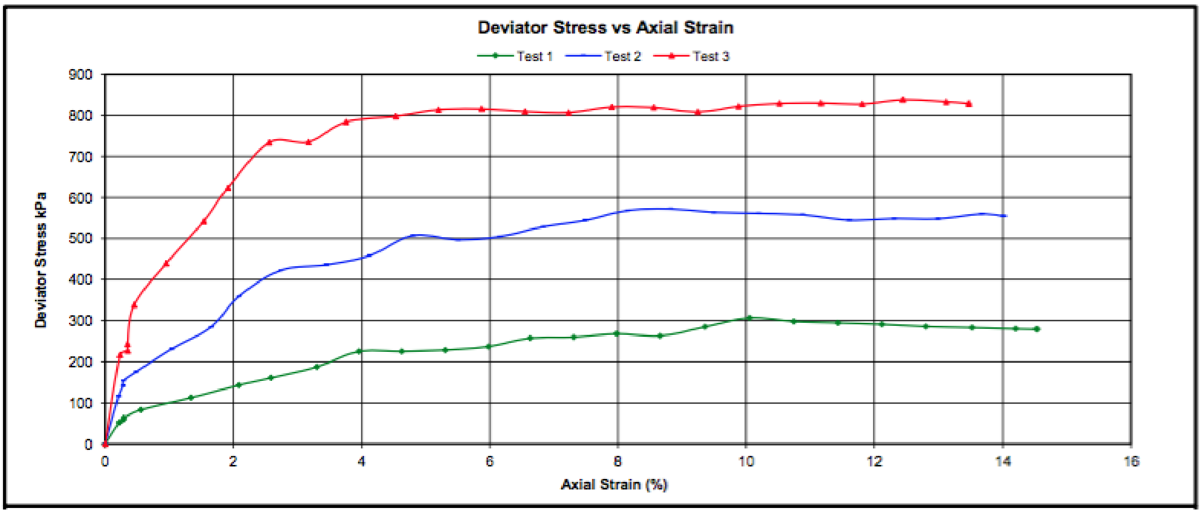

4.4. Test 4: 2- Layer Reinforced Mosquito Net

The fourth triaxial test was conducted using a material 'mosquito net' reinforcement, arranged in two layers, as seen in Figure 19 above. The axial strain results were observed to decrease with an increase in normal stress over the duration of the test with the axial strain being 13.5%, 13.7% and 7.2% over a normal stress of 100kPa, 200kPa and 300kPa respectively thereby indicating an indirectly proportional relationship and effectively displaying that strain reduces with an increase in load. The 0.2% decimal change in axial strain at 100kPa to 200kPa can be disregarded and kept as constant. A correlation can be seen with Test 1. The shear strength parameters namely, angle of internal friction and cohesion were found to be 31° and 13kPa, respectively.

The response of Berea Red sand mirrors that of the previous test which show an increase in deviator stress with an increase in confining pressure which increases steadily to a relatively constant plateau after 4% axial strain.

Graph 8: Test 4- 2 Layer mosquito net reinforced triaxial test showing deviator stress versus axial strain

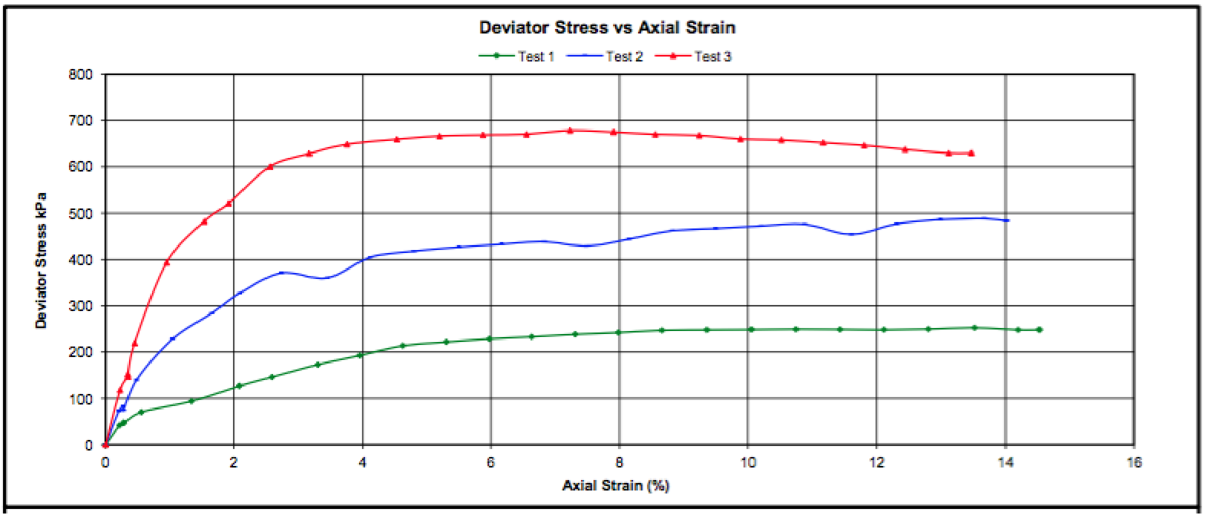

4.5. Test 5: 4- Layer Reinforced Mosquito Net

The fifth and final triaxial test was conducted using a material 'mosquito net' reinforcement, arranged in four layers, as seen in Figure 20 above. The axial strain results decreased with an increase in normal stress from 14.5%, 11.6% and 9.2% at 100kPa, 200kPa and 300kPa confining pressures, respectively. Thereby displaying axial strain decreases with an increase in load and displaying a correlation to Test 1 and Test 4. The shear strength parameters namely, angle of internal friction and cohesion were found to be 32° and 11kPa, respectively which is summarized in Table 6.

The response of Berea Red sand continues to mirror the trend observed in the previous samples which show an increase in deviator stress with an increase in confining pressure.

Graph 9: Test 5- 4 Layer mosquito net reinforced triaxial test showing deviator stress versus axial strain.

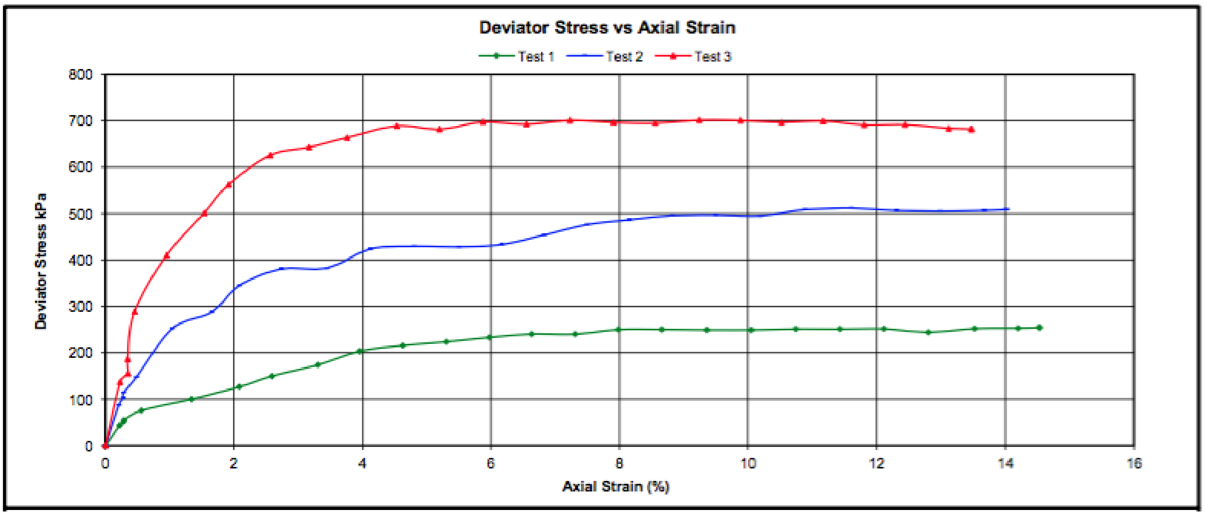

4.6. Variation in Deviator Stress

Typical stress-strain curves for unreinforced and reinforced samples under confining pressures of 100kPa, 200kPa and 300kPa with different numbers and types of geosynthetic layers are presented in Figure 23. It was noted that the reinforced samples greatly increase the deviator stress, in particular under low confining pressure, compared with the unreinforced samples. The figures also show that the maximum deviator stress increases with the increasing number of reinforcement layers, with the diamond mesh reinforcement having the peak deviator stress across all confining pressures. The most noted effect of the geosynthetic layers appears in the high strain, prior to reaching a constant level, whereas in the low strain (3%), where the reinforcement does not influence the behaviour of the axial stress- strain of the samples under all confining pressures. Continuous loading gradually slows the stress-strain growth due to the increased strain under all confining pressures. The geosynthetics increases the ductility of the Berea Red sand samples and allows for improvement of the soil strength and changing the strain-softening stress-strain behaviour to strain-hardening behaviour that would be able to prevent static liquefaction from occurring in saturated soils. The results observed agree with Denine et al., 2016 and Yi and Du, 2020, where the authors concluded that the presence of geosynthetic reinforcement improves the soil strength and observation of strain-hardening in the soils sampled.

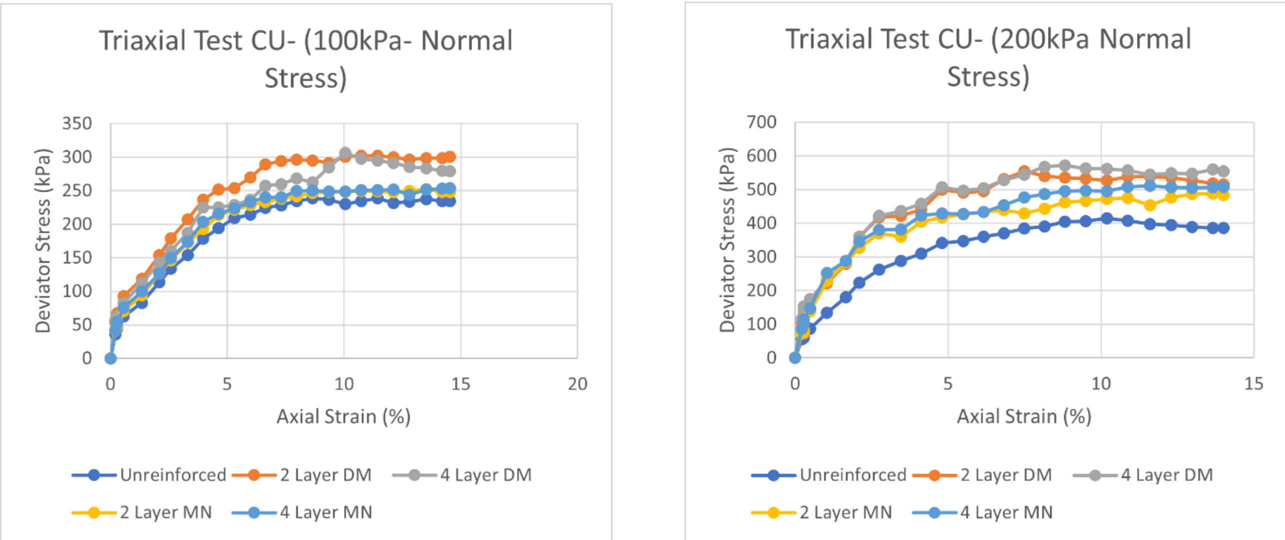

(b)

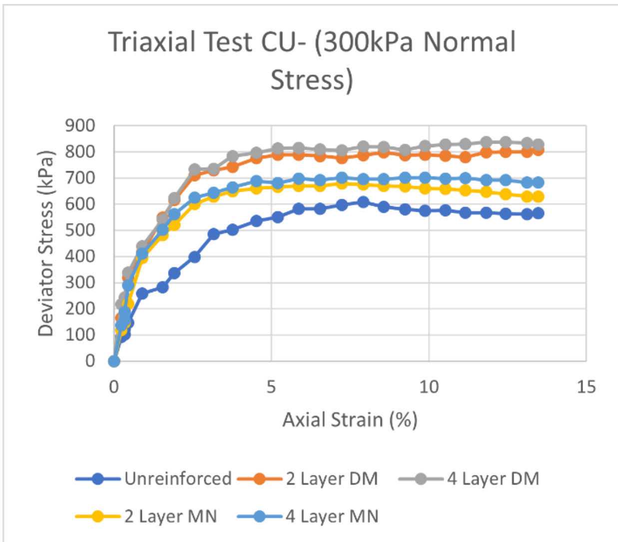

(c)

Figure 23: Deviator stress vs axial strain curves of Berea Red sand samples reinforced with several geosynthetic layers under different confining pressures: (a) 100kPa, (b) 200kPa, and (c) 300kPa

4.7. Variation of Pore Pressure

Figure 24 illustrates the evolution of pore water pressure on triaxial tests performed on unreinforced and reinforced Berea Red sand samples, drawn for the different confining pressures of 100kPa, 200kPa and 300kPa. The pore pressure development and dissipation of the tests have similar trends. The trends start off with a steady increase from 0% to 4% then followed by a sharp increase after 4% axial strain particularly for lower confining pressures of 100kPa and 200kPa whereas a more gradual increase is observed for confining pressures of 300kPa. It was seen that increasing the reinforcement layers increases the peak pore pressure of reinforced samples compared with unreinforced Berea Red sand samples as supported by Chen et al., 2014 and Denine et al., 2016.

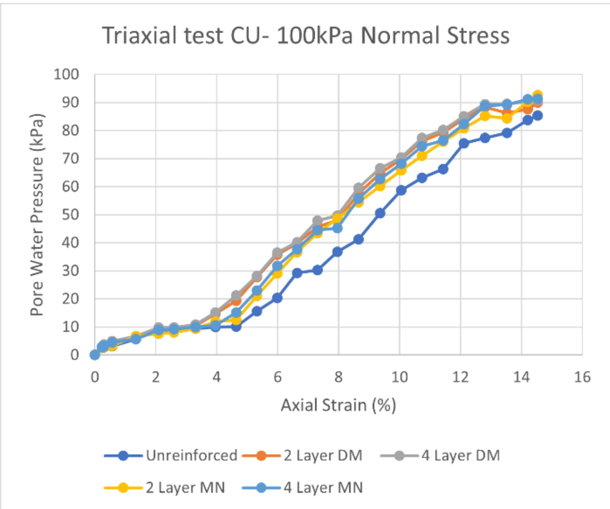

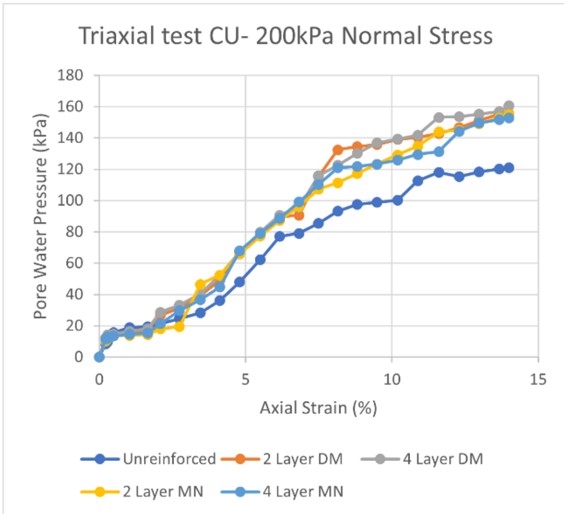

(a) (b)

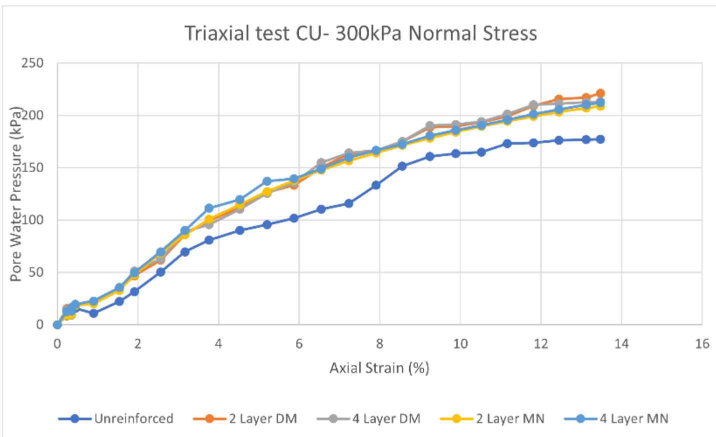

(c)

Figure 24: Pore water pressure vs axial strain curves of Berea Red sand samples reinforced with several geosynthetic layers under different confining pressures: (a) 100kPa, (b) 200kPa, and (c) 300kPa

4.8. Strength Properties

As indicated in Figure 25, the envelopes of all samples are linear and relatively parallel, with 4 Layer Diamond mesh being the peak deviator stress for all confining pressures. The triaxial test results show a decrease in cohesion with an increase in geosynthetic reinforcement and an increase in the friction angle with an increase in geosynthetic reinforcement (Table 6). These results could be attributed to the failure of geosynthetic reinforcement in reducing the number of contact points between the layers of soil particles, as supported by Latha and Murthy, 2007, where the authors conclude an increase in cohesion and decrease in friction angle contribute to interlocking soil particles thereby reducing the number of contact points between the soil particle layers.

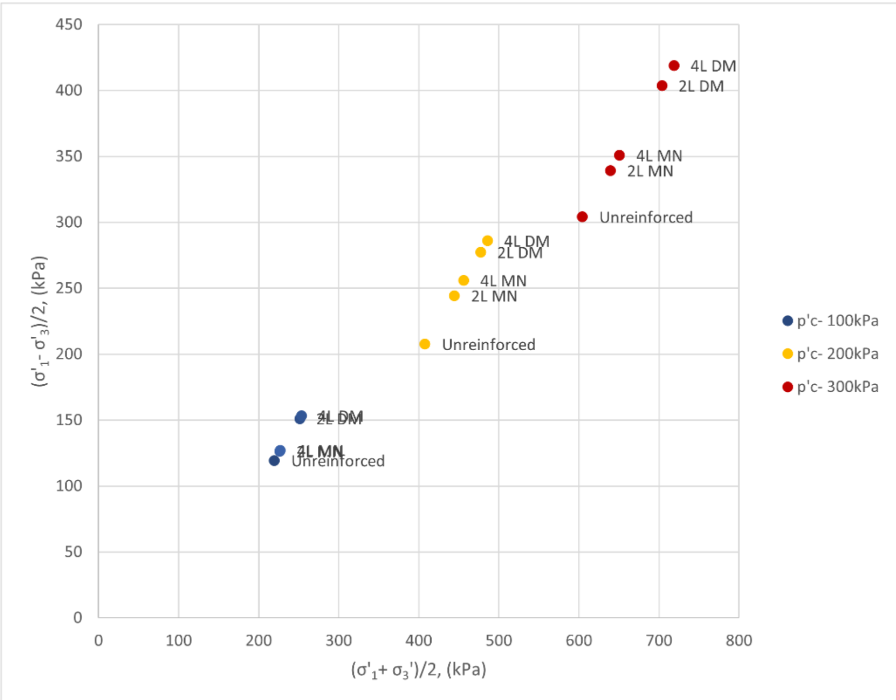

Figure 25: $(\sigma_1 - \sigma_3)/2$ vs $(\sigma_1 + \sigma_3)/2$ envelopes plot geosynthetic reinforced samples.

Table 6: The trend between cohesion and friction angle with and without geosynthetic reinforcement.

	Cohesion (kPa)	Friction Angle (°)
Unreinforced	15	29
2-Layer DM	13	34
4-Layer DM	11	35
2-Layer MN	13	31
4-Layer MN	11	32

By investigating the five consolidated undrained triaxial tests above it can be seen that Test 1, Test 4 and Test 5 show a trend in axial strain to normal stress results which represent the expectant behaviour of soils when under a load whereas Tests 2 and 3 show a significant increase for 200 kPa to 300kPa. This could be due to the failure of the reinforcement thereby resulting in a larger increase in deformation.

4.9. Shear Strength Analysis

The effective stress (σ') of the soil is considered a defining component when considering the shear strength (S') of the soil. The shear strength of the soils with and without reinforcing parameters were determined using the following formula below:

$$S' = c + \sigma' \tan \phi' \qquad \text{Eq. 19}$$

Where,

S' = shear strength

c = cohesion

σ' = normal stress

ϕ' = angle of internal friction

The shear strength of the unreinforced triaxial test at 100kPa is calculated as follows:

$$S' = c + \sigma' \tan \phi'$$

$$S' = 15 + 100\tan 29$$

$$S' = 70.43kPa$$

The shear strength results for all the triaxial tests at 100kPa normal stress can be observed in Table 7 below, with the lowest and highest shear strength presented in italics and bold, respectively.

Table 7: Shear strength results

Triaxial Test Name	**Shear strength (kPa)**
Test 1- Unreinforced	*70.43*
Test 2- 2 layer Diamond mesh	80.45
Test 3- 4 layer Diamond mesh	**81.02**
Test4- 2 layer Mosquito net	73.09
Test 5- 4 layer Mosquito net	73.49

After investigation of the above results, the shear strength increases with the implementation of reinforcements as supported by Kurre et al., 2018, with the authors' concluding that fabric reinforced soil upon cementation could lead to higher shear strength due to a proper reinforcement interaction; along with Goodarzi and Shahnazari, 2019, who state shear strength is increased by the inclusion of geotextile reinforcement in siliceous material. Shear strength increases with confining pressures as seen in Figure 25, due to an increase in frictional resistance, as supported by Fouche, 2021. It was also observed that shear strength increases with an increase in reinforcement layers, with Test 3- 4 layer diamond mesh having the highest shear strength. As supported by Clayton, 1989, the dilatancy of the samples maintains the high shear strength, by increasing confining stress through pore pressure reduction. Therefore, little reduction in the peak failure deviator stress could be attributed to the high degree of grain packing and dilatancy, even after 10% axial strain.

4.10. Sand- Geosynthetic Strength Ratio

The strength ratio (*SR*) of Berea Red sand is defined by the ratio of the maximum deviator stress of reinforced sand (q^{R}_{max}) to the maximum deviator stress of unreinforced sand (q^{Ur}_{max}) used in Latha and Murthy, 2007.

$$SR = (q^{R}_{max}/q^{Ur}_{max}) \quad \text{Eq. 20}$$

Table 8 summarizes the values of maximum deviator stress and strength ratio values of all tests. The results obtained indicate an increase in strength ratio with increasing geosynthetic reinforcement layers where samples reinforced with four geosynthetic layers, in the diamond mesh reinforcement, exhibit more strength than Berea Red sand alone or with two layers. With regards to confining pressure, all reinforced samples present a strength ratio of 1 or more with the peak strength ratio shown in the diamond mesh geosynthetic reinforcement. It should be noted the strength ratio increased with increase in confining pressure, from 100kPa to 200kPa, and reaching a constant thereafter. This could be due to a failure in the geosynthetic layers, however this cannot be confirmed as no photos, after deformation, were provided by the laboratory.

Table 8: Maximum deviator stress and strength ratio values of all triaxial tests.

Samples	Deviator stress (kPa)	Q max (kPa)	SR (-)
Unreinforced	100	238.7	-
	200	415.2	-
	300	608.4	-
2-Layer DM	100	302.3	1.27
	200	554.8	1.34
	300	807.3	1.34
4-Layer DM	100	306.7	1.28
	200	572	1.38
	300	838	1.38
2-Layer MN	100	252.6	1.06
	200	488.8	1.18
	300	678.6	1.12
4-Layer MN	100	254.1	1.06
	200	511.9	1.23
	300	701.7	1.15

4.11. Bearing capacity

In order for shallow foundations to perform adequately, it should be regarded as safe against overall shear failure of the soil, and it cannot undergo relative settlement (Das, 2011). The ultimate bearing capacity can be defined as "the load per unit area of the foundation at which shear failure in soil occurs" Das, 2011. The results show that the ultimate bearing capacity increases with the implementation of reinforcements. It was also observed that the ultimate bearing capacity increases with an increase in reinforcement layers, with 4 Layer Diamond mesh having the highest ultimate bearing capacity for circular foundations, continuous/strip footing foundations and square foundations. This could be a result of the lateral transferal of the load to adjacent soil by the geosynthetic as mentioned in Carlos et al., 2016. The ultimate bearing capacity and allowable load per unit area share a directly proportional relationship.

For this study bearing capacity regarding continuous/strip foundation; square foundations and circular foundations have been calculated as follows.

Continuous/Strip Footing Foundations:

The ultimate bearing capacity equation used to calculate ultimate bearing capacity for continuous/strip footing foundation is as follows:

$$q_u = c'N_c + qN_q + \frac{1}{2}\gamma BN_\gamma \qquad \text{Eq. 21}$$

D_f and B are given as 1m and 1.5m respectively.

The bearing capacity for the unreinforced triaxial test is calculated as follows:

$$q_u = c'N_c + qN_q + \frac{1}{2}\gamma BN_\gamma$$

$$q_u = (15 \times 34.24) + (16.2 \times 1 \times 19.98) + (0.5 \times 16.2 \times 1.5 \times 16.18)$$

$$q_u = 1033.86 kN/m^2$$

The allowable load per unit area of the foundation is calculated as follows:

$$q_{all} = \frac{q_u}{FS}$$

$$q_{all} = \frac{1033.86}{3}$$

$$q_{all} = 344.62$$

The ultimate bearing capacity and allowable load per unit area results for all the triaxial tests can be observed in Table 9 below, with the highest values presented in italics and bold, respectively.

Table 9: Ultimate bearing capacity and allowable load per unit area for continuous/strip footing foundations

Triaxial Test Name	**Ultimate Bearing Capacity (kN/m^2)**	**Allowable load per unit area (kN/m^2)**
Unreinforced	*1033.86*	*344.62*
2-layer Diamond mesh	1737.81	579.27
4-layer Diamond mesh	**1858.31**	**619.44**
2-layer Mosquito net	1210.06	403.35
4-layer Mosquito net	1272.93	424.31

Square Foundations:

The ultimate bearing capacity equation used to calculate ultimate bearing capacity for a square foundation is as follows:

$$q_u = 1.3c'N_c + qN_q + 0.4\gamma BN_\gamma \quad \text{Eq. 22}$$

D_f and B are given as 1.5m and 2m respectively.

The bearing capacity for the unreinforced triaxial test is calculated as follows:

$$q_u = 1.3c'N_c + qN_q + 0.4\gamma BN_\gamma$$

$$q_u = (1.3 \times 15 \times 34.24) + (16.2 \times 1.5 \times 19.98) + (0.4 \times 16.2 \times 2 \times 16.18)$$

$$q_u = 1362.89 kN/m^2$$

The allowable load per unit area of the foundation is calculated as follows:

$$q_{all} = \frac{q_u}{FS}$$

$$q_{all} = \frac{1362.89}{3}$$

$$q_{all} = 454.30$$

The ultimate bearing capacity and allowable load per unit area results for all the triaxial tests can be observed in Table 10 below, with the highest values presented in italics and bold, respectively.

Table 10: Ultimate bearing capacity and allowable load per unit area for square foundations

Triaxial Test Name	**Ultimate Bearing Capacity (kN/m²)**	**Allowable load per unit area (kN/m²)**
Unreinforced	*1362.89*	*454.30*
2-layer Diamond mesh	2269.56	756.52
4-layer Diamond mesh	**2421.33**	**807.11**
2-layer Mosquito net	1590.78	530.26
4-layer Mosquito net	1671.04	557.01

Circular Foundation:

The ultimate bearing capacity equation used to calculate ultimate bearing capacity for a circular foundation is as follows:

$$q_u = 1.3c'N_c + qN_q + 0.3\gamma BN_\gamma \qquad \text{Eq. 23}$$

D_f and B are given as 0.072m and 0.036m respectively, where B is equivalent to the diameter.

The bearing capacity for the unreinforced triaxial test is calculated as follows:

$$q_u = 1.3c'N_c + qN_q + 0.3\gamma BN_\gamma$$

$$q_u = (1.3 \times 15 \times 34.24) + (16.2 \times 0.072 \times 19.98) + (0.3 \times 16.2 \times 0.036 \times 16.18)$$

$$q_u = 1721.96kN/m^2$$

The allowable load per unit area of the foundation is calculated as follows:

$$q_{all} = \frac{q_u}{FS} \qquad \text{Eq. 24}$$

$$q_{all} = \frac{1721.96}{3}$$

$$q_{all} = 573.99$$

The ultimate bearing capacity and allowable load per unit area results for all the triaxial tests can be observed in Table 11 below, with the highest values presented in italics and bold, respectively.

Table 11: Ultimate bearing capacity and allowable load per unit area for circular foundations

Triaxial Test Name	**Ultimate Bearing Capacity (kN/m^2)**	**Allowable load per unit area (kN/m^2)**
Unreinforced	*1721.96*	*573.99*
2-layer Diamond mesh	2922.49	974.16
4-layer Diamond mesh	**3166.22**	**1055.41**
2-layer Mosquito net	2037.01	679.00
4-layer Mosquito net	2176.60	725.53

4.12. Modulus of Elasticity

The magnitudes of the elasticity modulus of soils are required when calculating the soil distribution of stress as well as discussing the elasticity of the soil mass (Das, 2011). The modulus of elasticity can be derived from the change in stress and the change in strain relation.

The modulus of elasticity is derived by the stress-strain curve obtained from the triaxial test results.

Table 12: Modulus of elasticity for all triaxial tests

Triaxial Test Name	*E* (MPa) at 100kPa	*E* (MPa) at 200kPa	*E* (MPa) at 300kPa
Unreinforced	0.15	0.2	0.3
2-layer Diamond mesh	0.2	0.6	1
4-layer Diamond mesh	0.2	0.6	1
2-layer Mosquito net	0.2	0.25	0.4
4-layer Mosquito net	0.2	0.25	0.4

After investigation of the above results, the modulus of elasticity increases with an increase in normal strain for all tests. It can also be seen that the modulus of elasticity increases with the implementation of reinforcement and remains constant with the increase of layers therefore indicating that the increase in layers of reinforcement does not have any effect to the modulus of elasticity.

5. Conclusion and Recommendations

This research was undertaken to establish the different strength parameters of Berea Red sands with and without geosynthetic reinforcement. Five triaxial consolidated undrained tests were carried out with four tests incorporating geosynthetic materials namely diamond mesh and mosquito net. The reinforced triaxial tests varied in the number of layers from two and four. The unreinforced test was used as a comparative in understanding the influence of the different reinforcements. The results of these tests show that the implementation of geosynthetics does increase the strength properties of Berea Red sand such as bearing capacity and shear strength. The analysis of the bearing capacity results for all three types of foundations indicates an increase with reinforcement as well as the quantity of reinforcing layers implemented with the 4 layer diamond mesh reinforcement exhibited the best strength properties when compared to unreinforced samples and 2 layer reinforced samples, across all confining pressures (100kPa, 200kPa and 300kPa). Shear strength results show an increase with confining pressures due to an increase in frictional resistance as well as with an increase in geosynthetic reinforcement. The stress-strain behaviour between the natural state and reinforced samples shows an increasing trend depicted in the deviator stress versus axial strain graphs. The strength ratio shows an increase with increasing geosynthetic reinforcement layers where samples reinforced with four geosynthetic layers, in the diamond mesh reinforcement, exhibit more strength than Berea Red sand alone or with two layers. A correlative trend is seen with the 4 layer diamond mesh reinforcement exhibiting the strongest strength properties. The results from the triaxial tests revealed that the internal angle of friction increased with the addition of reinforcing layers whereas the cohesion decreases. This could be attributed to the failure of geosynthetic reinforcement in reducing the number of contact points between the layers of soil particles. The implementation of reinforcement does not influence the modulus of elasticity due to it remaining constant with the increase of layers. It can be concluded that the shear strength and bearing capacity of Berea Red sands are enhanced with the addition of reinforcing agents however show adequate values without reinforcement, most likely due to the composition of the sand being silty sand with low levels of clay.

5.1. Limitations

The limitations to this study would be that the sampling of the Berea Red sand was carried out at a single site. This would limit the findings of this study to this site. However, the composition of Berea Red sands is known to be highly variable at various locations, particularly in terms of clay content. The number of geosynthetic reinforcement could also limit this study as it only focuses on two- and four-layer configurations as well as that representing a mesh or grid like nature.

5.2. Recommendations

Regarding construction, Berea Red sands is seen to be an adequate material to use and is in abundance along the eastern coast of South Africa. The use of reinforcement, in particular geosynthetic reinforcement with a permeable yet durable i.e., plastic composition, is highly recommended to enhance the shear strength and bearing capacity of Berea Red sands in construction and engineering disciplines. For future studies, an increase in reinforcement layers could be considered as well as sampling Berea Red sand from various locations with varying compositions, more specifically clay content, to better determine the shear strength and bearing capacity properties with and without reinforcing agents. This would also lead to more variety in the results as well as more variables to consider.

Acknowledgements

I would like to show my utmost gratitude and appreciation first and foremost to my Lord and savior Jesus Christ for all His blessings particularly during the course of my studies. To Professor J. Louis Van Rooy, my supervisor, thank you for the time, funding, support, and guidance you have shown me during this time.

To my mom and dad, thank you for your unconditional love and continuous support, not only during my studies but throughout my life. Thank you to my fur-son, Zakk, for patiently sharing me with my studies and your unconditional affection.

To my supportive and loving boyfriend, Nivek Ramsahai, thank you for being my accountability partner and encouraging me every day.

A big thank you to my bestie, Dayini Naidoo, for all your help, advice, and counselling- in life and studies.

I value and treasure each and every one of you!

I would like to thank the University of Pretoria for their continuous financial support via bursary for the duration of my studies. Thanks, must be extended to Paul Pratt, from Kaytech, for his assistance in providing tensile testing on the reinforcing materials used in this dissertation. A thank you to Sibaya Signature Estate and Luvan from 5th Dimension for allowing me to sample and test Berea Red sands from their site.

My gratitude is truly immeasurable to you all.

Ethical clearance was made for this study.

References

Bergh, A.O., Kleyn, E.G., and McKay, A.H. (2008). Preliminary studies on the utilisation of Berea Red sands for sub-base and base construction. *Southern African Transport Conference*, Pretoria.

Bishop, A. W. (1959). The principle of effective stress. Teknisk Ukeblad, **106**(39), 859-863.

Botha, J.P. (2015). Reinforcing unpaved roads on soft ground. BSc (Civil Engineering) Thesis, University of Pretoria, Pretoria.

Brink, A.B.A. (1985). Engineering Geology of Southern Africa, Volume 4, Building Publications, Pretoria.

Brink, G.E. (2011). The influence of soil suction on the collapse settlement of different soils in South Africa. *MSc. Thesis*, University of Pretoria, Pretoria.

Brink, G.E., and Van Rooy, J.L. (2015). The influence of the origin on soil volume change through collapse settlement. *Journal of African Earth Sciences*, **101**:113-118.

Carlos, D.M., Ponho-Lopes, M., and Lopes, M.L. (2016). Effect of geosynthetic reinforcement inclusion on the strength parameters and bearing ratio of a fine soil. *Advances in Transportation Geotechnics 3*, Vol. 143, Pp. 34-41.

Clayton, R.A. (1989). Investigation of stabilized Berea Red soil with emphasis on tensile and cyclic triaxial tests. *MSc Thesis*, University of Cape Town, Cape Town.

Christopher, B.R. (2014). Cost savings by using geosynthetics in the construction of civil works projects. German Geotechnical Society, 10ICG, **21**, Germany.

Das, B. (2008). Advanced soil mechanics. Third ed. Taylor and Francis, London and New York

Das, B. (2011). Principles of foundation engineering. Seventh ed. USA Cengage.

De Beer, E.E. and Martens, A. (1951). Method of computation of an upper limit for influence of heterogeneity of sand layers on the settlement of bridges. Proceedings 4th International Conference on Soil Mechanics and Foundation Engineering, London, Pp. 275-278.

Denine, S., Della, N., Muhammed, R.D., Feia, S., Canou, J., and Dulpa, J. (2016). Effect of geotextile reinforcement on shear strength of sandy soil: laboratory study. *Studia Geotechnica et Mechanica,* Vol. 38, No. 4.

Fredlund, D. G. (1979). Appropriate concepts and technology for unsaturated soils. *Canadian Geotech*. Vol. 1, No. 16, Pp. 121-139.

Fouche, N. (2021). Geotechnical charaterisation of upper quaternary sands of the cape flats. *PhD*. University of Stellenbosch, Stellenbosch.

Ghafoor, N., and Sharbaf, M.R. (2016). Use of geogrid for strengthening and reducing the roadway structural sections. *Nevada Department of Transportation*, Report No. 327-12-803.

Goodarzi, S., and Shahnazari, H. (2018). Strength enhancement of geotextile-reinforced carbonate sand. *Geotextiles and Geomembranes*, **47**(2019), Pp. 128-139.

Harikumar, M., Sankar, N., and Chrandrakaran. S. (2014). An alternate method of saturating sand specimens in triaxial tests. *International Journal of Engineering Research and Technology*, Vol. 3, Issue 9.

Heymann, G. (2000). Advances in triaxial testing. *Journal of South African institute of Civil Engineering*, **42(**1), Pp. 24-31.

Holtz, R.D. (2001). Geosynthetics for soil reinforcement. *The ninth Spencer J. Buchanan lecture.*

Jennings, J.E., and Knight, K. (1975). A Guide to Construction On or With Materials Exhibiting Additional Settlement Due to Collapse of Grain Structure, Proc. *Sixth Regional Conference for Africa on Soil Mechanics and Foundation Engineering*, Durban, South Africa, Pp. 99-105.

Jones, B.R. (2014). Geotechnical centrifuge modelling of the behaviour of a compressible clay horizon underlying a reinforced sand foundation. *MSc Thesis*, University of Pretoria, Pretoria.

Jones, B.R., Jacobsz, S.W., and Van Rooy, J.L. (2016). A qualitative model study on the effect of geosynthetic foundation reinforcement in sand overlaying very soft clay. *Journal of the South African Institute of Civil Engineering*, Vol. 58, No. 2, Pp. 25-34.

Klukanova, A., and Frankovska, J. (1995). The Slovak Carpathians loess sediments, their fabric and properties. Genesis and Properties of Collapsible Soils, Derbyshire et al. (Eds.), Pp. 129–147.

Kurre, P., Praveen, G.V., and Heeralal, M. (2018). Study of triaxial behaviour of geotextile reinforced marginal soil without and with cement modification for subgrade construction of pavements. *Journal of Engineering Research and Application*, Vol. 8, Issue 5, Pp. 40-44.

Latha, M.G., and Murthy, V.S. (2006). Investigations on sand reinforced with different geosynthetics. *Geotechnical Testing Journal*, Vol. 29, No. 6.

Latha, M.G., and Murthy, V.S. (2007). Effects of reinforcement form on the behaviour of geosynthetic reinforced sand. *Geotextile and Geomembranes*, Vol. 25, Pp. 23-32.

Mali, S., and Singh, B. (2014). Strength behaviour of cohesive soils reinforced with fibers. *International Journal of Civil Engineering Research*, Vol. 5, No. 4, Pp. 353-360.

Molla, I. (2017). Comparison of foundation settlements using soil parameter from consolidation test and drained triaxial test. *MSc Thesis*, Bangladesh University of Engineering and Technology.

Md.Noor, M.J., and Anderson, W.F. (2007). A Qualitative Framework for Loading and Wetting Collapses in Saturated and Unsaturated Soils. Proc. 16th Southeast Asian Geotechnical Conference, Kuala Lumpur, Malaysia.

Md.Noor, M.J., Jadin, R., and Hafez, M.A. (2008). Effective stress and complex soil settlement behaviour. *Faculty of Civil Engineering*, Vol. 3.

Nair, A.M., and Latha. G.M. (2014). Large diameter triaxial test on geosynthetic-reinforced granular subbases. Ph.D Thesis, *Journal of Materials in Civil Engineering*.

Noorzad, R., and Mirmoradi, S.H. (2010). Laboratory evaluation of the behaviour of a geotextile reinforced clay. *Geotextiles and Geomembranes*, **28** (2010), 386-392.

November, J.S. (2014). A study of soil to geotextile filtration behaviour in conjunction with Berea sand in South Africa. *MSc Thesis,* Stellenbosch University, Stellenbosch.

Okonta, F.N. (2005). Capacity of vertically loaded piles in low density sands. *PhD Thesis*. University of KwaZulu Natal, Durban.

Okonta, F.N., and Govender, E. (2011). Effect of desiccation on the geotechnical properties of lime-fly ash stabilized collapsible residual sand. *Journal of Engineering and Applied Sciences,* Vol. 6, No. 6.

Patil, P., Mena, I., Goski, S., and Urs, Y. (2016). Soil Reinforcement. Journal of Engineering Research and Application. Vol. 6, Issue 8, Pp. 25-31.

Pequenino, F.H., Van Der Merwe, F., Purchase, C., and Warren-Codrington, C.J. (2018). Case study: Mount Edgecombe interchange- investigation, design and construction of a complex geotechnical project.

Purchase, C., and Van Der Merwe, F. (2017). Case study and lessons learnt: The construction of mechanically stabilised earth walls at Mount Edgecombe interchange. *South African Young Geotechnical Engineers Conference*, Durban.

Rust, E., Heymann, G., and Jones, G. A. (2005). Collapse potential of partly saturated sandy soils from Mozal, Mozambique. *Journal of the South African Institution of Civil Engineering*, Vol. 47, No. 1, Pp. 8-14.

Sachan, A. (2015). Bearing capacity. Presentation, *Indian Institute of Technology,* Gandhinagar.

Schwartz, K. (1985). Collapsible Soils: Problems of Soils in South Africa, state-of-the-art. *The Civil Engineer in South Africa*, **27**, Pp. 379-393.

Singh, R.G. (2009). Landslide classification, characterization and susceptibility modelling in KwaZulu Natal. *MSc Thesis*, University of Witswatersand, Johannesburg.

Skempton, A.W. (1961). Effective stress in soils, concrete and rocks. Pore Pressure Conference, London.

Stucki, M., Büsser, S., Itten, R., Frischknecht, R., and Wallbaum H. (2011). Comparative Life Cycle Assessment of Geosynthetics versus Conventional Construction Materials. ESU-services Ltd. Uster, ETH Zürich, Switzerland.

Tennant, W.J., and van Heerdan, J. (1994). The influence of orography and local sea-surface temperature anomalies on the development of the 1987 Natal floods: a general circulation model study. *South African Journal of Science*, Vol. 90, Pp. 45-49.

Terzaghi, K. (1936). The shear resistance of saturated soils. Proceedings for the 1st. International Conference on Soil Mechanics and Foundation Engineering (Cambridge, MA), 1, Pp. 54 - 56.

Terzaghi, K. (1943). Theoretical Soil Mechanics. Wiley, New York.

Tuncer, E.R. (1976). Engineering behaviour and classification of lateritic soils in relation to soil genesis. PhD. Thesis, Iowa State University, Iowa.

Viswanadham, B. V. S., and König, D. (2004). Studies on scaling and instrumentation of a geogrid. *Geotextiles and Geomembranes*, **22**(5), 307-328.

Yi, F., and Du, Changbo. (2020). Triaxial testing on geosynthetic reinforced tailings with different reinforced layers. Materials, 13.

Zannoni, E. (2013). The use of geosynthetics in pavements: New technology for sustainable environment. *Imesa conference,* Maccaferri Southern Africa.

Appendices

Appendix A- Kaytech laboratory results

1 - 1 2020/09/21
Sample-Kaytech.xlsx

Test Report ELISHA GEOSURE

Product:	Diamond Mesh	Temperature:	23.000 °C
		Humidity:	65.000 AAA
Roll number:	ELLISHA-DM	Operator:	15000.000 N
Product code:	Cross Direction (CD)	Load range:	100.000 mm
Direction: Standard:		Gauge lenth:	20.000 mm/min
		Test speed:	20.000 N
Date: 2020/09/21 10:46:04		Preload:	

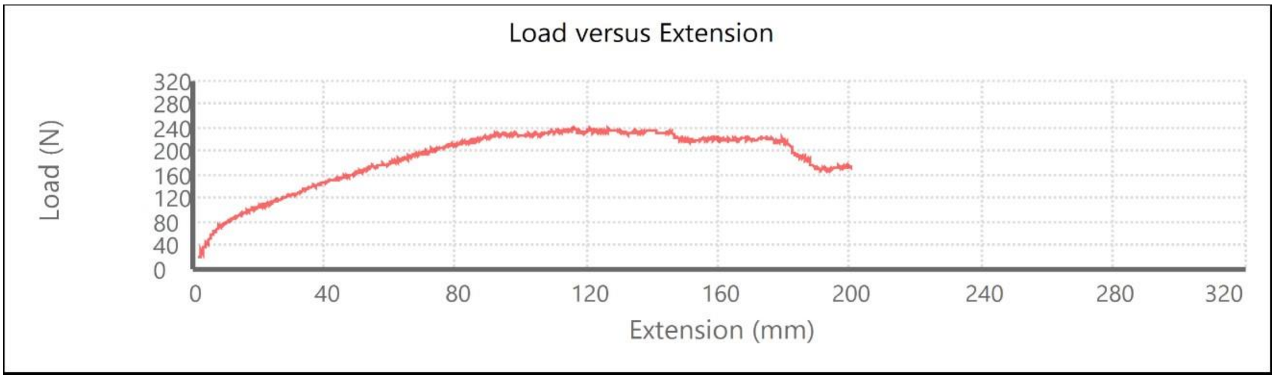

Specimen	Peak Load (kN)	Strain at Peak	Peak (kN/m)	Width (mm)
Test Run 1	0.240	116.010	1.199	200.000
Mean	0.240	116.010	1.199	200.000
[illegible]	0.240	116.010	1.199	200.000
[illegible]	0.240	116.010	1.199	200.000
[illegible]on	#NUM!	#NUM!	#NUM!	#NUM!
% Coefficient of Variance	#NUM!	#NUM!	#NUM!	#NUM!

1 - 1 2020/09/21
Sample-Kaytech.xlsx

Test Report Kaytech Development Tens

Product: GEOSURE
Roll number:

Temperature: 23.000 °C
Humidity: 65.000 unitless

Product code: ELLISHA

Operator: AAA

Direction: CD

Load range: 15000.000 N

Standard: WHITE NET

Gauge lenth: 100.000 mm

Date: 2020/09/21 11:17:52

Test speed: 20.000 mm/min
Preload: 20.000 N

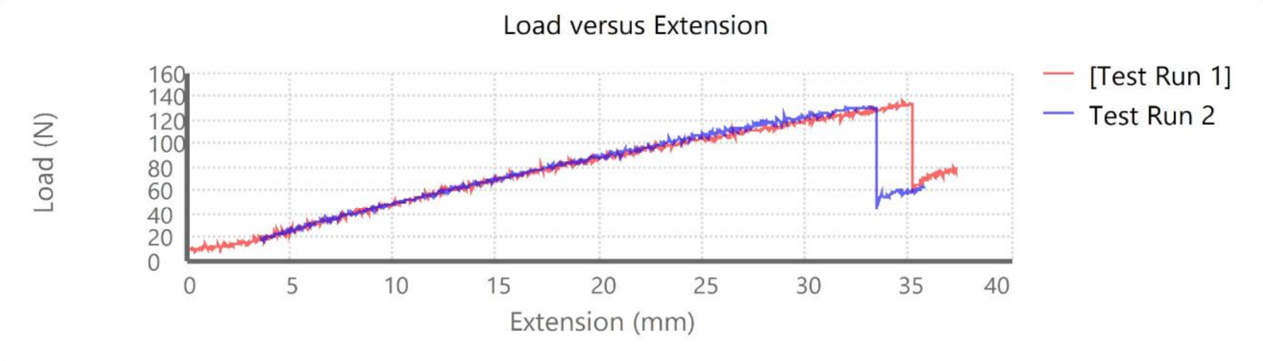

Specimen	Peak Load (kN)	Strain at Peak	Peak (kN/m)	Width (mm)
Test Run 1	0.136	34.756	0.678	200.000
Test Run 2	0.132	32.875	0.659	200.000
Mean	0.134	33.816	0.668	200.000
Minimum	0.132	32.875	0.659	200.000
Maximum	0.136	34.756	0.678	200.000
Standard Deviation	0.003	1.330	0.013	0.000
% Coefficient of Variance	1.974	3.934	1.974	0.000

Appendix B- TSL lab results

Laboratory Test Summary

THEKWINI SOILS LAB. CC
V.A.T. REGISTRATION NO. 4590210961.
68 Ridge Road, Tollgate, DURBAN Tel : (031) 201-8992
P.O. Box 30464, MAYVILLE, 4058 Fax : (031) 201-7920

Job Description: Sibaya

Job no.: 9236

Date: 02-02-2021

Lab no.		11122										
Location		S1										
Depth		-										
Description		-										
		-										
Binder Material		-										
Particle Size (mm)	75 53 37.5 26.5 19 13.2 9.5 4.75 2 0.425 0.25 0.15 0.075	Cumulative % Passing										

			100									
			97									
			63									
			15									
			9									
Hydrometer	0.05	% Passing	9									
	0.02		9									
	0.005		6									
	0.002		6									
Soil Mortar	Coarse Sand <2.0 >0.425mm	% Passing	3.0									
	Fine Sand <0.425>0.05mm		87.8									
	Silt <0.05 >0.005		3.0									
	Clay <0.005		6.2									
Atterberg Limits	Liquid Limit % (m/m)		19.7									
	Plasticity Index		0									
	Linear Shrinkage %		0									
	Natural MC %		-									
Mod AASHTO Density	Dry Density kg/m^3											
	OMC %											
CBR	100% MDD											
	98%											
	95%											
	93% (Inferred) *											
	90%											
	CBR Swell (%)											
AASHTO Soil Classification *			A - 3 (0)									

Grading Modulus	0.94									
TRH 14 (1985) * *WT = Worse Than										

Technical Signatory: ....

TEST REPORT

MATERIALS ANALYSIS

THEKWINI SOILS LAB. CC
V.A.T. REGISTRATION NO. 4590210961.
68 Ridge Road, Tollgate, DURBAN
Tel : (031) 201-8992
P.O. Box 30464, MAYVILLE, 4058
Fax : (031) 201-7920

Project: Sibaya

Ref no.: 9236 **Lab no.:** 11122 **Borehole/Pit no.:** S1
Description: -
Depth: - -

Test Methods: TMH1 METHOD A1(a), A2, A3 & A4, ASTMD422

Grading Analysis

Grain Size (mm)	%Passing
75	100.0
53	100.0
37.5	100.0
26.5	100.0
19	100.0
13.2	100.0
9.5	100.0
4.7	100.0
	100.0
	97.0
0.25	62.8
0.15	15.4
0.425	9.4
0.075	
0.05	9.4 9.4
0.02	6.4
0.005	6.4
0.002	

M.I.T SIZE CLASSIFICATION *

Cobble%		0.0
Gravel%	0.0	
Coarse		0.0
Medium		0.0
Fine		0.0
Sand%	90.6	
Coarse		2.7
Medium		58.2
Fine		29.7
Silt%	3.0	
Coarse		0.0
Medium		2.8
Fine		0.2
Clay%	6.4	

PLASTICITY

Liquid Limit, %	19.7
Plasticity Index	0
Linear Shrinkage, % (L/L)	0

GRADING

D10 Size (mm)	0.08
Uniformity Coefficient	3.03
Grading Modulus	0.94

CLASSIFICATION *

Potential Expansiveness	Low
Group Index	0
AASHTO Soil Classification	A - 3
Unified Classification	SP - SM

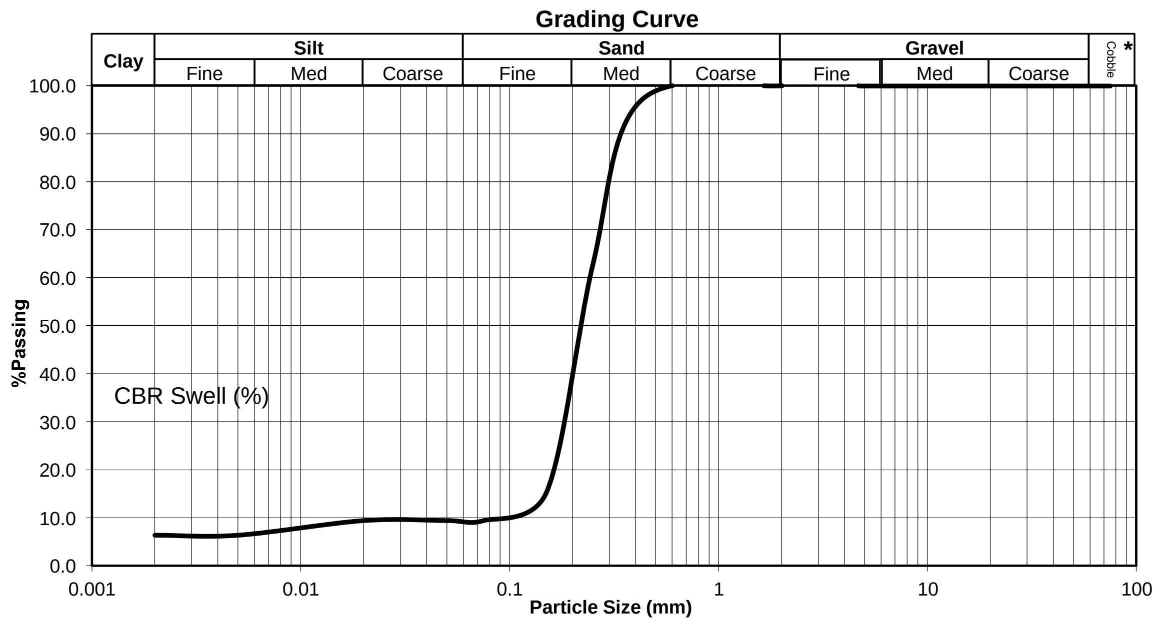

Ref no.: 9236 | Fig no.: -

* Information marked with an asterisk is outside the scope of Accreditation.
The results only relate to the samples tested.
The report may not be reproduced except in full.

CONSOLIDATED UNDRAINED TRIAXIAL TEST

SUMMARY OF RESULTS

THEKWINI SOILS LAB. CC

V.A.T. REGISTRATION NO. 4590210961.

68 Ridge Road, Tollgate, DURBAN
P.O. Box 30464, MAYVILLE, 4058
Tel : (031) 201-8992
Fax : (031) 201-7920

Project: Sibaya
Ref no.: 9236
Lab no.: 11122 **Depth:** **Description:** **Position:** S1
Standard Unreinforced

Test 1

Inputs

L (cm)	7.76	Lo (cm)	7.67	MC Before (%)	11.7
A (cm^2)	11.95	Ao (cm^2)	11.66	MC After (%)	18.8
V (cc)	92.70	Vo (cc)	89.40	Bulk Density (kg/m3)	1845
		Prooving Ring	0.43	Dry Density (kg/m3)	1652
		Sigma3	100		

Area at Test	%Strain	Deviator Stress (kPa)	Pore Water Pressurs (Kpa)	$F^1 + F^3$ / 2	$F^1 - F^3$ / 2	F^1 / F^3
11.66	0	0	0	0	0	0
11.69	0.22	36.2	2.58	118.1	18.1	1.36
11.70	0.28	44.2	2.74	122.1	22.1	1.44
11.70	0.29	45.1	2.85	122.5	22.5	1.45
11.73	0.56	62.6	3.12	131.3	31.3	1.63
11.82	1.34	83.1	5.62	141.5	41.5	1.83
11.91	2.09	113.8	8.78	156.9	56.9	2.14
11.97	2.59	134.0	9.01	167.0	67.0	2.34
12.06	3.30	154.2	9.45	177.1	77.1	2.54
12.14	3.95	178.3	10.00	189.1	89.1	2.78
12.23	4.63	194.0	10.11	197.0	97.0	2.94
12.32	5.31	209.6	15.60	204.8	104.8	3.10
12.40	5.97	214.2	20.37	207.1	107.1	3.14
12.49	6.63	224.3	29.21	212.2	112.2	3.24
12.58	7.30	228.4	30.33	214.2	114.2	3.28
12.67	7.97	234.2	36.81	217.1	117.1	3.34
12.77	8.65	238.5	41.23	219.2	119.2	3.38
12.87	9.35	236.5	50.62	218.3	118.3	3.37
12.97	10.05	230.4	58.78	215.2	115.2	3.30
13.07	10.74	234.8	63.21	217.4	117.4	3.35
13.17	11.43	238.7	66.31	219.4	119.4	3.39
13.27	12.11	231.3	75.54	215.6	115.6	3.31
13.37	12.80	234.0	77.34	217.0	117.0	3.34
13.48	13.51	237.4	79.21	218.7	118.7	3.37
13.59	14.19	234.7	83.72	217.4	117.4	3.35
13.64	14.52	234.3	85.42	217.1	117.1	3.34

Test 2

Inputs

L (cm)	7.76	Lo (cm)	7.63	MC Before (%)	11.7
A (cm^2)	11.95	Ao (cm^2)	11.53	MC After (%)	18.6
V (cc)	92.70	Vo (cc)	87.90	Bulk Density (kg/m3)	1845
		Prooving Ring	0.70	Dry Density (kg/m3)	1652
		Sigma3	200		

Area at Test	%Strain	Deviator Stress (kPa)	Pore Water Pressurs (Kpa)	$F^1 + F^3$ / 2	$F^1 - F^3$ / 2	F^1 / F^3
11.53	0	0	0	0	0	0
11.56	0.21	55.1	8.32	227.5	27.5	1.28
11.57	0.27	59.3	9.56	229.7	29.7	1.30
11.57	0.28	66.3	10.25	233.2	33.2	1.33
11.59	0.48	86.6	15.62	243.3	43.3	1.43
11.65	1.04	134.2	18.77	267.1	67.1	1.67
11.73	1.65	180.0	19.31	290.0	90.0	1.90
11.78	2.09	223.5	21.23	311.7	111.7	2.12
11.86	2.74	262.7	24.52	331.4	131.4	2.31
11.95	3.45	289.0	28.22	344.5	144.5	2.45
12.03	4.12	310.2	36.21	355.1	155.1	2.55
12.11	4.80	341.5	47.96	370.8	170.8	2.71
12.20	5.50	346.7	62.14	373.4	173.4	2.73
12.29	6.16	360.7	77.11	380.3	180.3	2.80
12.38	6.82	370.0	79.33	385.0	185.0	2.85
12.47	7.49	384.2	85.33	392.1	192.1	2.92
12.56	8.15	390.2	93.21	395.1	195.1	2.95
12.65	8.81	404.9	97.54	402.5	202.5	3.02
12.74	9.49	406.3	98.88	403.2	203.2	3.03
12.84	10.19	415.2	100.21	407.6	207.6	3.08
12.94	10.88	407.4	112.54	403.7	203.7	3.04
13.05	11.60	398.2	117.99	399.1	199.1	2.99
13.15	12.30	395.0	115.37	397.5	197.5	2.97
13.25	12.98	388.6	118.22	394.3	194.3	2.94
13.36	13.66	386.3	120.12	393.1	193.1	2.93
13.41	14.00	386.4	121.08	393.2	193.2	2.93

Test 3

Inputs

L (cm)	0.00	Lo (cm)	7.57	MC Before (%)	11.7
A (cm^2)	7.76	Ao (cm^2)	11.37	MC After (%)	18.5
V (cc)	11.95	Vo (cc)	86.00	Bulk Density (kg/m3)	1845
		Prooving Ring	0.85	Dry Density (kg/m3)	1652
		Sigma3	300		

Area at Test	%Strain	Deviator Stress (kPa)	Pore Water Pressurs (Kpa)	$F^1 + F^3$ / 2	$F^1 - F^3$ / 2	F^1 / F^3
11.37	0	0	0	0	0	0
11.40	0.23	92.0	8.44	346.0	46.0	1.31
11.41	0.35	102.0	9.31	351.0	51.0	1.34
11.41	0.35	122.7	9.49	361.4	61.4	1.41
11.42	0.45	145.5	15.63	372.7	72.7	1.48
11.48	0.95	258.1	10.89	429.1	129.1	1.86
11.55	1.54	282.6	22.35	441.3	141.3	1.94
11.59	1.91	336.1	31.55	468.1	168.1	2.12
11.67	2.56	398.8	50.23	499.4	199.4	2.33
11.74	3.17	485.7	69.74	542.8	242.8	2.62
11.81	3.76	501.9	81.01	550.9	250.9	2.67
11.91	4.53	534.9	90.21	567.5	267.5	2.78
11.99	5.20	551.3	95.64	575.6	275.6	2.84
12.08	5.87	582.7	101.74	591.4	291.4	2.94
12.17	6.55	583.0	110.34	591.5	291.5	2.94
12.26	7.23	598.0	115.94	599.0	299.0	2.99
12.35	7.91	608.4	133.21	604.2	304.2	3.03
12.43	8.56	590.1	151.62	595.1	295.1	2.97
12.53	9.24	580.9	160.67	590.4	290.4	2.94
12.62	9.88	575.5	163.42	587.7	287.7	2.92
12.71	10.52	575.9	165.02	587.9	287.9	2.92
12.80	11.16	568.2	173.21	584.1	284.1	2.89
12.89	11.81	567.2	174.00	583.6	283.6	2.89
12.99	12.44	563.5	176.21	581.7	281.7	2.88
13.09	13.12	562.6	177.06	581.3	281.3	2.88
13.14	13.47	565.4	177.10	582.7	282.7	2.88

CONSOLIDATED UNDRAINED TRIAXIAL TEST
SUMMARY OF RESULTS

THEKWINI SOILS LAB. CC
V.A.T. REGISTRATION NO. 4590210961.
68 Ridge Road, Tollgate, DURBAN Tel : (031) 201-8992
P.O. Box 30464, MAYVILLE, 4058 Fax : (031) 201-7920

Project: Sibaya
Ref no.: 9236
Lab no.: 11122
Depth: -
Position: S1

Description:
Standard unreinforced

	Test 1	Test 2	Test 3
Normal Stress (kN/m^2)	100	200	300
Dry Density (kg/m^3)	1652	1652	1652
NMC(%)	11.7	11.7	11.7
Axial Strain (%)	11.4	10.2	7.9
$F^1 + F^3$ **2**	219.4	407.6	604.2
$F^1 - F^3$ **2**	119.4	207.6	304.2
F_1 F_3	3.39	3.08	3.03

Shear Strength Parameters:

Angle of Internal Friction (0^0) 29

Cohesion (kPa) 15

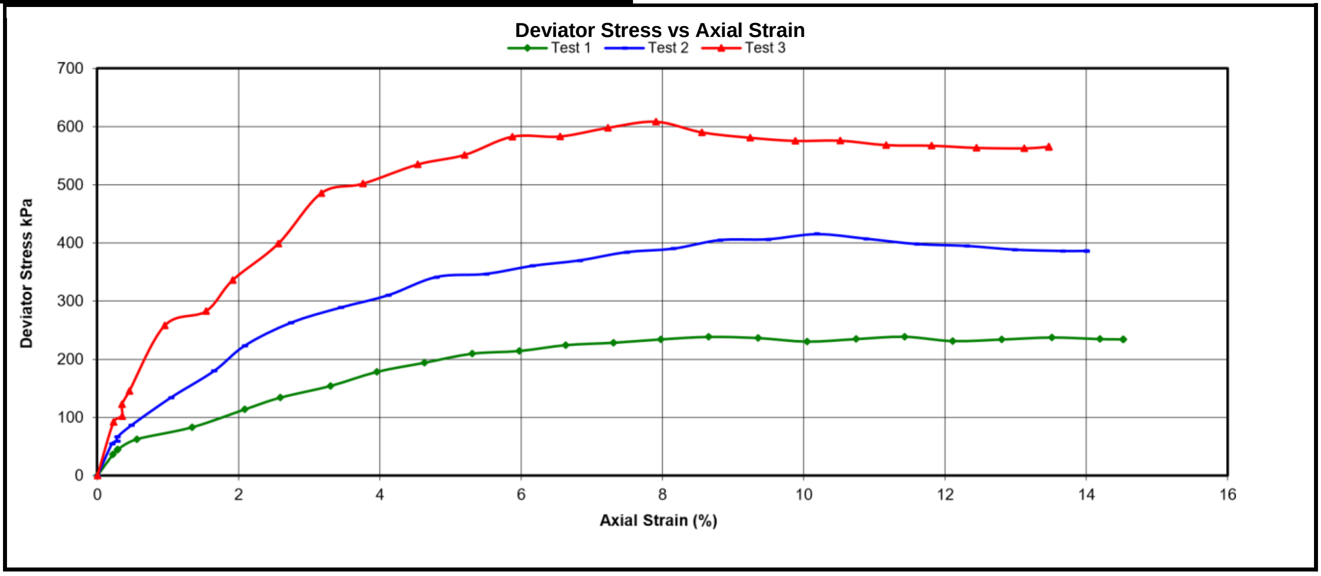

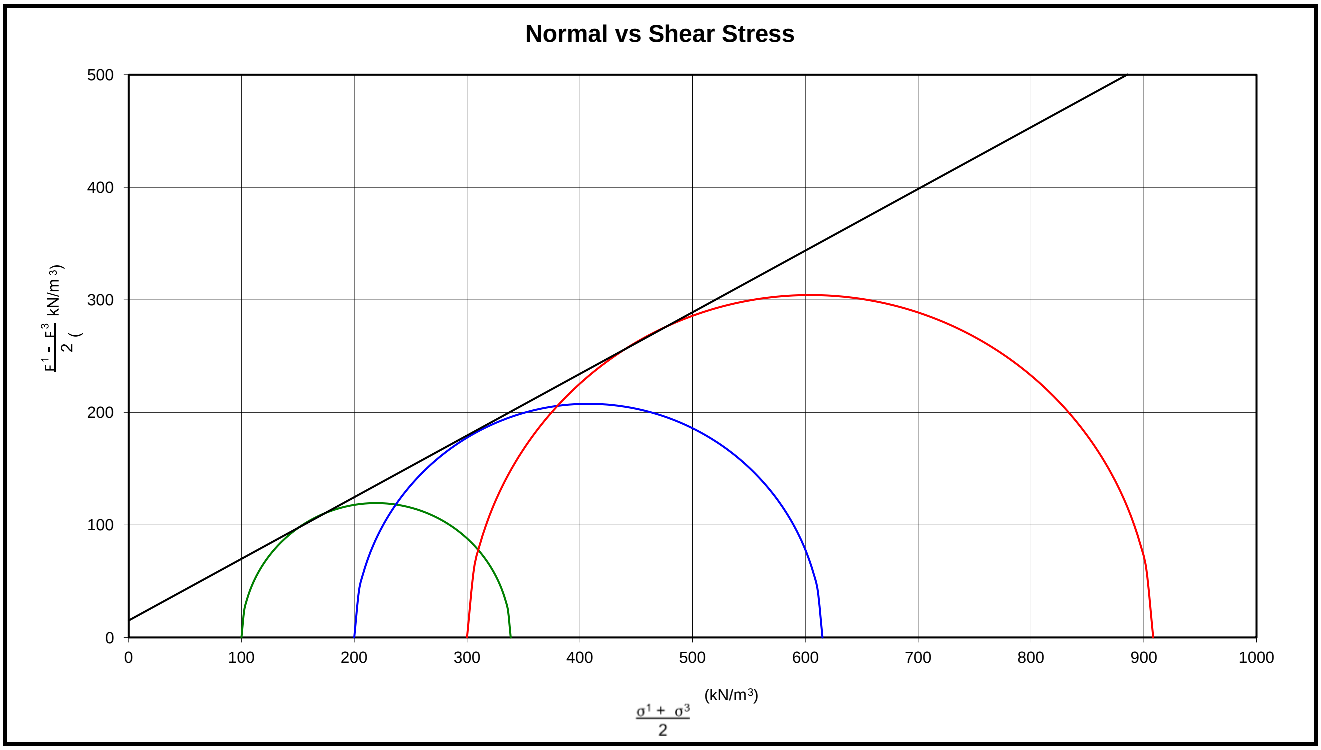
Normal vs Shear Stress
500
400
300
200
100
0
0
100
200
300
400
500
600
700
800
900
1000
E1 - E3 / 2 (kN/m3)
σ1 + σ3 / 2 (kN/m3)

CONSOLIDATED UNDRAINED TRIAXIAL TEST

SUMMARY OF RESULTS

THEKWINI SOILS LAB. CC
V.A.T. REGISTRATION NO. 4590210961.
68 Ridge Road, Tollgate, DURBAN
Tel : (031) 201-8992
P.O. Box 30464, MAYVILLE, 4058
Fax : (031) 201-7920

Project: Sibaya
Ref no.: 9236
Lab no.: 11122 **Depth:** **Description:** **Position:** S1
2 Layer Net- Mosquito

Test 1

Inputs

L (cm)	7.76	Lo (cm)	7.67	MC Before (%)	11.7
A (cm^2)	11.95	Ao (cm^2)	11.65	MC After (%)	19.5
V (cc)	92.70	Vo (cc)	89.30	Bulk Density (kg/m3)	1845
		Prooving Ring	0.45	Dry Density (kg/m3)	1652
		Sigma3	100		

Test 2

Inputs

L (cm)	7.76	Lo (cm)	7.62	MC Before (%)	11.7
A (cm^2)	11.95	Ao (cm^2)	11.52	MC After (%)	19.0
V (cc)	92.70	Vo (cc)	87.80	Bulk Density (kg/m3)	1845
		Prooving Ring	0.75	Dry Density (kg/m3)	1652
		Sigma3	200		

Test 3

Inputs

L (cm)	0.00	Lo (cm)	7.57	MC Before (%)	11.7
A (cm^2)	7.76	Ao (cm^2)	11.37	MC After (%)	19.0
V (cc)	11.95	Vo (cc)	86.00	Bulk Density (kg/m3)	1845
		Prooving Ring	0.90	Dry Density (kg/m3)	1652
		Sigma3	300		

Area at Test	%Strain	Deviator Stress (kPa)	Pore Water Pressurs (Kpa)	$(F^1+F^3)/2$	$(F^1-F^3)/2$	F^1/F^3	Area at Test	%Strain	Deviator Stress (kPa)	Pore Water Pressurs (Kpa)	$(F^1+F^3)/2$	$(F^1-F^3)/2$	F^1/F^3	Area at Test	%Strain	Deviator Stress (kPa)	Pore Water Pressurs (Kpa)	$(F^1+F^3)/2$	$(F^1-F^3)/2$	F^1/F^3
11.65	0	0	0	0	0	0	11.52	0	0	0	0	0	0	11.37	0	0	0	0	0	0
11.68	0.22	41.7	2.79	120.9	20.9	1.42	11.55	0.21	72.3	10.50	236.1	36.1	1.36	11.40	0.23	118.3	8.73	359.1	59.1	1.39
11.69	0.28	47.9	2.91	123.9	23.9	1.48	11.56	0.27	82.8	11.44	241.4	41.4	1.41	11.41	0.35	147.0	9.71	373.5	73.5	1.49
11.69	0.29	46.6	2.97	123.3	23.3	1.47	11.56	0.28	74.2	12.76	237.1	37.1	1.37	11.41	0.35	151.6	9.82	375.8	75.8	1.51
11.72	0.56	70.2	3.32	135.1	35.1	1.70	11.58	0.48	139.3	13.37	269.7	69.7	1.70	11.42	0.45	219.3	18.40	409.7	109.7	1.73
11.81	1.34	94.1	6.76	147.1	47.1	1.94	11.65	1.04	228.0	14.12	314.0	114.0	2.14	11.48	0.95	393.6	20.26	496.8	196.8	2.31
11.90	2.09	126.7	7.63	163.4	63.4	2.27	11.72	1.65	284.0	14.37	342.0	142.0	2.42	11.55	1.54	482.4	32.96	541.2	241.2	2.61
11.96	2.59	145.9	8.04	172.9	72.9	2.46	11.77	2.09	327.1	17.94	363.5	163.5	2.64	11.59	1.91	521.2	47.53	560.6	260.6	2.74
12.05	3.30	172.8	9.38	186.4	86.4	2.73	11.85	2.74	370.8	19.28	385.4	185.4	2.85	11.67	2.56	600.6	68.54	600.3	300.3	3.00
12.13	3.96	192.6	11.93	196.3	96.3	2.93	11.94	3.45	360.0	46.58	380.0	180.0	2.80	11.74	3.17	628.8	85.89	614.4	314.4	3.10
12.22	4.63	213.7	12.54	206.8	106.8	3.14	12.02	4.12	404.7	52.60	402.4	202.4	3.02	11.81	3.76	649.0	100.84	624.5	324.5	3.16
12.31	5.31	221.7	21.10	210.8	110.8	3.22	12.11	4.80	418.1	65.64	409.0	209.0	3.09	11.91	4.53	659.8	114.86	629.9	329.9	3.20
12.39	5.98	228.6	29.05	214.3	114.3	3.29	12.20	5.50	426.6	77.46	413.3	213.3	3.13	11.99	5.20	666.8	127.09	633.4	333.4	3.22
12.48	6.63	233.1	36.71	216.6	116.6	3.33	12.28	6.16	433.2	87.40	416.6	216.6	3.17	12.08	5.87	669.0	137.78	634.5	334.5	3.23
12.57	7.31	238.3	43.47	219.1	119.1	3.38	12.37	6.83	438.8	96.13	419.4	219.4	3.19	12.17	6.55	670.7	147.93	635.3	335.3	3.24
12.66	7.98	242.0	48.59	221.0	121.0	3.42	12.46	7.49	429.1	107.35	414.6	214.6	3.15	12.26	7.23	678.6	156.72	639.3	339.3	3.26
12.76	8.65	246.9	54.45	223.5	123.5	3.47	12.55	8.15	444.4	111.44	422.2	222.2	3.22	12.35	7.91	675.1	164.19	637.6	337.6	3.25
12.86	9.36	247.9	60.18	223.9	123.9	3.48	12.64	8.81	462.3	117.29	431.1	231.1	3.31	12.43	8.56	670.4	171.56	635.2	335.2	3.23

12.96	10.05	248.5	65.79	224.2	124.2	3.48	12.73	9.49	467.0	123.48	433.5	233.5	3.33	12.53	9.24	668.2	178.16	634.1	334.1	3.23
13.06	10.74	249.3	71.00	224.7	124.7	3.49	12.83	10.19	472.2	129.34	436.1	236.1	3.36	12.62	9.88	660.4	184.17	630.2	330.2	3.20
13.16	11.43	248.9	76.08	224.4	124.4	3.49	12.93	10.88	475.9	134.86	438.0	238.0	3.38	12.71	10.52	658.2	189.46	629.1	329.1	3.19
13.26	12.11	248.0	80.79	224.0	124.0	3.48	13.04	11.61	454.2	143.98	427.1	227.1	3.27	12.80	11.16	652.6	194.48	626.3	326.3	3.18
13.37	12.80	249.6	85.21	224.8	124.8	3.50	13.14	12.31	476.8	145.08	438.4	238.4	3.38	12.89	11.81	646.7	199.06	623.3	323.3	3.16
13.48	13.52	252.6	84.35	226.3	126.3	3.53	13.25	12.99	486.6	149.01	443.3	243.3	3.43	12.99	12.44	638.1	203.48	619.1	319.1	3.13
13.58	14.20	247.9	90.25	224.0	124.0	3.48	13.35	13.67	488.8	152.98	444.4	244.4	3.44	13.09	13.12	629.8	207.25	614.9	314.9	3.10
13.63	14.53	248.2	92.63	224.1	124.1	3.48	13.40	14.01	483.7	154.92	441.8	241.8	3.42	13.14	13.47	629.8	208.67	614.9	314.9	3.10

CONSOLIDATED UNDRAINED TRIAXIAL TEST
SUMMARY OF RESULTS

THEKWINI SOILS LAB. CC
V.A.T. REGISTRATION NO. 4590210961.
68 Ridge Road, Tollgate, DURBAN
Tel : (031) 201-8992
P.O. Box 30464, MAYVILLE, 4058
Fax : (031) 201-7920

Project: Sibaya
Ref no.: 9236
Lab no.: 11122
Depth: -
Position: S1

Description:
2 Layer Net-Mosquito

	Test 1	Test 2	Test 3
Normal Stress (kN/m^2)	100	200	300
Dry Density (kg/m^3)	1652	1652	1652
NMC(%)	11.7	11.7	11.7
Axial Strain (%)	13.5	13.7	7.2
$F^1 + F^3$ **2**	226.3	444.4	639.3
$F^1 - F^3$ **2**	126.3	244.4	339.3
F_1 F_3	3.53	3.44	3.26

Shear Strength Parameters

Angle of Internal Friction (0^0) 31

Cohesion (kPa) 13

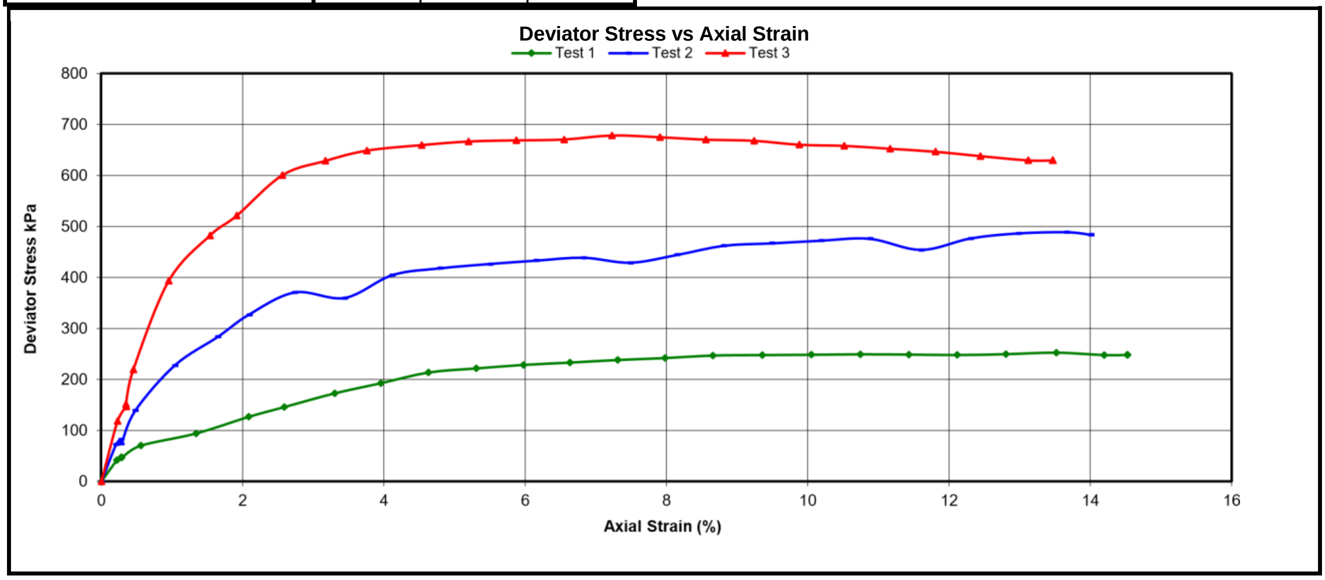

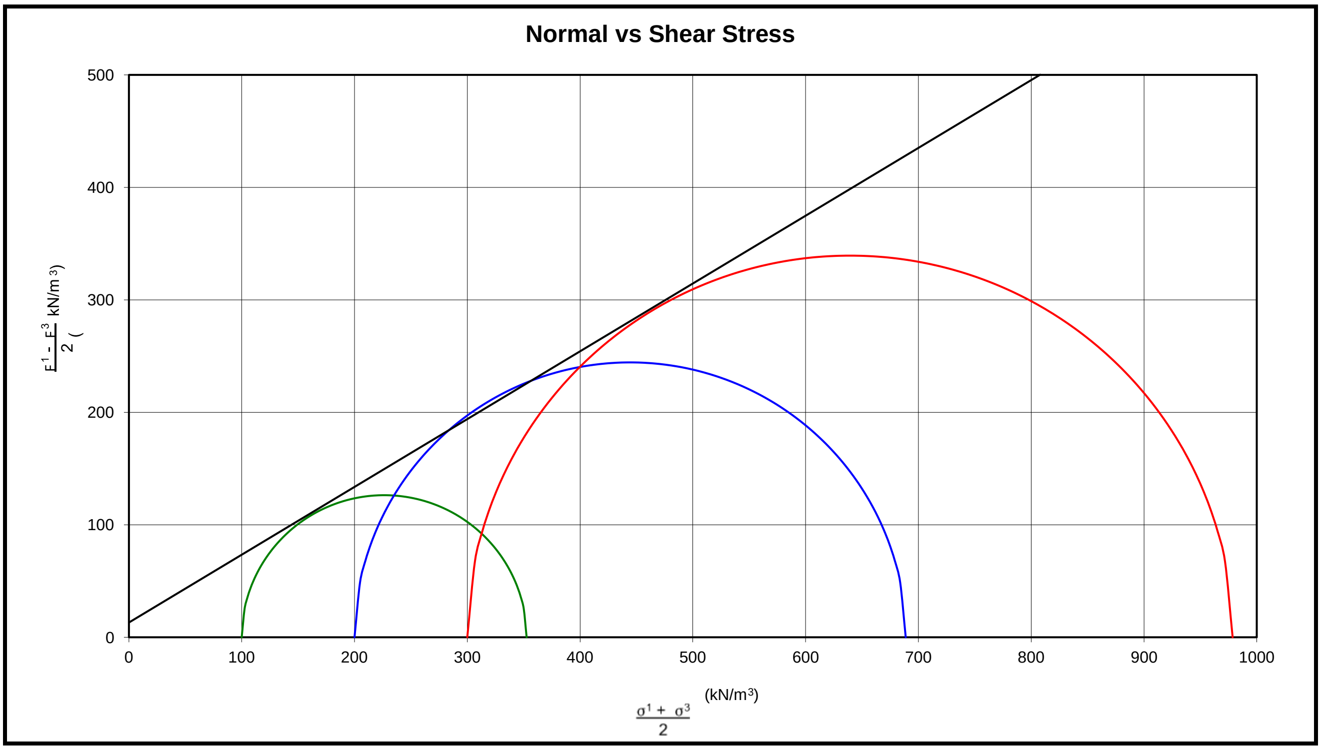

Normal vs Shear Stress
500
400
300
200
100
0
0
100
200
300
400
500
600
700
800
900
1000
(kN/m³)
σ1 + σ3
2

CONSOLIDATED UNDRAINED TRIAXIAL TEST

SUMMARY OF RESULTS

THEKWINI SOILS LAB. CC
V.A.T. REGISTRATION NO. 4590210961.
68 Ridge Road, Tollgate, DURBAN
Tel : (031) 201-8992
P.O. Box 30464, MAYVILLE, 4058
Fax : (031) 201-7920

Project: Sibaya
Ref no.: 9236
Lab no.: 11122 **Depth:** **Description:** **Position:** S1
4 Layer Net-Mosquito

Test 1

Inputs

L (cm)	7.76	Lo (cm)	7.67	MC Before (%)	11.7
A (cm^2)	11.95	Ao (cm^2)	11.65	MC After (%)	19.4
V (cc)	92.70	Vo (cc)	89.30	Bulk Density (kg/m3)	1845
		Prooving Ring	0.45	Dry Density (kg/m3)	1652
		Sigma3	100		

Test 2

Inputs

L (cm)	7.76	Lo (cm)	7.62	MC Before (%)	11.7
A (cm^2)	11.95	Ao (cm^2)	11.52	MC After (%)	19.3
V (cc)	92.70	Vo (cc)	87.80	Bulk Density (kg/m3)	1845
		Prooving Ring	0.75	Dry Density (kg/m3)	1652
		Sigma3	200		

Test 3

Inputs

L (cm)	0.00	Lo (cm)	7.57	MC Before (%)	11.7
A (cm^2)	7.76	Ao (cm^2)	11.37	MC After (%)	19.2
V (cc)	11.95	Vo (cc)	86.00	Bulk Density (kg/m3)	1845
		Prooving Ring	0.92	Dry Density (kg/m3)	1652
		Sigma3	300		

Test 1

Area at Test	%Strain	Deviator Stress (kPa)	Pore Water Pressurs (Kpa)	$F^1 + F^3$ / 2	$F^1 - F^3$ / 2	F^1 / F^3
11.65	0	0	0	0	0	0
11.68	0.22	42.8	2.83	121.4	21.4	1.43
11.69	0.28	51.6	2.97	125.8	25.8	1.52
11.69	0.29	54.8	3.28	127.4	27.4	1.55
11.72	0.56	75.7	4.43	137.8	37.8	1.76
11.81	1.34	100.1	5.68	150.1	50.1	2.00
11.90	2.09	126.9	8.97	163.4	63.4	2.27
11.96	2.59	149.6	9.17	174.8	74.8	2.50
12.05	3.30	174.0	10.00	187.0	87.0	2.74
12.13	3.96	203.3	10.56	201.6	101.6	3.03
12.22	4.63	215.9	15.13	207.9	107.9	3.16
12.31	5.31	223.8	22.97	211.9	111.9	3.24
12.39	5.98	233.2	31.71	216.6	116.6	3.33
12.48	6.63	240.4	37.74	220.2	120.2	3.40
12.57	7.31	240.0	44.56	220.0	120.0	3.40
12.66	7.98	249.9	45.27	225.0	125.0	3.50
12.76	8.65	250.2	55.73	225.1	125.1	3.50
12.86	9.36	249.2	62.75	224.6	124.6	3.49

Test 2

Area at Test	%Strain	Deviator Stress (kPa)	Pore Water Pressurs (Kpa)	$F^1 + F^3$ / 2	$F^1 - F^3$ / 2	F^1 / F^3
11.52	0	0	0	0	0	0
11.55	0.21	87.5	11.67	243.7	43.7	1.44
11.56	0.27	102.5	11.99	251.2	51.2	1.51
11.56	0.28	114.3	12.84	257.2	57.2	1.57
11.58	0.48	147.5	13.50	273.7	73.7	1.74
11.65	1.04	252.3	14.50	326.2	126.2	2.26
11.72	1.65	287.7	15.37	343.9	143.9	2.44
11.77	2.09	345.3	21.37	372.6	172.6	2.73
11.85	2.74	380.6	29.77	390.3	190.3	2.90
11.94	3.45	382.4	36.74	391.2	191.2	2.91
12.02	4.12	423.8	44.78	411.9	211.9	3.12
12.11	4.80	429.6	67.79	414.8	214.8	3.15
12.20	5.50	428.5	79.27	414.2	214.2	3.14
12.28	6.16	433.0	88.75	416.5	216.5	3.17
12.37	6.83	454.0	99.12	427.0	227.0	3.27
12.46	7.49	476.3	110.17	438.1	238.1	3.38
12.55	8.15	486.7	121.11	443.4	243.4	3.43
12.64	8.81	495.8	121.74	447.9	247.9	3.48

Test 3

Area at Test	%Strain	Deviator Stress (kPa)	Pore Water Pressurs (Kpa)	$F^1 + F^3$ / 2	$F^1 - F^3$ / 2	F^1 / F^3
11.37	0	0	0	0	0	0
11.40	0.23	137.4	12.67	368.7	68.7	1.46
11.41	0.35	155.2	13.13	377.6	77.6	1.52
11.41	0.35	187.0	15.99	393.5	93.5	1.62
11.42	0.45	289.0	19.34	444.5	144.5	1.96
11.48	0.95	410.1	22.74	505.0	205.0	2.37
11.55	1.54	501.7	35.72	550.8	250.8	2.67
11.59	1.91	562.2	49.58	581.1	281.1	2.87
11.67	2.56	625.6	69.73	612.8	312.8	3.09
11.74	3.17	643.2	90.04	621.6	321.6	3.14
11.81	3.76	664.0	111.37	632.0	332.0	3.21
11.91	4.53	688.9	119.52	644.4	344.4	3.30
11.99	5.20	681.6	137.23	640.8	340.8	3.27
12.08	5.87	697.7	139.55	648.8	348.8	3.33
12.17	6.55	692.7	148.97	646.4	346.4	3.31
12.26	7.23	701.3	159.66	650.7	350.7	3.34
12.35	7.91	696.8	166.73	648.4	348.4	3.32
12.43	8.56	695.4	172.31	647.7	347.7	3.32

12.96	10.05	249.2	68.17	224.6	124.6	3.49	12.73	9.49	497.1	123.47	448.5	248.5	3.49	12.53	9.24	701.7	180.73	650.8	350.8	3.34
13.06	10.74	251.1	74.44	225.5	125.5	3.51	12.83	10.19	495.1	125.78	447.5	247.5	3.48	12.62	9.88	701.0	185.97	650.5	350.5	3.34
13.16	11.43	250.9	76.45	225.4	125.4	3.51	12.93	10.88	508.9	129.72	454.4	254.4	3.54	12.71	10.52	697.1	190.73	648.6	348.6	3.32
13.26	12.11	251.6	82.29	225.8	125.8	3.52	13.04	11.61	511.9	131.14	456.0	256.0	3.56	12.80	11.16	699.9	195.77	650.0	350.0	3.33
13.37	12.80	244.0	88.78	222.0	122.0	3.44	13.14	12.31	506.6	144.38	453.3	253.3	3.53	12.89	11.81	691.4	201.27	645.7	345.7	3.30
13.48	13.52	252.1	89.22	226.0	126.0	3.52	13.25	12.99	505.3	149.56	452.6	252.6	3.53	12.99	12.44	691.8	205.68	645.9	345.9	3.31
13.58	14.20	253.0	91.12	226.5	126.5	3.53	13.35	13.67	506.9	151.67	453.5	253.5	3.53	13.09	13.12	683.7	210.20	641.9	341.9	3.28
13.63	14.53	254.1	91.27	227.1	127.1	3.54	13.40	14.01	508.8	152.72	454.4	254.4	3.54	13.14	13.47	682.2	212.34	641.1	341.1	3.27

CONSOLIDATED UNDRAINED TRIAXIAL TEST
SUMMARY OF RESULTS

THEKWINI SOILS LAB. CC
V.A.T. REGISTRATION NO. 4590210961.
68 Ridge Road, Tollgate, DURBAN
Tel : (031) 201-8992
P.O. Box 30464, MAYVILLE, 4058
Fax : (031) 201-7920

Project: Sibaya
Ref no.: 9236
Lab no.: 11122
Depth: -
Position: S1

Description:
4 Layer Net-Mosquito

	Test 1	Test 2	Test 3
Normal Stress (kN/m^2)	100	200	300
Dry Density (kg/m^3)	1652	1652	1652
NMC(%)	11.7	11.7	11.7
Axial Strain (%)	14.5	11.6	9.2
F^1 **+** F^3 **2**	227.1	456.0	650.8
F^1 **-** F^3 **2**	127.1	256.0	350.8
F1 F3	3.54	3.56	3.34

Shear Strength Parameters

Angle of Internal Friction (0^0) 32

Cohesion (kPa) 11

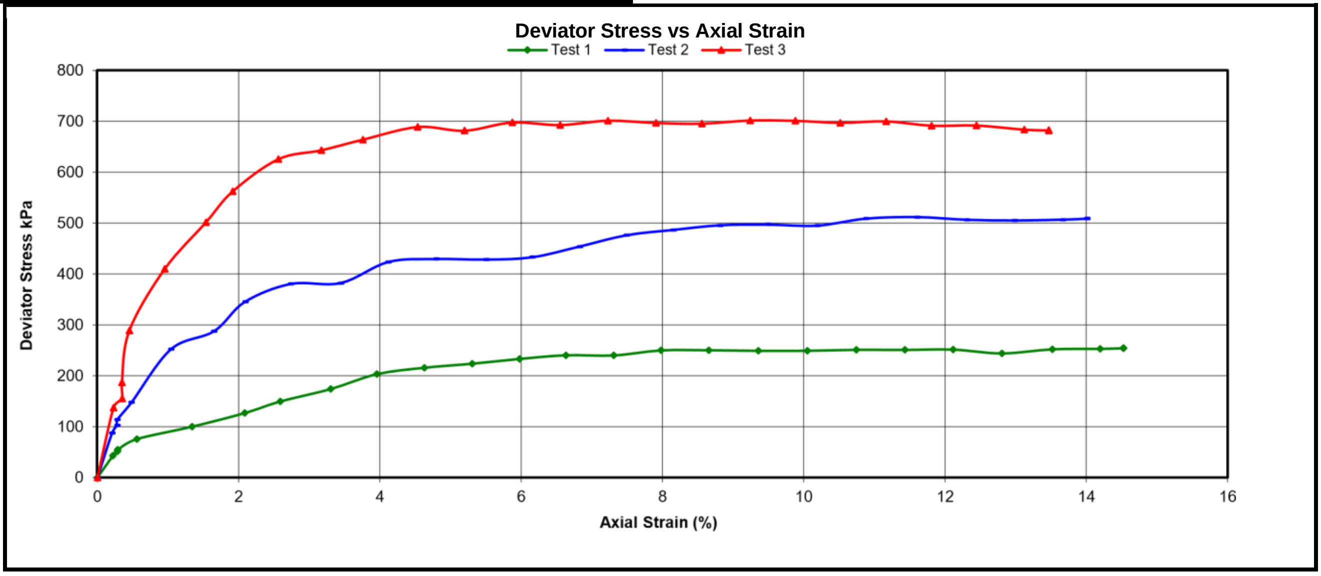

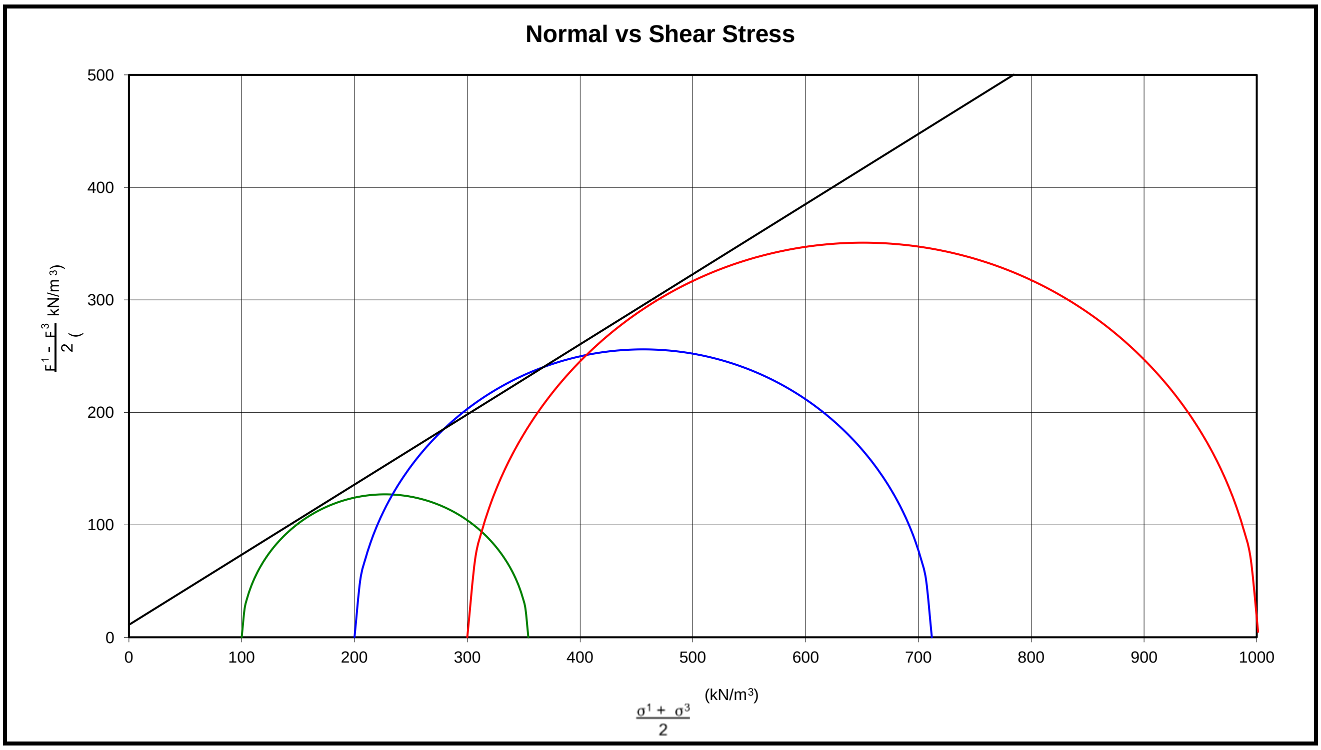

Normal vs Shear Stress
500
400
300
200
100
0
0
100
200
300
400
500
600
700
800
900
1000
(kN/m³)
σ¹ + σ³
2

CONSOLIDATED UNDRAINED TRIAXIAL TEST

SUMMARY OF RESULTS

THEKWINI SOILS LAB. CC
V.A.T. REGISTRATION NO. 4590210961.
68 Ridge Road, Tollgate, DURBAN
Tel : (031) 201-8992
P.O. Box 30464, MAYVILLE, 4058
Fax : (031) 201-7920

Project: Sibaya
Ref no.: 9236
Lab no.: 11122 **Depth:** **Description:** **Position:** S1
2 Layer Mesh-Diamond

Test 1

Inputs

L (cm)	7.76	Lo (cm)	7.67	MC Before (%)	11.7
A (cm^2)	11.95	Ao (cm^2)	11.65	MC After (%)	19.3
V (cc)	92.70	Vo (cc)	89.30	Bulk Density (kg/m3)	1845
		Prooving Ring	0.50	Dry Density (kg/m3)	1652
		Sigma3	100		

Area at Test	%Strain	Deviator Stress (kPa)	Pore Water Pressurs (Kpa)	$\frac{F^1 + F^3}{2}$	$\frac{F^1 - F^3}{2}$	F^1 / F^3
11.65	0	0	0	0	0	0
11.68	0.22	55.8	2.94	127.9	27.9	1.56
11.69	0.28	63.7	3.23	131.9	31.9	1.64
11.69	0.29	67.9	3.67	134.0	34.0	1.68
11.72	0.56	92.7	4.91	146.3	46.3	1.93
11.81	1.34	118.4	5.84	159.2	59.2	2.18
11.90	2.09	154.2	9.35	177.1	77.1	2.54
11.96	2.59	179.3	9.67	189.6	89.6	2.79
12.05	3.30	207.4	10.38	203.7	103.7	3.07
12.13	3.96	236.9	14.68	218.5	118.5	3.37
12.22	4.63	251.7	19.27	225.9	125.9	3.52
12.31	5.31	253.8	27.77	226.9	126.9	3.54
12.39	5.98	269.6	35.72	234.8	134.8	3.70
12.48	6.63	289.3	39.77	244.7	144.7	3.89
12.57	7.31	294.4	45.70	247.2	147.2	3.94
12.66	7.98	296.6	48.11	248.3	148.3	3.97
12.76	8.65	294.7	57.55	247.3	147.3	3.95
12.86	9.36	291.7	64.73	245.8	145.8	3.92

Test 2

Inputs

L (cm)	7.76	Lo (cm)	7.62	MC Before (%)	11.7
A (cm^2)	11.95	Ao (cm^2)	11.52	MC After (%)	19.1
V (cc)	92.70	Vo (cc)	87.80	Bulk Density (kg/m3)	1845
		Prooving Ring	0.80	Dry Density (kg/m3)	1652
		Sigma3	200		

Area at Test	%Strain	Deviator Stress (kPa)	Pore Water Pressurs (Kpa)	$\frac{F^1 + F^3}{2}$	$\frac{F^1 - F^3}{2}$	F^1 / F^3
11.52	0	0	0	0	0	0
11.55	0.21	104.2	12.22	252.1	52.1	1.52
11.56	0.27	122.8	12.68	261.4	61.4	1.61
11.56	0.28	139.9	13.45	269.9	69.9	1.70
11.58	0.48	172.6	13.78	286.3	86.3	1.86
11.65	1.04	221.9	15.67	310.9	110.9	2.11
11.72	1.65	279.8	17.43	339.9	139.9	2.40
11.77	2.09	359.9	26.79	379.9	179.9	2.80
11.85	2.74	418.2	31.28	409.1	209.1	3.09
11.94	3.45	422.7	39.45	411.4	211.4	3.11
12.02	4.12	440.5	48.98	420.3	220.3	3.20
12.11	4.80	499.4	66.42	449.7	249.7	3.50
12.20	5.50	491.1	78.33	445.6	245.6	3.46
12.28	6.16	496.2	89.43	448.1	248.1	3.48
12.37	6.83	532.0	90.74	466.0	266.0	3.66
12.46	7.49	554.8	115.40	477.4	277.4	3.77
12.55	8.15	540.4	132.47	470.2	270.2	3.70
12.64	8.81	535.4	134.44	467.7	267.7	3.68

Test 3

Inputs

L (cm)	0.00	Lo (cm)	7.57	MC Before (%)	11.7
A (cm^2)	7.76	Ao (cm^2)	11.37	MC After (%)	19.0
V (cc)	11.95	Vo (cc)	86.00	Bulk Density (kg/m3)	1845
		Prooving Ring	0.98	Dry Density (kg/m3)	1652
		Sigma3	300		

Area at Test	%Strain	Deviator Stress (kPa)	Pore Water Pressurs (Kpa)	$\frac{F^1 + F^3}{2}$	$\frac{F^1 - F^3}{2}$	F^1 / F^3
11.37	0	0	0	0	0	0
11.40	0.23	164.3	15.44	382.1	82.1	1.55
11.41	0.35	200.1	14.55	400.1	100.1	1.67
11.41	0.35	211.4	16.23	405.7	105.7	1.70
11.42	0.45	319.1	19.02	459.5	159.5	2.06
11.48	0.95	416.2	22.29	508.1	208.1	2.39
11.55	1.54	548.2	33.47	574.1	274.1	2.83
11.59	1.91	615.2	46.75	607.6	307.6	3.05
11.67	2.56	710.2	61.76	655.1	355.1	3.37
11.74	3.17	729.1	86.27	664.6	364.6	3.43
11.81	3.76	742.5	99.37	671.2	371.2	3.47
11.91	4.53	776.2	112.23	688.1	388.1	3.59
11.99	5.20	788.3	126.58	694.1	394.1	3.63
12.08	5.87	789.4	133.46	694.7	394.7	3.63
12.17	6.55	784.4	150.16	692.2	392.2	3.61
12.26	7.23	775.6	163.33	687.8	387.8	3.59
12.35	7.91	787.8	165.56	693.9	393.9	3.63
12.43	8.56	798.3	174.99	699.2	399.2	3.66

12.96	10.05	300.7	69.80	250.4	150.4	4.01	12.73	9.49	532.8	135.78	466.4	266.4	3.66	12.53	9.24	787.7	188.44	693.8	393.8	3.63
13.06	10.74	302.0	76.25	251.0	151.0	4.02	12.83	10.19	526.8	138.99	463.4	263.4	3.63	12.62	9.88	788.7	189.74	694.4	394.4	3.63
13.16	11.43	302.3	79.37	251.2	151.2	4.02	12.93	10.88	538.8	140.27	469.4	269.4	3.69	12.71	10.52	785.7	193.42	692.9	392.9	3.62
13.26	12.11	300.0	84.28	250.0	150.0	4.00	13.04	11.61	538.1	142.74	469.0	269.0	3.69	12.80	11.16	780.3	199.35	690.1	390.1	3.60
13.37	12.80	296.5	88.37	248.3	148.3	3.97	13.14	12.31	535.9	146.70	467.9	267.9	3.68	12.89	11.81	797.5	209.14	698.7	398.7	3.66
13.48	13.52	298.4	86.22	249.2	149.2	3.98	13.25	12.99	527.1	151.24	463.6	263.6	3.64	12.99	12.44	801.1	215.55	700.5	400.5	3.67
13.58	14.20	298.3	87.65	249.1	149.1	3.98	13.35	13.67	518.2	155.34	459.1	259.1	3.59	13.09	13.12	800.5	217.07	700.3	400.3	3.67
13.63	14.53	301.0	89.97	250.5	150.5	4.01	13.40	14.01	515.4	155.47	457.7	257.7	3.58	13.14	13.47	807.3	221.08	703.7	403.7	3.69

CONSOLIDATED UNDRAINED TRIAXIAL TEST
SUMMARY OF RESULTS

THEKWINI SOILS LAB. CC
V.A.T. REGISTRATION NO. 4590210961.
68 Ridge Road, Tollgate, DURBAN
Tel : (031) 201-8992
P.O. Box 30464, MAYVILLE, 4058
Fax : (031) 201-7920

Project: Sibaya
Ref no.: 9236
Lab no.: 11122
Depth: -
Position: S1

Description:
2 Layer Mesh-Diamond

	Test 1	Test 2	Test 3
Normal Stress (kN/m²)	100	200	300
Dry Density (kg/m³)	1652	1652	1652
NMC(%)	11.7	11.7	11.7
Axial Strain (%)	11.4	7.5	13.5
$\frac{F^1 + F^3}{2}$	251.2	477.4	703.7
$\frac{F^1 - F^3}{2}$	151.2	277.4	403.7
F1 F3	4.02	3.77	3.69

Shear Strength Parameters

Angle of Internal Friction (0^0) 34

Cohesion (kPa) 13

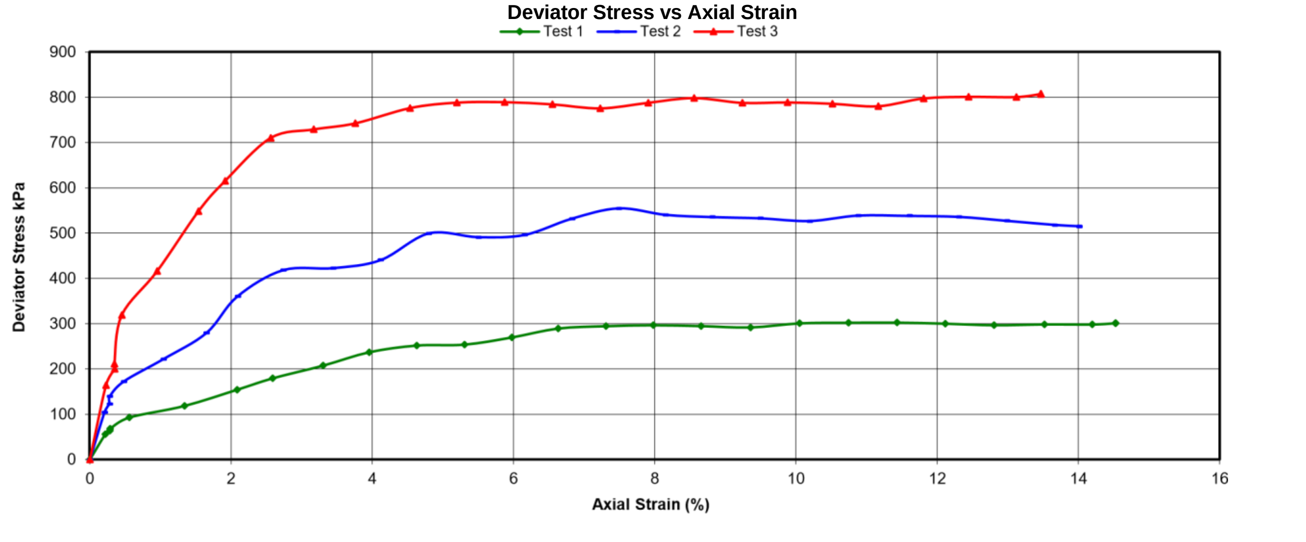

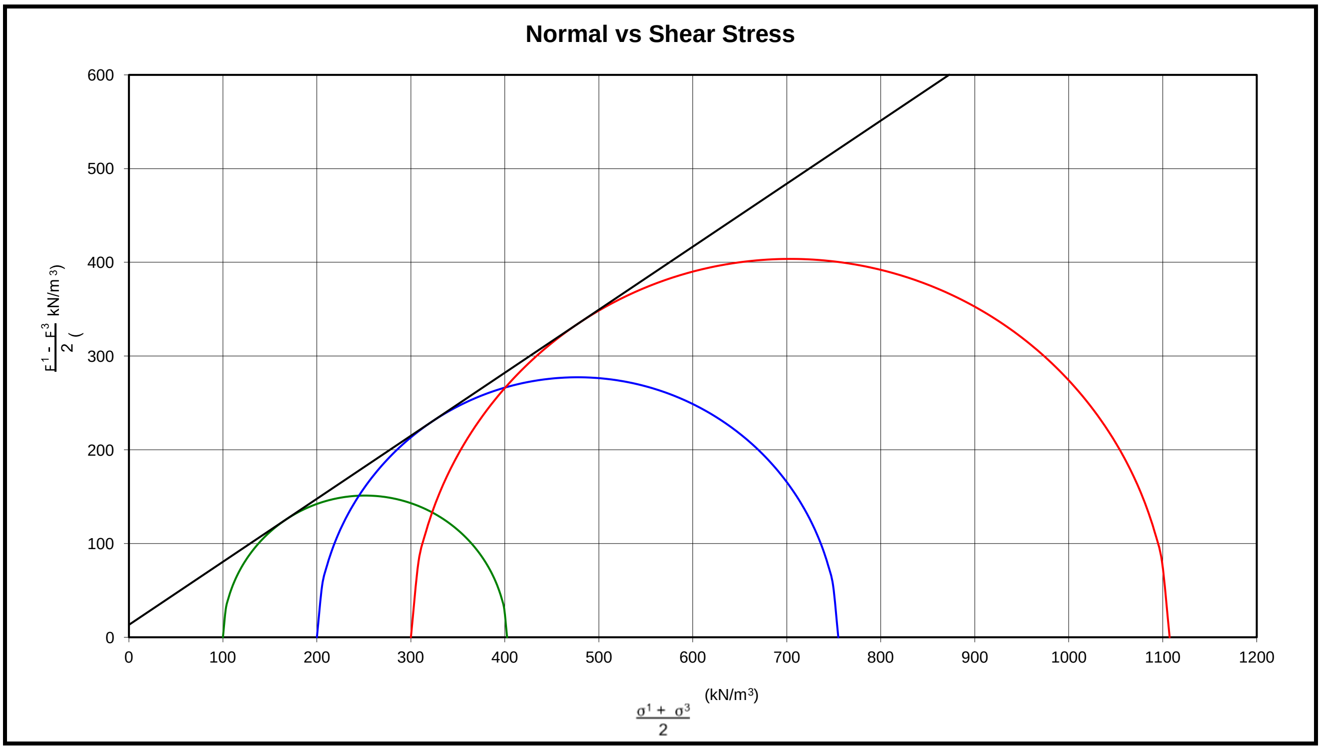
Normal vs Shear Stress
600
500
400
300
200
100
0
0
100
200
300
400
500
600
700
800
900
1000
1100
1200
(kN/m³)
σ1 + σ3 / 2

CONSOLIDATED UNDRAINED TRIAXIAL TEST

SUMMARY OF RESULTS

THEKWINI SOILS LAB. CC
V.A.T. REGISTRATION NO. 4590210961.
68 Ridge Road, Tollgate, DURBAN
Tel : (031) 201-8992
P.O. Box 30464, MAYVILLE, 4058
Fax : (031) 201-7920

Project: Sibaya
Ref no.: 9236
Lab no.: 11122 **Depth:** **Description:** **Position:** S1
4 Layer Net-Diamond

Test 1

Inputs

L (cm)	7.76	Lo (cm)	7.67	MC Before (%)	11.7
A (cm^2)	11.95	Ao (cm^2)	11.65	MC After (%)	19.3
V (cc)	92.70	Vo (cc)	89.30	Bulk Density (kg/m3)	1845
		Prooving Ring	0.45	Dry Density (kg/m3)	1652
		Sigma3	100		

Test 2

Inputs

L (cm)	7.76	Lo (cm)	7.62	MC Before (%)	11.7
A (cm^2)	11.95	Ao (cm^2)	11.52	MC After (%)	19.1
V (cc)	92.70	Vo (cc)	87.80	Bulk Density (kg/m3)	1845
		Prooving Ring	0.80	Dry Density (kg/m3)	1652
		Sigma3	200		

Test 3

Inputs

L (cm)	0.00	Lo (cm)	7.57	MC Before (%)	11.7
A (cm^2)	7.76	Ao (cm^2)	11.37	MC After (%)	19.0
V (cc)	11.95	Vo (cc)	86.00	Bulk Density (kg/m3)	1845
		Prooving Ring	1.00	Dry Density (kg/m3)	1652
		Sigma3	300		

Test 1

Area at Test	%Strain	Deviator Stress (kPa)	Pore Water Pressurs (Kpa)	$\frac{F^1 + F^3}{2}$	$\frac{F^1 - F^3}{2}$	F^1 / F^3
11.65	0	0	0	0	0	0
11.68	0.22	52.2	2.94	126.1	26.1	1.52
11.69	0.28	59.2	3.43	129.6	29.6	1.59
11.69	0.29	63.2	3.71	131.6	31.6	1.63
11.72	0.56	82.9	5.01	141.5	41.5	1.83
11.81	1.34	112.4	6.75	156.2	56.2	2.12
11.90	2.09	143.0	9.90	171.5	71.5	2.43
11.96	2.59	160.7	9.79	180.3	80.3	2.61
12.05	3.30	187.4	10.80	193.7	93.7	2.87
12.13	3.96	225.0	15.14	212.5	112.5	3.25
12.22	4.63	225.2	21.25	212.6	112.6	3.25
12.31	5.31	228.5	28.17	214.3	114.3	3.29
12.39	5.98	236.8	36.47	218.4	118.4	3.37
12.48	6.63	257.4	40.22	228.7	128.7	3.57
12.57	7.31	259.6	47.89	229.8	129.8	3.60
12.66	7.98	268.2	49.71	234.1	134.1	3.68
12.76	8.65	262.9	59.65	231.5	131.5	3.63
12.86	9.36	284.9	66.54	242.5	142.5	3.85

Test 2

Area at Test	%Strain	Deviator Stress (kPa)	Pore Water Pressurs (Kpa)	$\frac{F^1 + F^3}{2}$	$\frac{F^1 - F^3}{2}$	F^1 / F^3
11.52	0	0	0	0	0	0
11.55	0.21	115.6	10.00	257.8	57.8	1.58
11.56	0.27	141.4	13.75	270.7	70.7	1.71
11.56	0.28	153.9	14.37	277.0	77.0	1.77
11.58	0.48	175.2	14.56	287.6	87.6	1.88
11.65	1.04	231.4	16.72	315.7	115.7	2.16
11.72	1.65	284.8	17.97	342.4	142.4	2.42
11.77	2.09	359.3	28.74	379.6	179.6	2.80
11.85	2.74	422.3	33.28	411.2	211.2	3.11
11.94	3.45	435.9	40.37	417.9	217.9	3.18
12.02	4.12	457.9	52.20	429.0	229.0	3.29
12.11	4.80	507.3	67.18	453.6	253.6	3.54
12.20	5.50	496.9	79.78	448.5	248.5	3.48
12.28	6.16	504.6	90.75	452.3	252.3	3.52
12.37	6.83	528.3	95.74	464.1	264.1	3.64
12.46	7.49	544.1	115.77	472.1	272.1	3.72
12.55	8.15	568.2	122.58	484.1	284.1	3.84
12.64	8.81	572.0	130.18	486.0	286.0	3.86

Test 3

Area at Test	%Strain	Deviator Stress (kPa)	Pore Water Pressurs (Kpa)	$\frac{F^1 + F^3}{2}$	$\frac{F^1 - F^3}{2}$	F^1 / F^3
11.37	0	0	0	0	0	0
11.40	0.23	216.4	14.38	408.2	108.2	1.72
11.41	0.35	226.5	14.56	413.2	113.2	1.75
11.41	0.35	243.1	16.38	421.5	121.5	1.81
11.42	0.45	338.3	18.14	469.2	169.2	2.13
11.48	0.95	439.3	21.30	519.7	219.7	2.46
11.55	1.54	542.1	34.38	571.0	271.0	2.81
11.59	1.91	623.4	51.49	611.7	311.7	3.08
11.67	2.56	733.8	62.76	666.9	366.9	3.45
11.74	3.17	734.9	88.94	667.4	367.4	3.45
11.81	3.76	783.9	95.75	692.0	392.0	3.61
11.91	4.53	797.4	110.28	698.7	398.7	3.66
11.99	5.20	813.3	125.58	706.6	406.6	3.71
12.08	5.87	815.2	135.89	707.6	407.6	3.72
12.17	6.55	809.0	154.89	704.5	404.5	3.70
12.26	7.23	806.2	164.38	703.1	403.1	3.69
12.35	7.91	820.2	166.76	710.1	410.1	3.73
12.43	8.56	818.9	175.37	709.5	409.5	3.73

12.96	10.05	306.7	70.44	253.3	153.3	4.07	12.73	9.49	563.8	136.77	481.9	281.9	3.82	12.53	9.24	807.7	190.25	703.9	403.9	3.69
13.06	10.74	298.1	77.41	249.0	149.0	3.98	12.83	10.19	561.2	139.42	480.6	280.6	3.81	12.62	9.88	821.7	191.27	710.9	410.9	3.74
13.16	11.43	294.7	80.14	247.4	147.4	3.95	12.93	10.88	557.8	141.75	478.9	278.9	3.79	12.71	10.52	828.9	194.15	714.4	414.4	3.76
13.26	12.11	291.2	85.13	245.6	145.6	3.91	13.04	11.61	544.6	153.41	472.3	272.3	3.72	12.80	11.16	829.9	201.22	715.0	415.0	3.77
13.37	12.80	285.8	89.47	242.9	142.9	3.86	13.14	12.31	548.6	153.50	474.3	274.3	3.74	12.89	11.81	827.3	210.22	713.7	413.7	3.76
13.48	13.52	283.2	89.55	241.6	141.6	3.83	13.25	12.99	547.9	155.23	474.0	274.0	3.74	12.99	12.44	838.0	211.19	719.0	419.0	3.79
13.58	14.20	280.1	90.27	240.0	140.0	3.80	13.35	13.67	560.0	156.74	480.0	280.0	3.80	13.09	13.12	833.1	212.48	716.5	416.5	3.78
13.63	14.53	279.1	90.78	239.5	139.5	3.79	13.40	14.01	554.0	160.47	477.0	277.0	3.77	13.14	13.47	828.6	213.45	714.3	414.3	3.76

CONSOLIDATED UNDRAINED TRIAXIAL TEST
SUMMARY OF RESULTS

THEKWINI SOILS LAB. CC
V.A.T. REGISTRATION NO. 4590210961.
68 Ridge Road,
Tollgate, DURBAN
Tel : (031) 201-8992
P.O. Box 30464,
MAYVILLE, 4058
Fax : (031) 201-7920

Project: Sibaya
Ref no.: 9236
Lab no.: 11122
Depth: -
Position: S1

Description:
4 Layer Net-Diamond

	Test 1	Test 2	Test 3
Normal Stress (kN/m^2)	100	200	300
Dry Density (kg/m^3)	1652	1652	1652
NMC(%)	11.7	11.7	11.7
Axial Strain (%)	10.1	8.8	12.4
$\frac{F^1 + F^3}{2}$	253.3	486.0	719.0
$\frac{F^1 - F^3}{2}$	153.3	286.0	419.0
F_1 F_3	4.07	3.86	3.79

Shear Strength Parameters

Angle of Internal Friction (0^0) 35

Cohesion (kPa) 11

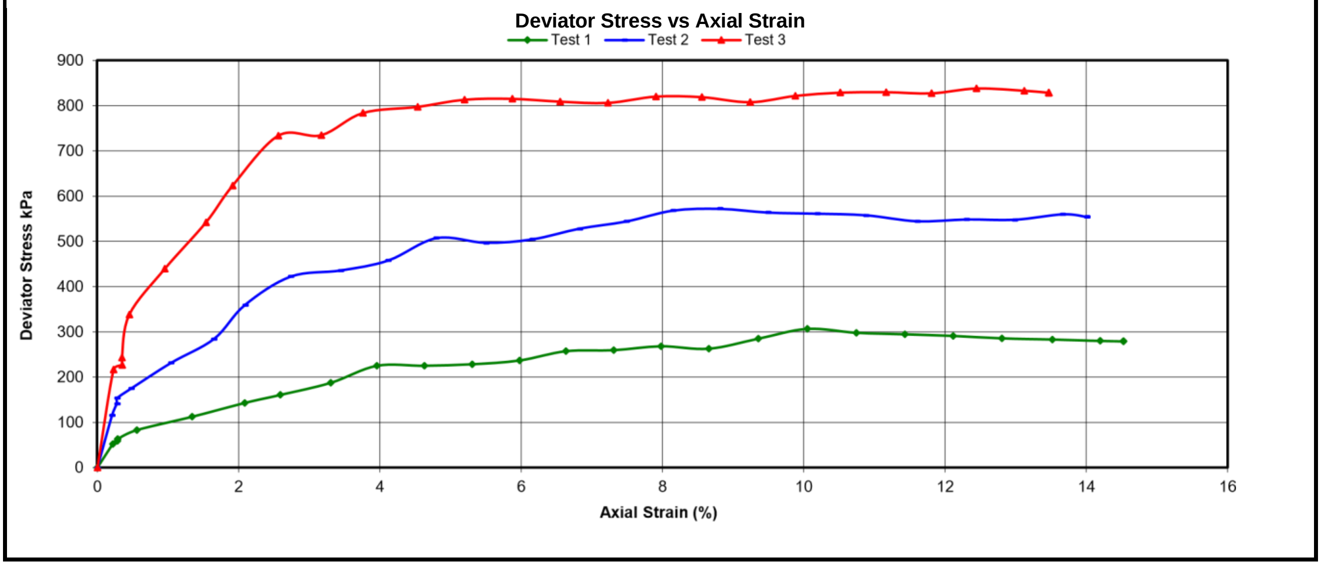

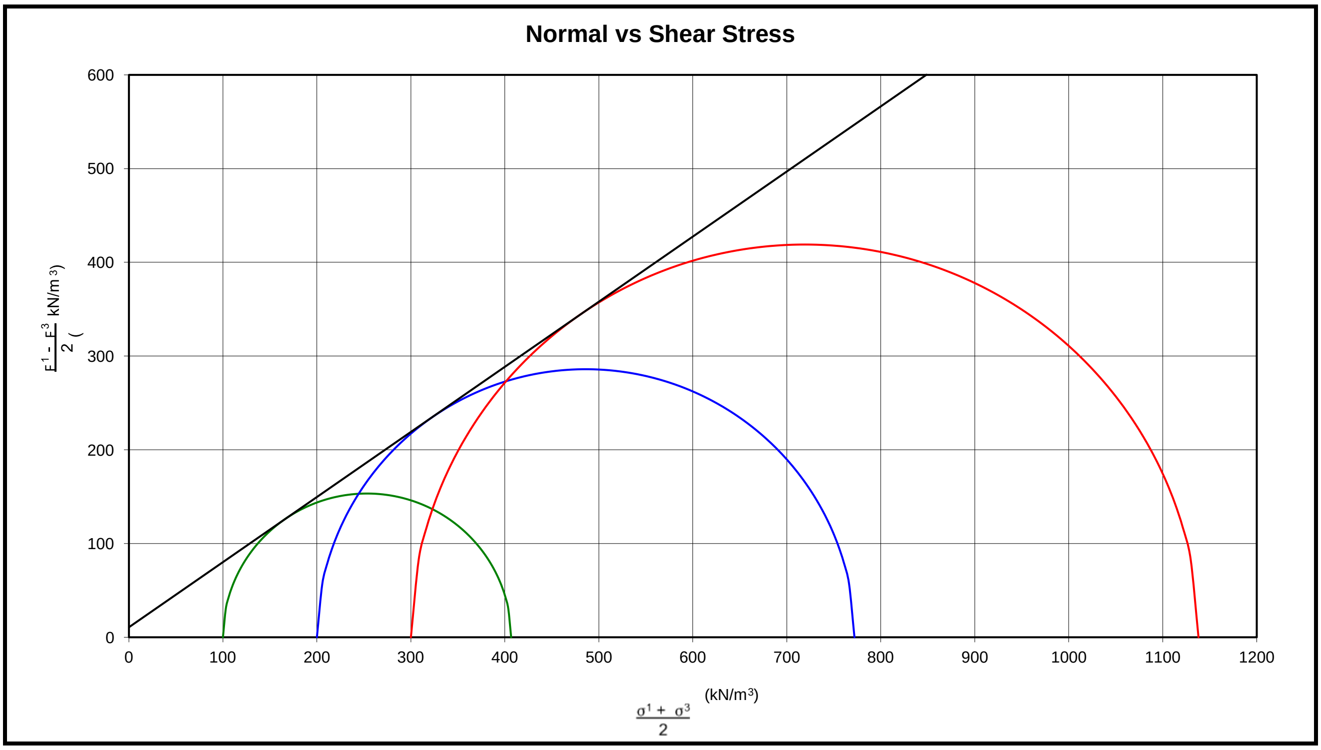
Normal vs Shear Stress
600
500
400
300
200
100
0
0
100
200
300
400
500
600
700
800
900
1000
1100
1200
(kN/m³)
σ1 + σ3
2